MOLECULAR MECHANISMS AND CONTROL OF CELLULOSE CARBONIZATION FOR EFFICIENT PRODUCTION OF LEVOGLUCOSAN

Takashi Nomura

Contents

List of Figures

List of Tables

List of Abbreviations

LG	lecoglucosan
AGF	1,6-anhydro-β-D-glucofuranose
5-HMF	5-Hydroxymethyl-2-furaldehyde
GA	glycolaldehyde
BPH	benzophenone
DPS	diphenyl sulfide
DPB	1,3-diphenoxybenzene
DMSO	dimethylsulfoxide

Chapter 1

Introduction

1.1 Biomass as an alternative to fossil resources

We use large amounts of fossil resources (oil, coal and natural gas) as energy and organic chemicals sources. However, the reserves of fossil resources are known to be limited, (oil: 50.0 years, natural gas: 49.8 years and coal: 132 years) (BP, 2020). The use of fossil fuels releases huge amount of carbon dioxide, which cause global warming, into atmosphere (IPCC, 2013). In addition, SOx and NOx produced by the burning of fossil resources are the sources of air pollution and acid rain (Ando et al., 1996). Therefore, in order to realize the sustainable society and solve environmental problems, reproducible and clean energy and chemical resources are needed to replace fossil resources.

Solar, wind, geothermal or other renewable energies are the energy sources, which can replace fossil resources. On the other hand, biomass can be utilized not only as the energy sources, but also as the renewable organic compound resources. This is the feature found only in biomass. The amount of biomass resources on earth is very large, estimated 1.8 Gt, and 10 % of the amount of biomass is renewed by photosynthesis every year (Saka, 2001; Whittaker, 1979). This annual production amount is six times the total energy consumption of the world. In addition, when carbon dioxide is generated using biomass, the produced carbon dioxide becomes a resource again through photosynthesis. The total amount of carbon dioxide in the atmosphere does not increase (carbon neutral). Therefore, the use of biomass as a source of energy and chemicals needs to be expanded.

There are various forms of biomass on the earth, but the woody biomass in the forest accounts for the majority of biomass resources. Woody biomass is mainly composed of cellulose, hemicellulose and lignin. These biomass resources are

collectively called lignocellulose resources. Rice straw and corn stover are also lignocellulose. These lignocellulose resources contain almost no sulfur and nitrogen. The utilization of biomass can reduce air pollution and acid rain generation as mentioned above. Therefore, lignocellulose resources have excellent potential as renewable chemicals and energy sources, and their utilization is important for building the sustainable society.

However, lignocellulose is difficult to use as energy and chemical sources. Lignocellulose is a solid, has a high-water content and a low specific gravity, which makes it unsuitable for transportation and inefficient as an energy source (Tillman, 1978). In addition, the structural components of biomass (cellulose, hemicellulose and lignin) are all polymer materials, and to use them as chemical sources for organic compounds is difficult. These indicate that the establishment of conversion technology of lignocellulose is necessary for its utilization.

1.2 Pyrolysis as a biomass conversion technology

Pyrolysis is degradation method by heating in the absence of oxygen, which produce solid, liquid, and gaseous products from biomass. The selectivity of the products can be changed depending on the pyrolysis conditions (temperature, heating rate or gas residence time). Low heating rate and short gas residence time process increase the yield of solid products. High heating rate and short gas residence time process maximize the yield of liquid products from biomass pyrolysis. Biomass gasification is normally conducted at high temperatures > 800 °C to maximize the gas formation. From the next section, solid, liquid and gas production are briefly introduced along with their situation.

1.2.1 Carbonization

Slow pyrolysis is a batch process performed at low temperatures and long heating rates. Heating rates as low as 0.1–2 °C, have been reported (Antal and Grønli,

2003). This process increases the yield of solid carbonized products by inhibiting volatilizing the pyrolysis products. Carbonization is the traditional technique for biomass processing to produce charcoal from wood. The resulting charcoal has a high carbon content and a high energy density (Pereira et al., 2012). On the other hand, torrefaction is another technology for producing solid fuel. Torrefaction is conducted in the temperature of range of 225–300 °C. This is a mild pyrolysis process for increasing the energy density and fuel properties of biomass (Prins et al., 2006). During the torrefaction process, water and volatiles in the biomass are removed. In addition, the biopolymers of biomass are partially degraded. The biomass treated by torrefaction requires less energy to crush, grind, or pulverize (Bridgeman et al., 2008).

Solid products from biomass have long been used as fuel. In recent years, concerns about climate change and food productivity have led to increased interest in bio--char to improve soil productivity and carbon sequestration (Manyà, 2012). Biochar is a carbon-rich, fine-grained, porous material that is produced by pyrolyzing biomass at low temperatures under oxygen limited conditions, which is as same as carbonization. One of the interesting properties of biochar is its porous structure, which is believed to be responsible for improved water retention and increased soil surface area. The nutrients contained in the biochar and the ability of the soil to adsorb and retain cations (e.g., Mg^{2+}, Ca^{2+}, K^{+}, and NH^{4+}) improves nutrient utilization efficiently (Yuan et al., 2011). In addition, due to its biological and chemical stability properties, biochar acts as a carbon sequestration material (McHenry, 2009). The use of biochar is a promising technique for solving environmental problems.

1.2.2 Fast pyrolysis for bio-oil production

Fast pyrolysis is a pyrolysis technique that rapidly heats biomass and instantly cools the produced volatiles to convert them into liquid products (bio-oil). The purpose of fast pyrolysis is to suppress further carbonization of the volatiles into solid carbonized compounds. Biomass is heated in the temperature range of 450-600 °C with a short

residence time (less than about 2 seconds). The yield of liquid product has been reported to reach 70 % on a dry feed basis (Dasappa, 2014).

Bio-oil is expected to be used as fuels and sources of chemicals. However, it is difficult to use bio-oil as an alternative resource to petroleum-derived oil. Bio-oil usually includes a high water and oxygen content, which decrease the energy density. The energy density of bio-oil (Higher Heating Value: 16-19 MJ/kg) is less than 50 % of that of heavy fuel oil (40 MJ/kg). On the other hand, the high-water content of bio-oil reduces the oil viscosity and improves the flow characteristics. This is beneficial for combustion, for example pumping and atomization. Since it contains organic acids such as acetic acid and formic acid, the pH of bio-oil is 2-3. Therefore, bio-oils are corrosive to common construction materials (Czernik and Bridgwater, 2004). From these reasons, reforming of bio-oil is important to utilize as alternative of fossil fuels. On the other hand, because bio-oil contains many compounds, the separation and purification costs is a problem when using it as chemical sources. It is important to improve the properties of bio-oil by controlling the pyrolysis reaction.

1.2.3 Gasification

Gasification is an important process for the thermochemical conversion of biomass. In this process, biomass is converted to producer gas at temperatures above 800 °C in the presence of oxidizing agent (also called a gasifying agent). The gasification temperature is much higher than the temperature of other thermochemical conversion technologies such as carbonization, torrefaction and fast pyrolysis. Oxidizing agents are usually air, vapors, N_2, CO_2, O_2, and a combination of these gases, which promotes the gasification of biomass. Producer gases include CO, H_2, CH_4, and small amounts of other hydrocarbon gases such as ethylene and acetylene (Demirbaş, 2001; Kumar et al., 2009).

Producer gas obtained by gasification of biomass can be directly used for engine or gas turbine to generate electricity. Alternatively, various catalytic conversion methods such as Fischer-Tropsch (FT) synthesis or methanation produce different types of gas and

liquid fuels and chemicals via CO and H2 in the producer gas (Kumar et al., 2009). Biogas could be utilized as an alternative resource to fossil fuels. The problem of biogas production is tar trouble. Tar is the volatile products which give condensable materials by cooling during the gas production from gasifier. Tar is easily decomposed to solid products, causing tar troubles such as clogging of pipeline and engine damage (Milne et al., 1998). Coke formation on the catalyst surface of FT synthesis and methanation causes the catalyst's deactivation (Paethanom et al., 2012). Therefore, the tar problem is an important problem to be solved in order to establish a reliable biomass gasification process.

1.3 Cellulose

The major pyrolysis products obtained from biomass can be controlled to some extent by the thermal decomposition conditions. However, further control of the reaction is essential for practical use of thermochemical conversion of biomass. Therefore, we try to reveal the molecular mechanism of pyrolysis reactions of biomass.

Biomass is mainly composed of cellulose, hemicellulose, and lignin. The contents of cellulose, hemicellulose and lignin are 40-50%, 15-30% and 20-30%, respectively (Wang et al., 2017). Cellulose is a linear high molecular weight polysaccharide, and the framework substance of plant cell wall. Hemicellulose is a heterogeneous branched polysaccharide, which mostly composed of sugars such as glucose, mannose, xylose and arabinose. Hemicellulose binds to the surface of each cellulose microfibril. Lignin is an amorphous three-dimensional polyphenol polymer, a coating material that solidifies the cell walls associated with matrix materials. In present studies, we investigated the pyrolysis of cellulose, which is the largest constituent of biomass. This section shows the chemical and crystal structure of cellulose.

1.3.1 Chemical structure

Cellulose is an unbranched homopolysaccharide composed of β-D-glucopyranose units linked by (1→4) glycosides (Figure 1-1). These pyranose rings are in the chair conformation $^4C_1$, with the hydroxy groups in an equatorial position. Every second pyranose ring is rotated 180° in the plane to accommodate the preferred bond angles of the acetal oxygen bridges. In nature, the degree of polymerization (DP) of cellulose chains is about 10,000 glucopyranose units for wood cellulose and about 15,000 for native cotton cellulose. The cellulose chain contains two ends. One is nonreducing end, which is an original C4-OH group. The other is reducing end, which is an original C1-OH group and in equilibrium with aldehyde structure (Klemm et al., 2005; O'Sullivan, 1997).

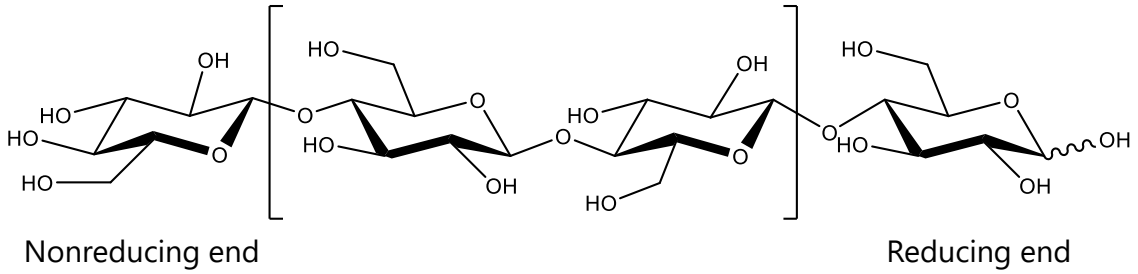

Figure 1-1. Chemical structure of cellulose chain.

1.3.2 Physical structure

There are several types of cellulose crystal types, but here we take Cellulose I as an example. Cellulose I has two intramolecular hydrogen bonds at (C2OH) - (HOC6) and (C3OH) - (OC5) and an interchain hydrogen bond between (C6OH) - (C3OH) as shown in Figure 1-2 (Klemm et al., 2005; O'Sullivan, 1997). On the other hand, C-H groups are arranged in the vertical direction of the pyranose ring of the glucose unit and show hydrophobicity in this direction (Figure 1-3). Cellulose crystals are formed by arranging them in the plane direction by intermolecular and interchain hydrogen bonds and

arranging them perpendicularly to the hydrophobic surface. Figure 1-4 shows the cross-sectional view of cellulose fibers and the structure of cellulose crystallites (Elazzouzi-Hafraoui et al., 2008). The width of crystallites is reported to be 6.1 nm and most of their surfaces are hydrophilic. The thermal decomposition of crystalline cellulose was studied by X-ray diffraction, and the thermal decomposition of cellulose crystallite was reported to proceed from its surface (Kawamoto and Saka, 2006; Kim et al., 2001b; Zickler et al., 2007). In addition, because the glycosidic bonds are exposed, the cleavage of the glycosidic bonds is expected to occur from this surface.

Microcrystals come together to form fibers. A cotton fiber is 10 μm in diameter. This indicates that about 300 cellulose crystallites line up in the thickness direction of the cell wall. Cellulose is composed of β-D-glucopyranose as the basic unit, but its reactivity is complicated because of its heterogeneous structure as described above.

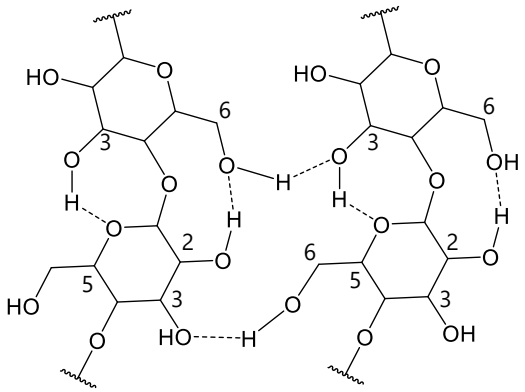

Figure 1-2. Hydrogen bonding pattern for cellulose I.

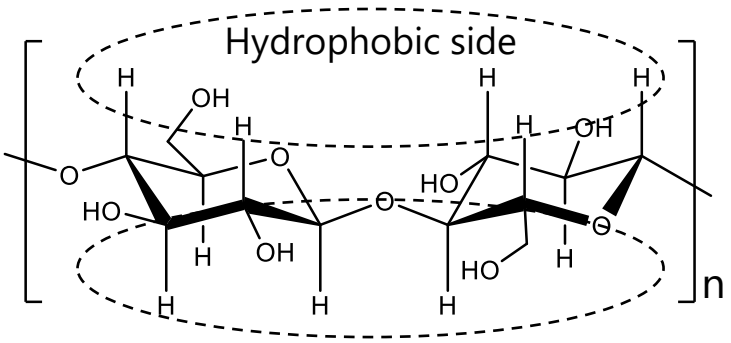

Figure 1-3. Hydrophobic side of glucose unit of cellulose in the vertical direction of the pyranose ring.

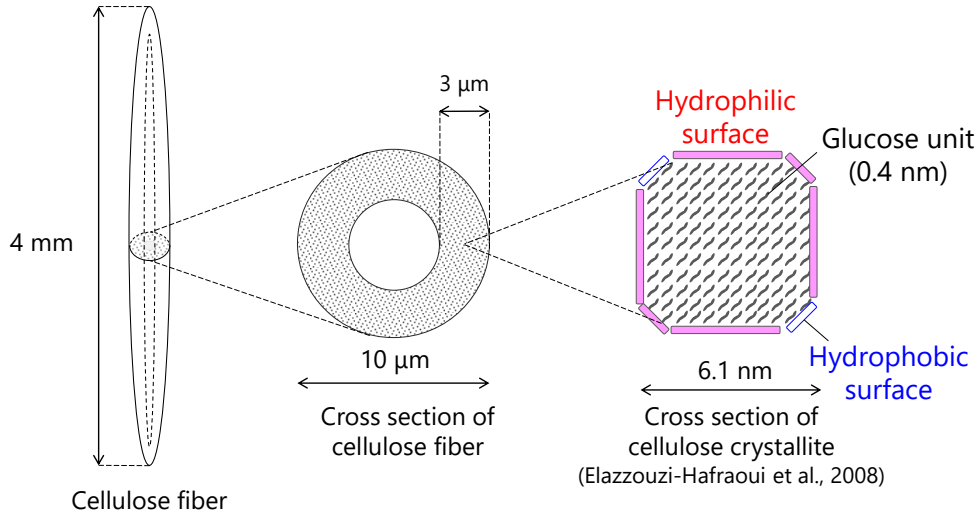

Figure 1-4. Cross section of cotton cellulose fibers and crystallite.

1.4 Pyrolysis reactions of cellulose

Pyrolysis of cellulose proceeds in two stages, primary pyrolysis reactions and secondary pyrolysis reactions. In the primary pyrolysis reactions, cellulose is converted into volatile intermediates and primary char. The selectivity of primary pyrolysis products depends on pyrolysis conditions such as temperature and heating rate. Generally, the thermal decomposition temperature of cellulose is reported to be around 350 °C based on thermogravimetry analysis (TGA) (Fisher et al., 2002). In this temperature range, cellulose is rapidly converted to large amounts of volatile products and 10% of residues. However, even if the temperature is under 300 °C, thermal decomposition of cellulose proceeds by heating for a long time. At low temperatures, char, water and gas are the major products. The boundary temperature is thought to be around 300 °C (F. Shafizadeh, 1982). Therefore, similar to the thermochemical conversion of biomass, liquid products are mainly obtained at high temperatures and solid products are mainly obtained at low temperatures. This section describes the primary and secondary pyrolysis reactions.

1.4.1 Primary pyrolysis reactions

The first event of pyrolysis of cellulose is a decrease in the degree of polymerization (DP) to a level-off degree of polymerization (LODP, DP: about 200) (Broido, Javier-Son, Ouano, Barrall, et al., 1973; Matsuoka et al., 2014; F Shafizadeh and Bradbury, 1979). Broido et al. reported that the DP of Whatman cellulose dropped rapidly from DP 2650 to DP 200-400 in the temperature range of 175-225 °C (Broido, Javier-Son, Ouano, Barrall, et al., 1973). On the other hand, the DP of ammonia-swelled cellulose changed only gradually in the early stages. In heat treatment of ammonia-swelled cellulose, crystallization of cellulose proceeded before the DP of cellulose drops, and the decrease of DP was delayed. Therefore, they suggested that initial rupture of cellulose molecule occurs at strain points at the crystalline-amorphous boundaries (Broido, Javier-Son, Ouano, Barrall, et al., 1973).

After the DP decreases, dehydration is the significant reaction in cellulose pyrolysis. Tang and Bacon determined that dehydration is the main reaction in the pyrolysis of cellulose at 200–280 °C based on the van Kreveken diagram of the elemental composition of cellulose char (Tang and Bacon, 1964b). Scheirs et al. showed that dehydration of Whatman cellulose occurred from 220 °C to 350 °C, and that the total amount of water remaining was 14.3% (w/w) (Scheirs et al., 2001). Early in cellulose pyrolysis, characteristic two IR bands appear at 1600 and 1700 cm^{-1} (Julien et al., 1991; Pastorova et al., 1994; Sekiguchi et al., 1983; Tang and Bacon, 1964a). These bands were assigned to conjugated C=C bonds, such as in benzene rings, and carbonyl (C=O) groups, respectively, both of which are thought to form through dehydration reactions (Julien et al., 1991; Pastorova et al., 1994; Sekiguchi et al., 1983; Tang and Bacon, 1964a).

Thermal discoloration and carbonization of glycerol- or $NaBH_4$-treated cellulose, in which the reducing ends were eliminated, were remarkably suppressed in the heat treatment of cellulose at 160–280 °C (Matsuoka et al., 2011a, 2011b). This indicates that the reducing ends of cellulose have the important role of pyrolysis reactions of cellulose. Figure 1-5 shows the proposed activation mechanism of crystalline cellulose starting from

the formation and decomposition of reducing ends. Reduction of cellulose DP to LODP and decomposition of the paracrystalline region proceed, which produce new reducing end of cellulose, and oligosaccharides. Decomposition of the reducing ends and oligosaccharides produce various pyrolysis products including water. Since the thermal decomposed products promote the next reactions, dehydration and carbonization, reactions progress in a chain from reducing ends of cellulose (Matsuoka et al., 2011a, 2011b).

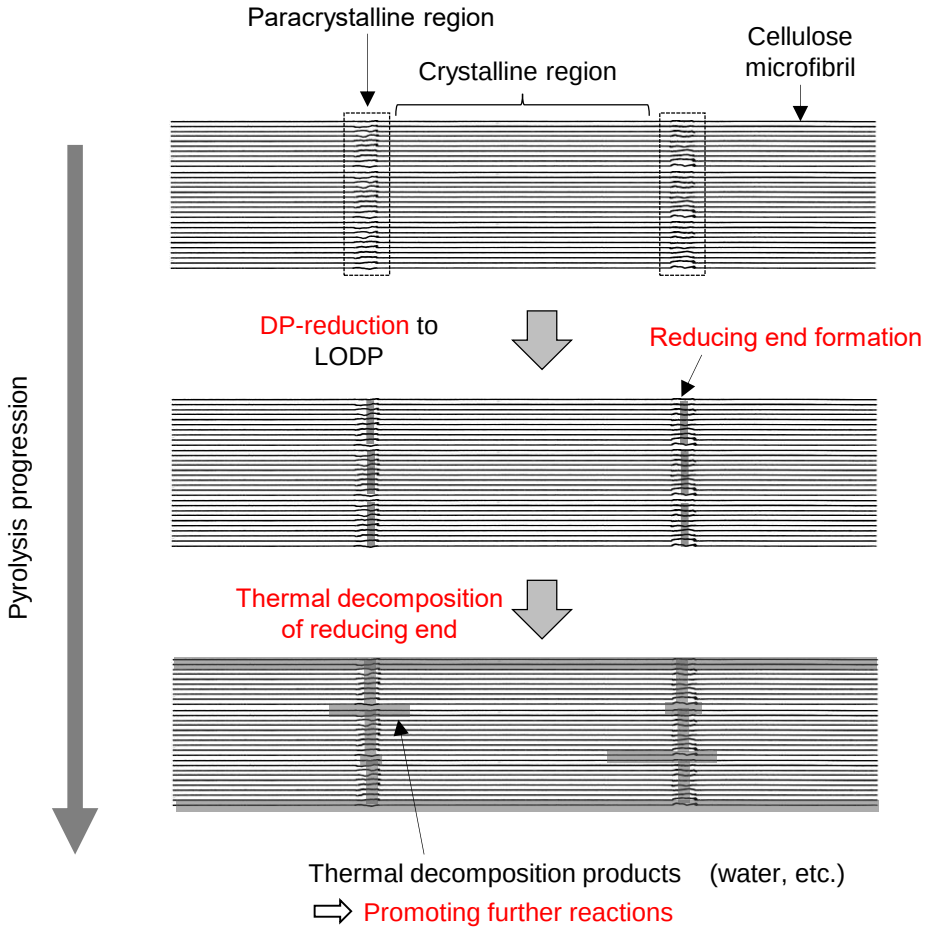

Figure 1-5. A proposed activation mechanism of cellulose starting from reducing ends.

At the temperature range over 300 °C, thermal decomposition reaction cellulose proceeds rapidly in a short time, and a large amount of volatile products are produced instead of char. The chemical structures of the major volatile products are shown in Figure

1-6. Cleavage of glycosidic bonds in cellulose produces lecoglucosan (LG), a pyranose-type anhydrous sugar, and 1,6-anhydro-β-D-glucofuranose (AGF), a furanose-type anhydrous sugar. By further dehydration of anhydosugar, 1,4; 3,6-dianhydro-α-D-glucopyranose, levoglucosenone, γ-lactone are formed. Furfural and 5-Hydroxymethyl-2-furaldehyde (5-HMF) are also dehydration products from cellulose in pyrolysis. Furan-type chemicals are produced by the conversion of pyranose to furanose via reducing sugars. Hydroxyacetaldehyde, hydroxyacetone, formaldehyde, acrolein, glyoxal, acetic acid and formic acid are the fragmentation products from cellulose. The formation of these pyrolysis products shows that glycosyl transfer reactions, dehydration reactions and fragmentation reactions proceed in pyrolysis.

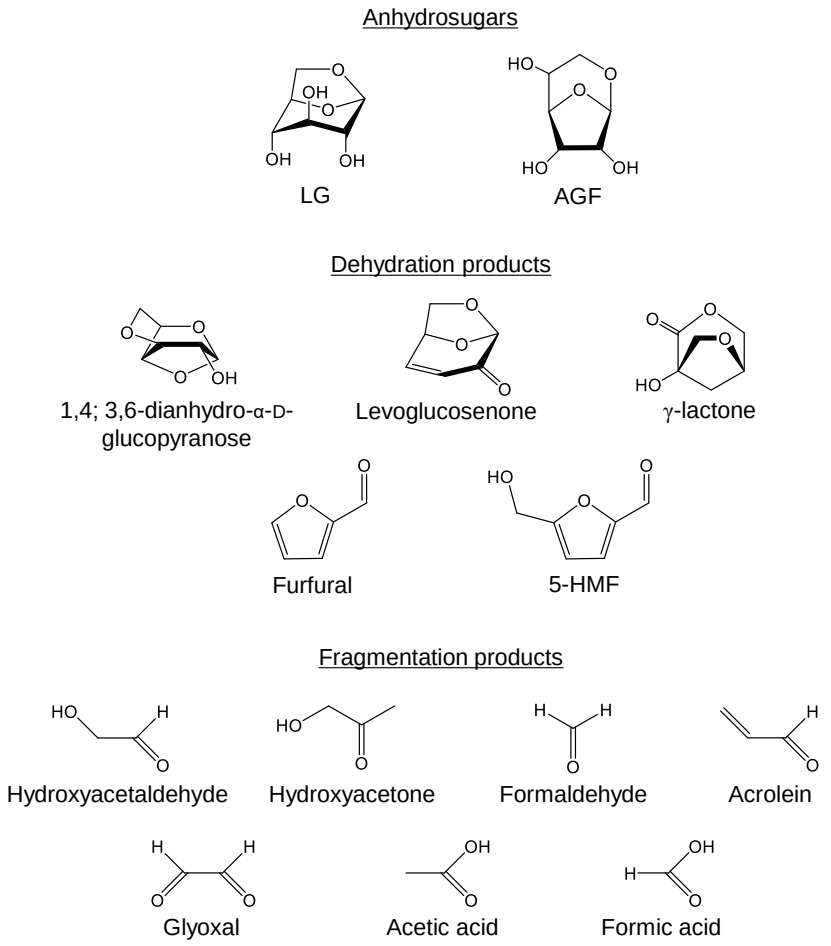

Figure 1-6. Low molecular-weight products obtained during cellulose pyrolysis.

Heating rate affects the product composition in pyrolysis of cellulose in this high temperature range. Fast pyrolysis is a method of raising the temperature of samples rapidly by using a high-temperature furnace (Radlein et al., 1987; Shoji et al., 2014), radiation flash (O. Boutin et al., 1998; Olivier Boutin et al., 2002; Nordin et al., 1974; Schroeter and Felix, 2005) or pressing on a hot metal disk (Dauenhauer et al., 2009; Lédé et al., 1987; Teixeira et al., 2011). In fast pyrolysis, cellulose is reported to be pyrolyzed via liquid intermediates. In addition, the thermal decomposition temperature of cellulose shifts to a higher temperature range in fast pyrolysis. The temperature change when a small amount of Avicel cellulose was inserted into a tubular furnace at various temperatures at once was measured by thermocouple (Figure 1-7) (Shoji et al., 2014). In the case of pyrolysis in a furnace under 550 °C, there was a region where the temperature rise was suppressed at 360-380 °C, which indicated that pyrolysis products was formed and evaporated in this temperature area. On the

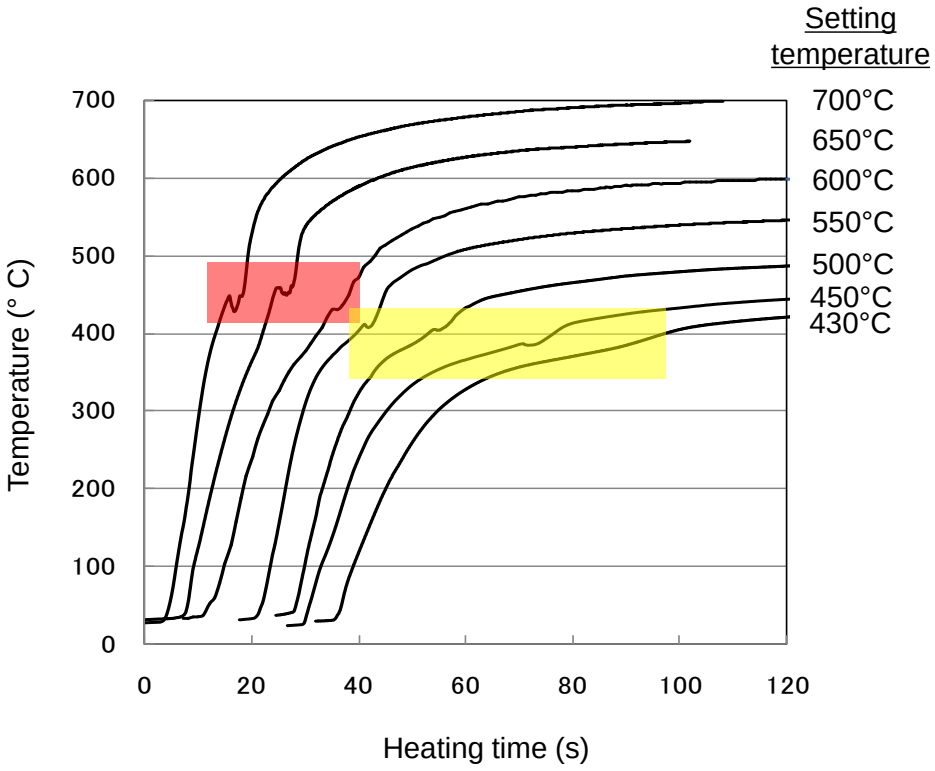

Figure 1-7. Temperature profiles obtained by in situ measurement of cellulose pyrolysis at various temperatures (430-700 °C) (Shoji et al., 2014).

other hand, in the furnace above 600 °C, the endothermic devolatilization plateau rose to 400-450 °C. This indicates that the thermal decomposition of cellulose proceeds at a higher temperature in a fast pyrolysis condition. By fast pyrolysis, the yield of liquid products increases and the yield of char (solid products) decreases. Fast pyrolysis is attracting attention as a method of producing bio-oil, which is a biofuel suitable for transportation and storage.

1.4.2 Secondary pyrolysis reactions and hydrogen-bond theory

One of the most important intermediate in pyrolysis of cellulose is LG. Under fast pyrolysis or vacuum conditions, the yield of LG was reported to be 60-70 wt% (G.J. Kwon et al., 2007; Fred Shafizadeh et al., 1979). However, the secondary pyrolysis reactions reduce the yield and selectivity of LG. For example, thermal polymerization and dehydration reactions of LG begin at 250 °C in liquid phase (Pictet, 1918), which is much lower than the decomposition temperature of cellulose (350 °C). Therefore, secondary pyrolysis reaction of LG proceeds immediately after its formation, and the final product becomes a complex mixture of gas, liquid, and solid products. In addition, since the boiling point of LG (385 °C) (Shoji et al., 2014) is higher than the polymerization temperature, secondary pyrolysis reactions of LG proceeds when the volatilized LG aggregates. Figure 1-8 shows the reactor after pyrolysis of cellulose with the temperature profile of the furnace (Hosoya et al., 2014). After tar extraction, solid carbonized products were found in the upper and bottom parts of the reactor. The solid carbonized product at the bottom (char) of reactor was formed directly from cellulose. On the other hand, the solid carbonized product in the upper side of reactor was generated from the volatile products from cellulose after aggregation. The solid carbonized product from volatiles, commonly referred to as coke, causes tar problems in the thermochemical conversion of biomass. Such carbonization reduces the yield and selectivity of the products during bio-oil and bio-gas generation.

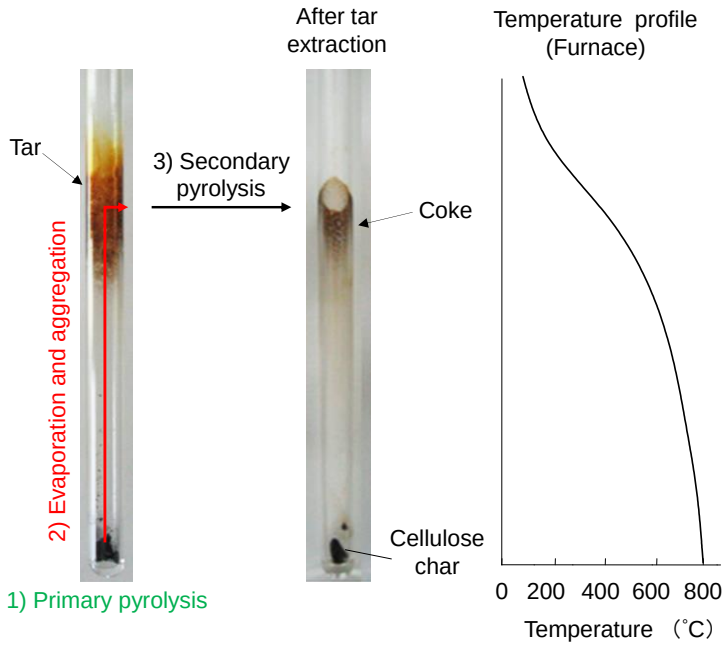

Figure 1-8. The reactor after pyrolysis of cellulose in N_2 at 800 °C for 30 s with the temperature profile of the furnace. (Hosoya et al., 2014).

The char produced from primary pyrolysis products is further decomposed to form benzene-ring structures. The cellulose chars prepared at different temperatures were characterized by using pyrolysis–gas chromatography–mass spectrometry (Py-GC/MS) (Pastorova et al., 1994). The major product detected from cellulose char heated at 250 °C was LG, because the char included much unreacted cellulose. By increasing the pyrolysis temperature of char preparation, the major compounds changed to furans and benzenes in the temperature range of 270–350 °C, which has also been supported by solid ^{13}C NMR. The furan structure was suggested to be converted to benzene-ring structures by secondary pyrolysis reactions of char. Smith and Howard also reported that benzenecarboxylic acids were obtained from cellulose char by alkaline permanganate oxidation and that the benzene ring structures were formed at temperatures above 250 °C by slow pyrolysis (Smith and Howard, 1937). Shafizadeh and Sekiguchi reported that, under fast pyrolysis conditions, benzene rings developed rapidly in the temperature range of 350–400 °C (Fred Shafizadeh and Sekiguchi, 1983).

1.4.3 Hydrogen-bond theory in pyrolysis of cellulose

The LG and other glycosides are shown to be stabilized to about 350 °C in polyether (Hosoya et al., 2008) and aromatic solvents (Hosoya et al., 2006a; Kawamoto et al., 2014). These solvents suppressed the pyrolysis reactions, which are promoted by acid catalysts. The ether oxygen of polyether or π-electron of aromatic solvent act as hydrogen bond acceptors for the hydroxyl groups of glycosides. Therefore, they proposed a molecular mechanism in which proton donation by intermolecular hydrogen bonds acts as an acid catalyst in the liquid phase (hydrogen-bond theory, Figure 1-9) (Kawamoto et al., 2013, 2014; Matsuoka et al., 2012). In the gas phase, LG is shown to be stable up to 500 °C, and gasification by fragmentation proceeds in the temperature range of 600-700 °C (Fukutome et al., 2015). This stability of LG is thought to be due to the weak intermolecular hydrogen bonds in the gas phase. These results suggest that by controlling the proton donation of intermolecular hydrogen bonds, we can suppress secondary pyrolysis reactions and improve product selectivity.

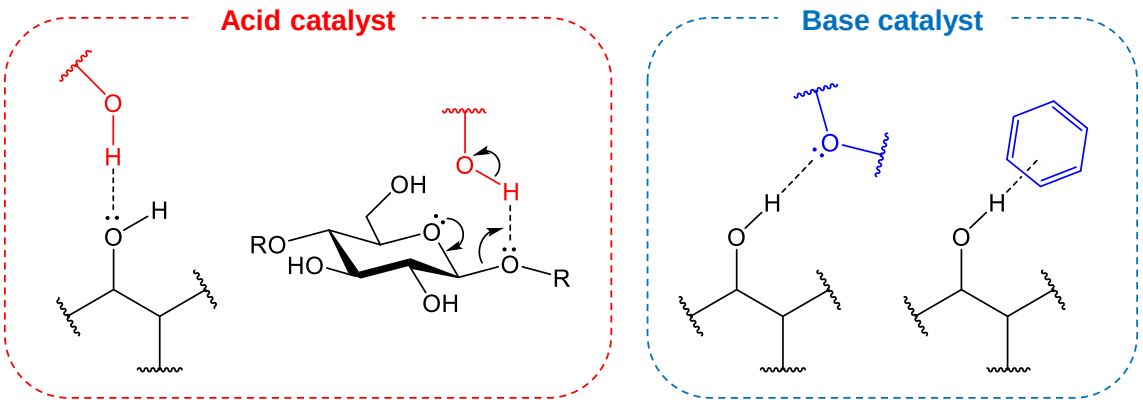

Figure 1-9. Hydrogen-bond theory acting as acid and base catalysts in pyrolysis.

1.5 Objectives of this thesis

The molecular mechanisms of cellulose pyrolysis, especially those associated with secondary pyrolysis, provide insight into the development of highly selective

product conversion methods. This dissertation primarily deals with improving the selectivity of pyrolysis products by suppressing secondary reactions of the products in aromatic solvents or gas phases.

In *Chapter 1*, the background of this dissertation is briefly summarized, which includes the importance of utilizing cellulosic biomass, the characteristics of pyrolysis conversion and the molecular mechanism of cellulose pyrolysis reactions with a focus on hydrogen bonding.

In *Chapter 2*, cellulose (Whatman filter paper) was pyrolyzed in aromatic solvents under nitrogen at 280 °C. Aromatic solvents delayed thermal degradation and carbonization and enhanced the yields of LG and 5-HMF. These results give important suggestions of carbonization mechanisms of cellulose. To reveal cellulose carbonization in the interior of cell walls, the pyrolyzed cellulose under nitrogen or in aromatic solvents was examined using ultraviolet (UV) microscopy (*Chapter 3*). From the results, the mechanism of cellulose carbonization in cell walls is discussed along with the influence of aromatic solvents.

As shown in *Chapter 2*, the formation of solid carbonized products was completely inhibited during cellulose pyrolysis in aromatic solvents, with 5-HMF recovered in certain yields instead. This indicated that 5-HMF is an intermediate in cellulose carbonization. In *Chapter 4 and 5*, carbonization and benzene formation mechanisms of cellulose via 5-HMF was investigated.

Based on the studies (*Chapter 2-5*), we proposed a mechanism that secondary pyrolysis reactions including carbonization via 5-HMF proceeds within the cell wall consisting of large number of cellulose crystallites. Because some of the surface of cellulose crystallites are inaccessible even with polar aromatic solvents, it is difficult to control all of cellulose pyrolysis by aromatic solvents. These results suggest that cellulose crystallinity is the key point in controlling the reactions. In fast pyrolysis, cellulose is melted at high temperature, and large amount of LG is produced. Therefore, fast pyrolysis can convert cellulose into low molecular weight products before the secondary reaction proceeds between the crystallites. However, in order to convert cellulose by fast pyrolysis,

the temperature of the furnace must be raised to over 600 °C. In these high temperature ranges, secondary pyrolysis reactions in gas phase reduce the yield of LG. Another problem is the progress of the polymerization / carbonization reaction after aggregation. In *Chapter 6*, fast pyrolysis of cellulose by infrared heating under nitrogen flow was investigated. Since infrared can heat only cellulose selectively, LG would be stably recovered by cooling immediately under nitrogen flow. The characteristics of infrared heating were also discussed. In addition, as basic research to expand the use of LG, we studied the conversion of LG and the pyrolyzed products obtained by infrared heating into glucose by using solid acid and microwaves (*Chapter 7*).

Finally, concluding remarks of these investigations are summarized in *Chapter 8* along with the prospects of these studies.

Chapter 2

Pyrolysis of cellulose in aromatic solvents: Reactivity, product yield, and char morphology

2.1 Introduction

Pyrolysis is defined as thermal degradation occurring under limited oxygen supply and is the fundamental basis of various thermochemical conversion technologies, like fast pyrolysis, gasification, carbonization, and torrefaction, for production of biofuels, biochemicals, and biomaterials from biomass resources. However, these technologies are limited by their low product selectivity, which usually makes their practical application difficult. For example, separation of desired products from a complex pyrolysis mixture is a tedious and costly process for biochemical production, and char formation makes the composition more complex along with decreasing productivity. Better understanding of the chemistry involved in biomass pyrolysis could provide insights to aid the development of controlled pyrolysis systems for sustainable utilization of biomass, which is the only renewable organic resource on Earth.

Pyrolysis of cellulose, the most abundant component of biomass, produces a substantial yield of LG (Kwon et al., 2007; Fred Shafizadeh et al., 1979), which is an important intermediate. Thus, LG and related compounds are promising biochemicals. However, the efficient production of LG is not easy, because thermal polymerization and dehydration reactions of LG occur at >250 °C (A. Pictet, 1918; Kawamoto et al., 2014), which is much lower than the temperature required for the formation of LG from cellulose (around 350 °C) (Kawamoto, 2016). Accordingly, cellulose-derived pyrolysis vapor forms coke by changing into the molten phase through cooling (Hosoya et al., 2007). This

apparently contradicting observation can be explained by the stability of gaseous LG (Fukutome et al., 2015), in which intermolecular hydrogen bonding is much less effective than in the molten LG, because the pyrolysis reactions of molten LG are believed to be promoted by hydrogen bonding (Agarwal et al., 2012; Hosoya et al., 2009; Kawamoto, 2016; Kawamoto et al., 2013, 2014; Mayes and Broadbelt, 2012; Seshadri and Westmoreland, 2012). Intermolecular hydrogen bonds act as an acid catalyst to promote transglycosylation and dehydration reactions. Such features may also exhibit complex effects on the mass-transfer efficiency of LG out of the cell wall, which affects the progression of secondary reactions including char formation.

LG and other glycosides are known to be stabilized in aromatic (Hosoya et al., 2006; Kawamoto et al., 2014) and polyether (Kawamoto et al., 2013) solvents up to around 350 °C. Hosoya et al. (2006) reported that the stabilization efficiency increased in direct correlation with the π-electron density of aromatic solvents. This is because π electrons of aromatic solvents (Kawamoto et al., 2014) and ether oxygens of polyethers (Kawamoto et al., 2013) act as hydrogen bond acceptors for hydroxyl groups of these glycosides, inhibiting proton donation to the carbohydrate molecules. Based on this stabilization mechanism, complete solvation of carbohydrate molecules would be critical to maximize this stabilization effect, so insoluble cellulose is expected to behave very differently from soluble compounds.

The ultrastructure of cellulose may affect its pyrolysis behavior. The cotton cellulose used in this study has cell walls consisting of cellulose microfibrils. Cellulose pyrolysis starts with a decrease of the degree of polymerization (DP) to around 200 (Broido et al., 1973; Halpern and Patai, 1969; F Shafizadeh and Bradbury, 1979), corresponding to the length of cellulose crystallites (Elazzouzi-Hafraoui et al., 2008; Nelson and Tripp, 1953; Nishiyama, 2009; Nishiyama et al., 2003; Rowland and Roberts, 1972) and subsequent thermal decomposition occurs from the crystallite surface (Kawamoto and Saka, 2006; Kim et al., 2001; Zickler et al., 2007). Accordingly, the formation of primary pyrolysis products and their secondary reactions including char

formation occur inside the cell wall volume. Thus, the aromatic solvent must penetrate into the cell wall volume to control the pyrolysis reactions.

Shoji et al. (2017) reported that cellulose was completely converted into volatile products by fast pyrolysis of cellulose–aromatic solvent mixtures with the complete inhibition of char formation. They also claimed that polar aromatic substituents are necessary to realize this behavior. Such substituents may help the aromatic compound to penetrate into the space between crystallites. Nevertheless, the action of aromatic solvents on the cell wall remains unclear. In this dissertation, the influences of aromatic solvents during cellulose pyrolysis are investigated focusing on the accessibility of the solvent to the cellulose crystallite surface by careful analysis of the pyrolyzed cellulose in the presence of aromatic solvents in nitrogen at 280 °C.

2.2 Materials and Methods

2.2.1 Materials

Whatman No. 42 filter paper (Whatman PLC, UK, cotton, moisture content: 4.9 wt%, dry basis) was used as a cellulose sample. Diphenyl sulfide [DPS, melting point (mp) −40 °C, boiling point (bp) 296 °C], 1,3-diphenoxybenzene (DPB, mp 166–171 °C, bp 375 °C), and benzophenone (BPH, mp 47–51 °C, bp 305 °C) were purchased from Tokyo Chemical Industry Co., Ltd. (Tokyo, Japan), Wako Pure Chemical Industries, Ltd. (Osaka, Japan) and Nacalai Tesque, Inc (Kyoto, Japan), respectively, (Figure 2-1) and used without further purification. The DPS is a thioether derivative with lower molar mass than that of DPB, while BPH has a carbonyl substituent that is expected to interact effectively with the hydrophilic surface of cellulose crystallites. Although DPB and BPH are solids at room temperature, they melted during the heating process to form liquids. All these solvents were stable up to the temperatures corresponding to their respective bp.

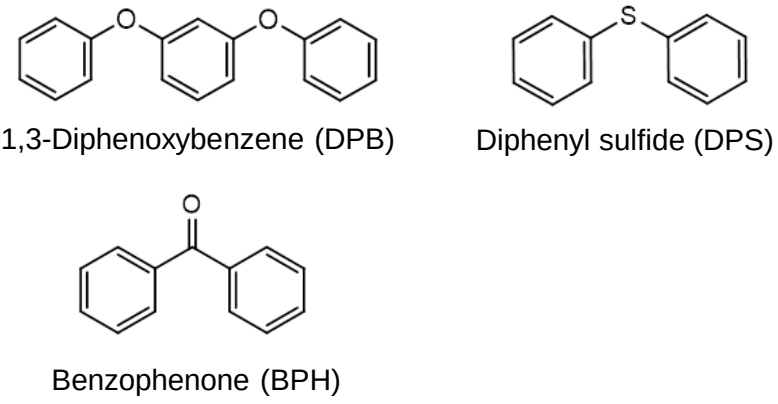

Figure 2-1. Chemical structures of aromatic solvents used in cellulose pyrolysis experiments.

2.2.2 Pyrolysis and characterization of low-molecular-weight products

Cellulose (40 mg, 38 mg dry basis) and aromatic solvent (400 mg) were placed at the bottom of a Pyrex glass tube reactor (internal diameter 8.0 mm, wall thickness 1.0 mm, length 300 mm), and then the reactor was connected to a nitrogen bag through a three-way tap. After the air inside the reactor was replaced with nitrogen using an aspirator, the reactor was inserted into a muffle furnace preheated to 280 °C. After heating for 60 min, the reactor was removed from the furnace and immediately cooled with an air flow.

The resulting pyrolysis mixture was extracted in dimethylsulfoxide (DMSO)- d_6 (0.7 mL) containing maleic acid as an internal standard and hydroxylamine hydrochloride LG (10 mg), an oximation reagent. The soluble portion was analyzed by ^{1}H NMR spectroscopy with a Bruker AC-400 (400 MHz) spectrometer (Bruker, MA, USA). The residue was washed successively with chloroform (5 mL, five times) and methanol (5 mL, five times), dried in an oven at 105 °C for 24 h, and then analyzed by various methods described in Section 2.2.3.

To determinate the low-molecular-weight products, the pyrolyzed cellulose was extracted with a binary mixture of D_2O (1.0 mL) and $CDCl_3$ (1.0 mL) containing maleic

acid (internal standard) and the oximation reagent (10 mg). With this procedure, the aromatic solvents were nicely separated into the $CDCl_3$-solbule fraction, whereas the cellulose-derived pyrolysis products were recovered in the D_2O-soluble fractions. The resulting residues were further extracted with DMSO-d_6 (1.0 mL) containing the oximation reagent (10 mg). The cellulose-derived products were determined with the first D_2O-soluble and second DMSO-d_6-soluble fractions by ^{1}H-NMR spectroscopy. Identification of the products was conducted by comparing the spectra with those of authentic compounds.

Control experiments were conducted in a similar manner without the addition of aromatic solvent. A heating period of 58 min was used for the control experiments because the presence of aromatic solvent delayed the heating process by 2 min based on the results of direct temperature measurement with a fine thermocouple (0.25 mm in diameter, type K, Shinnetsu Co., Ltd., Ibaraki, Japan). Experiments with a shorter pyrolysis period (10 min in aromatic solvent and 8 min for control) at 280 °C were also conducted following a similar process. All experiments were repeated at least twice to confirm the reproducibility of the results, although the data have not been treated statistically.

2.2.3 Characterization of the pyrolysis residue

Unreacted cellulose was determined as anhydroglucose that was obtained by the acid hydrolysis of the pyrolysis residue. First, aq. H_2SO_4 (72 wt%, 0.1 mL) was added to the residue and then the mixture was heated at 30 °C for 60 min with frequent agitation by a glass rod. The resulting transparent liquid was diluted with water (2.8 mL) and then heated in an autoclave at 121 °C for an additional 60 min. The hydrolyzate (1.0 mL) was added to a vial and diluted with water (9.0 mL). After removing the sulfuric acid in the solution using an OnGuard II/A ion-exchange cartridge (Dionex, Sunnyvale, USA), the glucose yield in the solution was determined by ion chromatography (IC) on an ICS-3000 ion chromatograph (Dionex) under the following conditions: column, CarboPac PA1 (4

× 250 mm, Dionex); column temperature, 25 °C; eluent, 2 M NaOH (8%) in ion-exchanged water; flow rate, 1.0 mL min−1; carrier gas, N_2. The obtained glucose yield was converted to that corresponding to anhydroglucose by multiplying by 162/180.

Small portions of pyrolysis residue and the residue after acid hydrolysis were sampled using a micromanipulator (Micro Support Co., Ltd., Shizuoka, Japan). Their infrared (IR) spectra were recorded in transmission mode with a Nicolet Continuum FT-IR microscope attached to a Nicolet iS10 FT-IR spectrometer (Thermo Scientific, Madison, WI, USA).

The color of cellulose and its pyrolysis residue was measured with a ZE6000 color meter (Nippon Denshoku Industries Co., Ltd., Tokyo, Japan). CIELAB parameters [brightness (L^*), redness (a^*), and yellowness (b^*)] were determined in reflectance mode according to standard JIS Z-8722 using illuminant C and an observation angle of 2°. Total color difference (ΔE^*) was calculated from the following equation (Matsuoka et al., 2011b):

$$\Delta E^* = [(\Delta L^*)^2 + (\Delta a^*)^2 + (\Delta b^*)^2]^{\frac{1}{2}} \quad (1)$$

Molecular weight (MW) distribution was evaluated by gel-permeation chromatography (GPC) for phenyl carbamate derivatives of cellulose and its pyrolysis residues. Phenyl isocyanate (0.2 mL) was added to a suspension of each sample (5 mg) in pyridine (2 mL), and then the mixture was stirred at 80 °C. After reaction for 24 h, the mixture formed a transparent solution. Methanol (0.5 mL) was added to the reaction mixture to terminate the reaction, and then the solvent was removed by evaporation in vacuo. The resulting residue was dissolved in tetrahydrofuran (THF) and analyzed by GPC with a chromatograph (Shimadzu LC-10A, Kyoto, Japan) under the following conditions: column, Shodex LF-804 (Showa Denko KK, Tokyo, Japan); column temperature, 40 °C; eluent, THF; flow rate, 1.0 mL min−1; detection wavelength, 254 nm.

2.3 Results and Discussion

2.3.1 Cellulose reactivity in aromatic solvents

Figure 2-2 shows photographs of the residues after pyrolysis in various aromatic solvents under nitrogen at 280 °C for 60 min followed by extraction with DMSO-d_6. Photographs of the DMSO-d_6-soluble fractions are also included. The color of the residues, which remained dark brown even after pyrolysis in the aromatic solvents, tended to be slightly brighter than that of the control pyrolysis sample obtained without the addition of aromatic solvent.

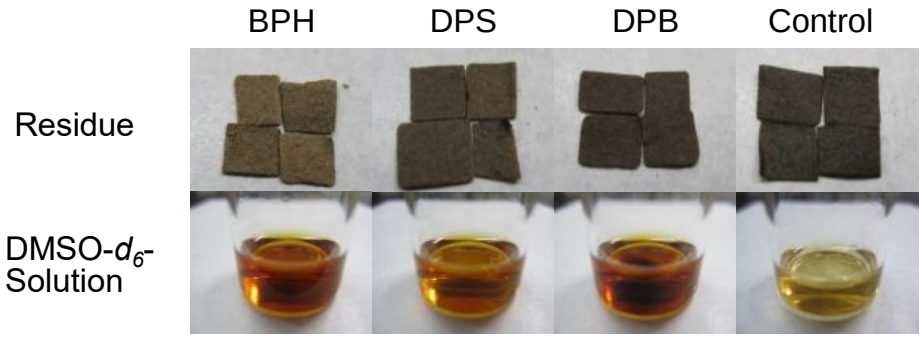

Figure 2-2. Photographs of residues after pyrolysis under N_2 at 280 °C and subsequent extraction with DMSO- d_6 along with the soluble fractions. Heating period: 60 min for BPH, DPS, and DPB; 58 min for the control.

Sample color can be discussed quantitatively using the CIELAB color parameters (L^*, a^*, b^*, and ΔE^*) listed in Table 1. The data measured for the residues obtained after pyrolysis for 10 min are also included for comparison. For the samples pyrolyzed for 60 min, ΔE^* was lower in the presence of aromatic solvent, with the order of control (60.6) > DPB (57.0) > DPS (56.1) > BPH (49.9). This order reflects the suppression efficiency of the color development of pyrolysis residues. The decrease of color development relied on the suppression of the decrease of L^* values. Alternatively, a shorter pyrolysis period of 10 min rather slightly enhanced color development (L^*, a^*, and ΔE^*) in aromatic solvents. Accordingly, pyrolysis in aromatic solvents may influence

color development, but the influence is not great. In contrast, the DMSO-d_6-soluble fractions obtained from the pyrolysis in aromatic solvents were darker than the control pyrolysis sample. This indicates that some chromophores formed from cellulose may be solubilized in aromatic solvents during pyrolysis.

Table 2-1. CIE color parameters (L^*, a^*, b^*, and ΔE^*) of cellulose and residues obtained after pyrolysis under N_2 at 280 °C and subsequent extraction with DMSO-d_6. Heating period: 10 or 60 min for BPH, DPS, and DPB; 58 min for the control.

280 ˚C/ 60min					
	Cellulose	BPH	DPS	DPB	Control
L^*	96.9	49.8	42.3	40.7	36.3
a^*	-0.5	6.8	5.9	1.7	1.2
b^*	3.4	18.3	14.8	12.4	4.5
ΔE	0.0	49.9	56.1	57.0	60.6
280 ˚C/ 10min					
	Cellulose	BPH	DPS	DPB	Control
L^*	96.9	71.5	71.0	73.1	74.4
a^*	-0.5	4.1	3.8	3.7	3.2
b^*	3.4	22.7	22.1	22.8	22.6
ΔE	0.0	32.2	32.2	30.9	29.8

Figure 2-3 summarizes the recoveries of cellulose and yields of hydrolysis residues (defined as “char” in this dissertation). Cellulose recovery was evaluated as anhydroglucose from the glucose yields obtained after hydrolysis. Unlike the influence on the color development, pyrolysis in the aromatic solvents strongly stabilized cellulose against thermal degradation, and the char yield dramatically decreased from 50.7 wt% (oven-dry basis for reacted cellulose, which is defined as the sum of char and pyrolysis products other than char in Figure 2-3) for the control pyrolysis sample to 14.5 wt% for DPB, 9.6 wt% for DPS, and 0.0 wt% for BPH. Interestingly, the char yield using BPH

was below the detection level even though color developed substantially (Figure 2-2). This indicates that the color development is not directly related to the char yield.

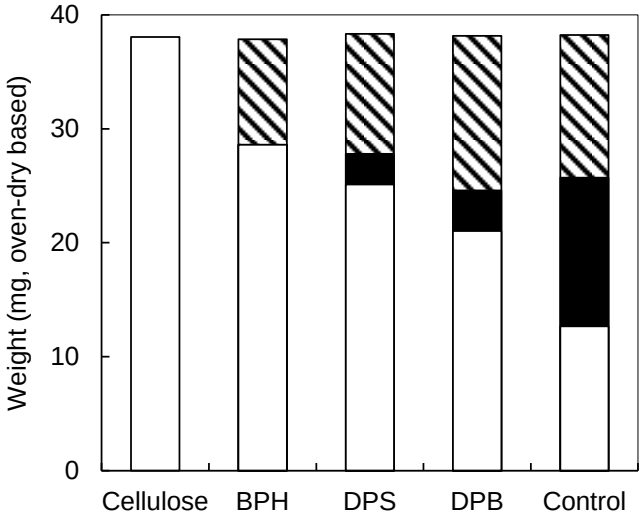

Figure 2-3. Recovery of unreacted cellulose and the yields of char and other pyrolysis products under N_2 at 280 °C. Heating period: 60 min for BPH, DPS, and DPB; 58 min for the control. □ : unreacted cellulose; ■ : char; ▨ : pyrolysis products other than char. Char is defined as residue obtained after hydrolysis of unreacted cellulose.

Char yields were well correlated with the appearance of two IR signals at 1620 and 1735 cm^{-1} (Figure 2-4), which were assigned to the stretching of C=C and C=O moieties, respectively. The appearance of these signals is associated with the dehydration reactions that occur during cellulose carbonization (Julien et al., 1991; Pastorova et al., 1994; Sekiguchi et al., 1983; Tang and Bacon, 1964a). The relative peak areas of these signals become smaller in the order of control > DPB, DPS > BPH, which is the same order as that of char yield, and the signals of the residue obtained using BPH were negligible. Accordingly, the peak areas of the 1620 and 1735 cm^{-1} signals directly relate to the extent of char formation, but not to color development. Large signals remain at 900–1300 cm^{-1} (C–O), 2800–3000 cm^{-1} (C–H), and 3000–3600 cm^{-1} (O–H) after

pyrolysis, which confirms that the pyranose structure of cellulose is preserved in the pyrolysis residues.

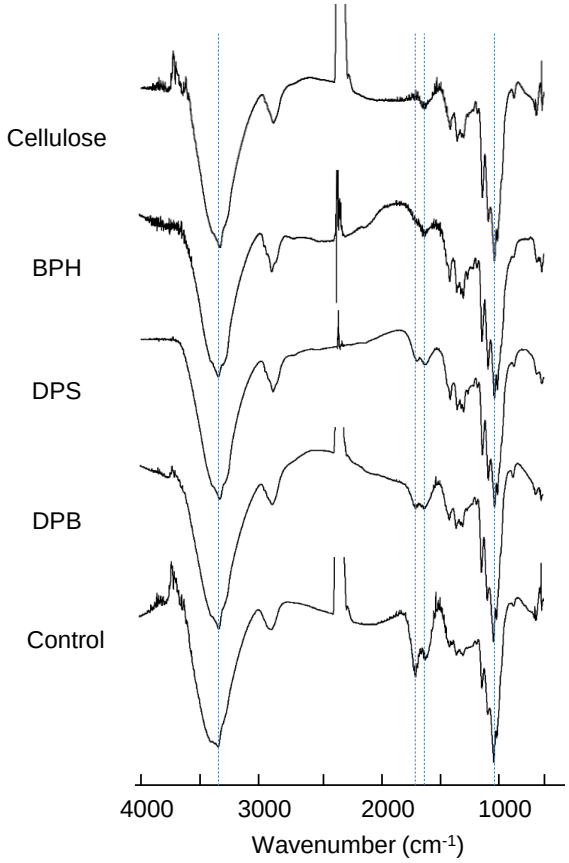

Figure 2-4. IR spectra of cellulose and residues after pyrolysis under N_2 at 280 °C and subsequent extraction with DMSO-d_6. Heating period: 60 min for BPH, DPS, and DPB; 58 min for the control.

It is well known that the DP of cellulose readily lowers to the leveling-off DP (approximately 200) during pyrolysis (Broido, Javier-Son, Ouano, and Barrall, 1973; Halpern and Patai, 1969; F Shafizadeh and Bradbury, 1979). The GPC analysis data (Figure 2-5, as phenyl carbamate derivatives) for cellulose and residues obtained for a shorter pyrolysis period of 10 min at 280 °C revealed that the decrease of DP to the leveling-off value occurred even during pyrolysis in aromatic solvents. Thus, pyrolysis in aromatic solvents could not suppress the initial DP decrease.

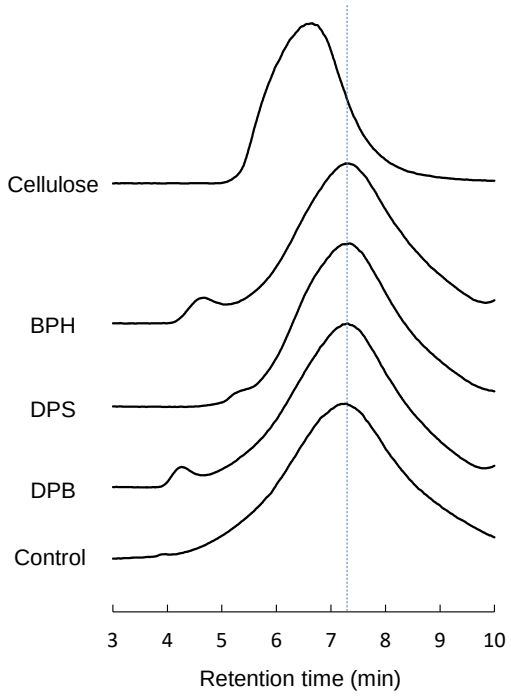

Figure 2-5. GPC analysis data for cellulose and residues after pyrolysis under N_2 at 280 °C and subsequent extraction with DMSO-d_6 (as phenyl carbamate derivatives). Heating period: 10 min for BPH, DPS, and DPB; 8 min for the control.

2.3.2 Char chemical structure and morphology

Figure 2-6 displays microscopy images of the char attached to filter paper and suspended in water; corresponding IR spectra are illustrated in Figure 2-7. All the IR spectra are similar in shape and contain two signals at 1620 and 1735 cm^{-1} characteristic of the char fraction. Sharp signals at 900–1300 cm^{-1} (C–O) that are observed for the pyrolysis residues (Figure 2-4) disappear after the removal of unreacted cellulose through hydrolysis, whereas strong O–H signals at 3000–3600 cm^{-1} remain in the char (Figure 2-7). This indicates that the char fractions obtained here still contain a large number of hydroxyl groups. Although further studies are necessary to unravel the details of the char chemical structure, our results indicate that carbonization does not proceed extensively under the present pyrolysis conditions, while dehydration may occur to some extent, which alters the cellulose to form non-hydrolyzable materials.

The very similar IR spectra (Figure 2-7) indicate that these char fractions have similar chemical structures, although their yields varied substantially depending on the pyrolysis conditions. These results indicate that carbonization reactions are inhibited locally by the influence of aromatic solvent but occur like that in the control sample for the cellulose molecules that cannot be accessed by aromatic solvent. Thus, the accessibility of aromatic solvent molecules to cellulose crystallites may result in the variation of char yield.

The morphologies of the char fractions were quite different depending on the pyrolysis conditions (Figure 2-6). Char fractions of the control and DPB samples retained the fiber shape of cellulose, whereas pyrolysis in BPH and DPS gave char as a thin film. In particular, the width of the film-like char obtained in DPS was much greater than that of the fiber-shaped char obtained under the control and DPB pyrolysis conditions. These observations, which imply that the scrolls unroll to form char sheets in the pyrolysis residue, are discussed below in terms of the superstructure of the cell wall of cellulose.

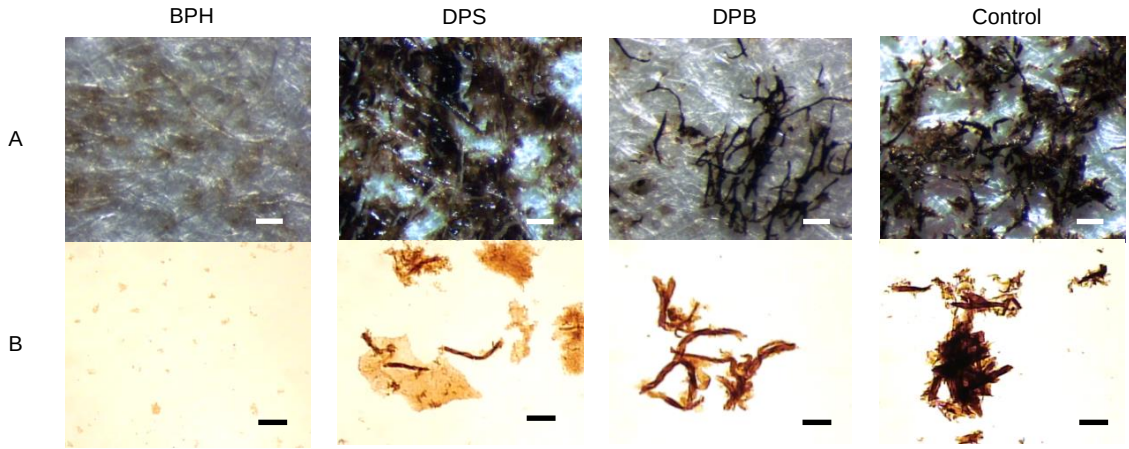

Figure 2-6. Microscopy images of char (A) attached to filter paper and (B) suspended in water obtained after pyrolysis under N_2 at 280 °C and subsequent extraction with DMSO-d_6. Heating period: 60 min for BPH, DPS, and DPB; 58 min for the control.

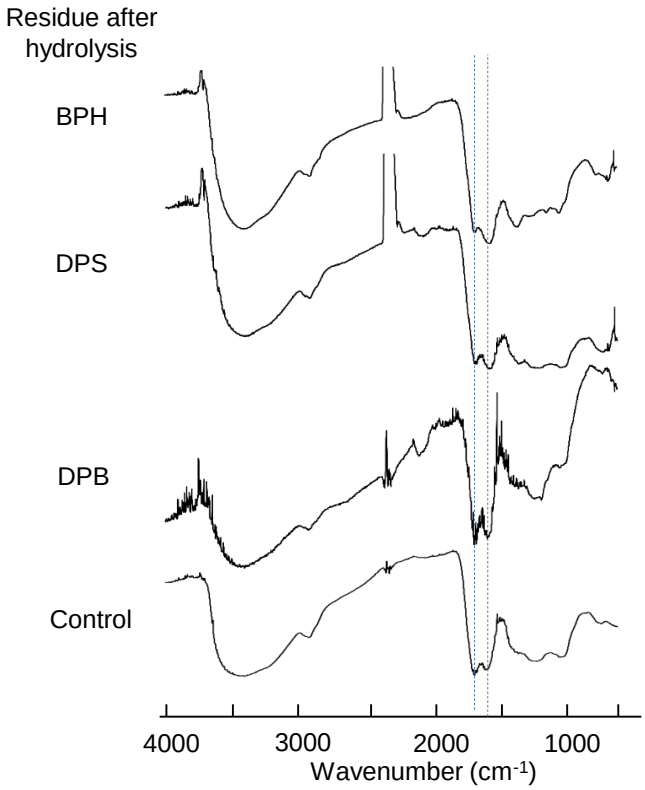

Figure 2-7. IR spectra of char obtained after pyrolysis under N_2 at 280 °C and subsequent extraction with DMSO-d_6. Heating period: 60 min for BPH, DPS, and DPB; 58 min for the control.

2.3.3 Influence of aromatic solvents on the selectivity for low-molecular-mass products

The ^{1}H NMR spectra of the DMSO-d_6-soluble fractions contained large signals derived from aromatic solvents with chemical shifts ranging from 6.0 to 8.0 ppm (Figure 2-8). These solvent signals made it difficult to identify the product signals, particularly furans and oxime derivatives of aldehydes and ketones. To overcome this problem, we tried to separate the aromatic compounds by solvent extraction, and found that extraction with a binary mixture of $CDCl_3$ and D_2O effectively separated the aromatic compounds from the pyrolysis mixtures. As illustrated in Figure 2-8 B-2, only the aromatic

compounds were extracted into the $CDCl_3$ layer, whereas the pyrolysis products including oxime derivatives were contained in the D_2O layer.

However, the extraction with $CDCl_3/D_2O$ could not recover the products completely from the pyrolysis residue; some of the products, particularly LG, were further solubilized by additional extraction with DMSO-d_6 (Figure 2-8C). For example, 51.2% and 13.5% (C-based, for reacted cellulose, BPH) of LG were recovered from the first $CDCl_3/D_2O$ extraction and subsequent DMSO-d_6 extraction, respectively. These results provide an important insight into the pyrolysis of cellulose in aromatic solvents; during pyrolysis, the products including LG could not be removed very efficiently from inside the cell wall, where the products exist in higher concentration than in solution outside

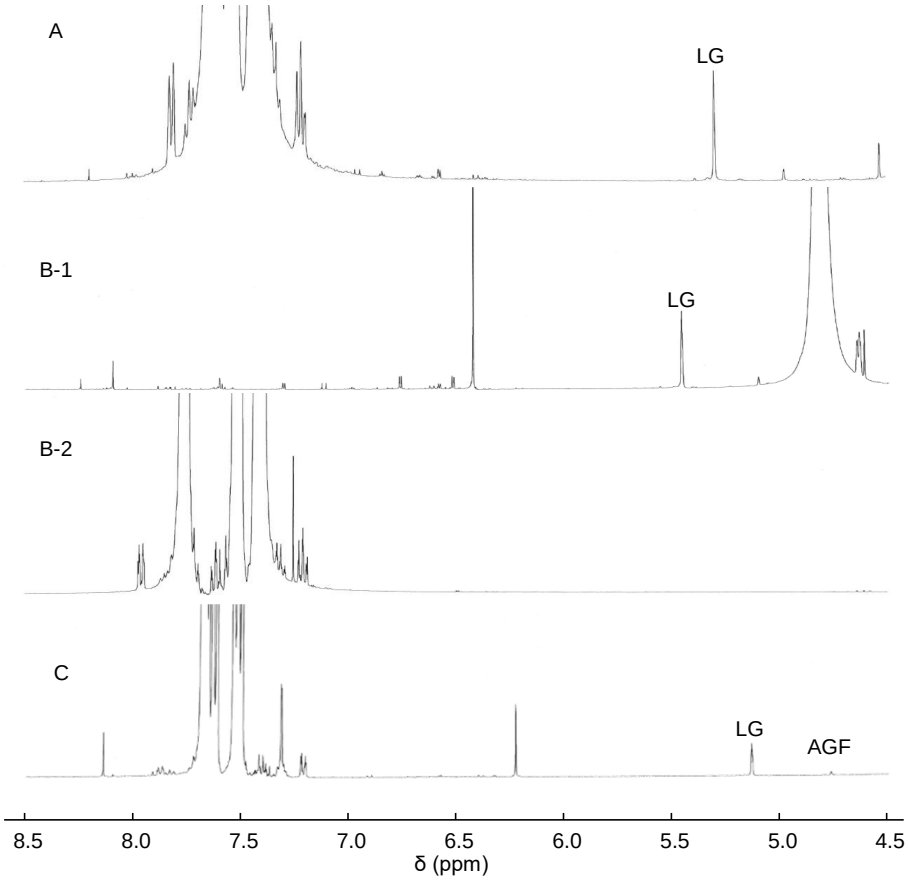

Figure 2-8. ^{1}H-NMR spectra of products from cellulose after pyrolysis in BPH at 280 °C soluble in DMSO-d_6 (A), D_2O (B-1), $CDCl_3$ (B-2) and DMSO-d_6 (C).

cellulose. $CDCl_3$ and D_2O could not access inside the cell wall where the pyrolysis products and aromatic solvent were located. In contrast, DMSO-d_6 could penetrate into the cell wall volume more efficiently, because DMSO-d_6 dissolves pyrolysis products with aromatic solvents and is more polar than $CDCl_3$. For these reasons, identification and determination of the yields of pyrolysis products were conducted using the first D_2O-soluble and second DMSO-d_6-soluble fractions by ^1H NMR spectroscopy.

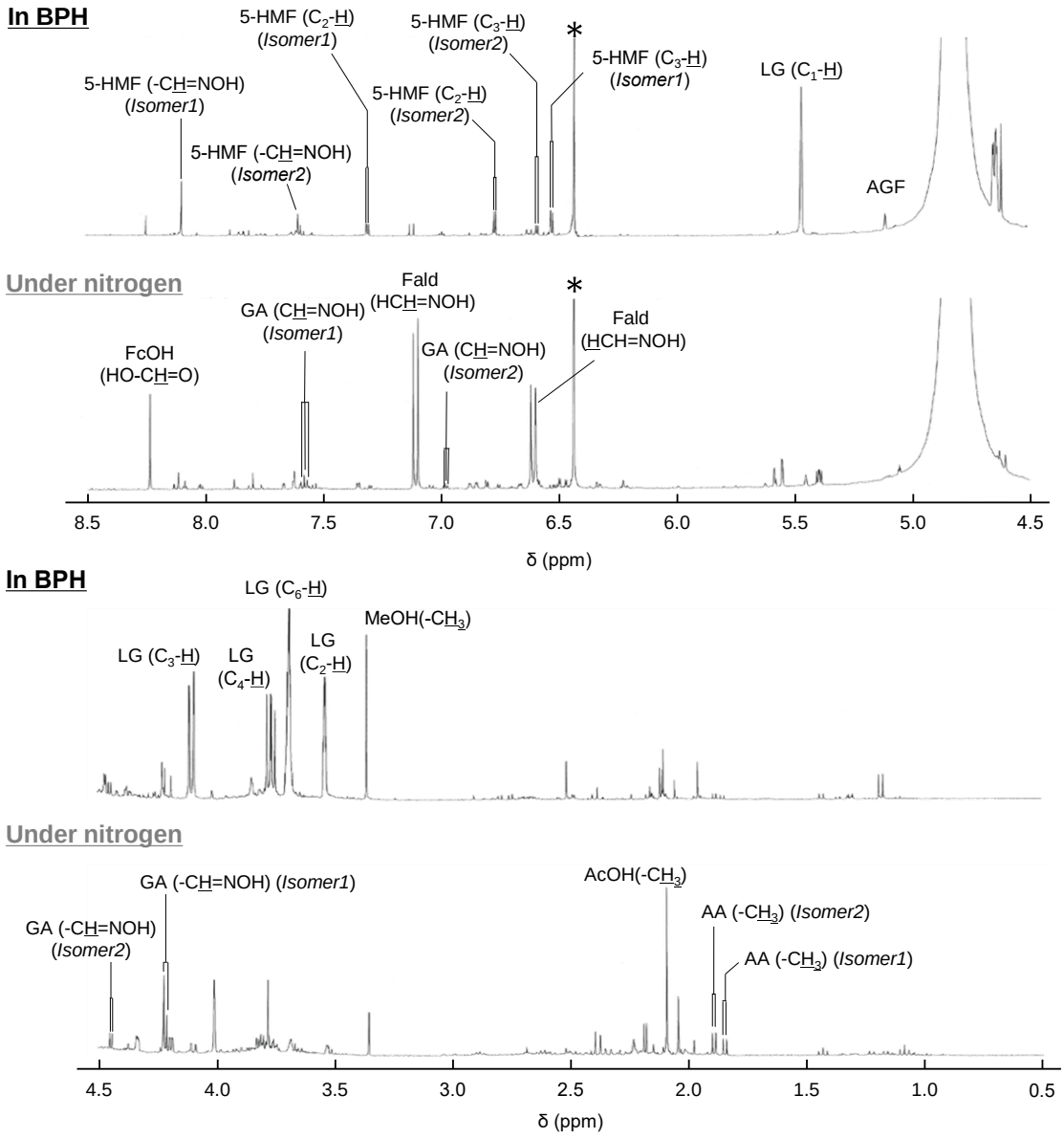

Figure 2-9. ^1H-NMR spectra of D_2O-soluble fractions obtained after pyrolysis in BPH and under N_2 at 280 °C.

The compositions of the products obtained from the control pyrolysis andpyrolysis in aromatic solvent varied considerably. Examples of ^{1}H NMR spectra of D_2O-soluble fractions obtained from cellulose under the control conditions and in BPH are shown in Figure 2-9, in which peaks of the internal standard (maleic acid) were normalized to enable quantitative comparison. In the spectrum of the control sample, formaldehyde, acetaldehyde, formic acid, and acetic acid were observed with relatively large signals, while the signals assigned to LG and 5-HMF were quite small. The LG and 5-HMF signals were more intense in the spectrum of the sample obtained using BPH.

Figure 2-10 summarizes the yields (%, C-based, for reacted cellulose) of LG, 5-HMF, AGF, and formaldehyde as the major products of cellulose pyrolysis, along with the total yields of the identified products. The individual yields including those of other products are listed in Table 2-2. Although the yield of LG from the control pyrolysis experiment was only 8.5%, it increased to 31.9% using DPB, 55.2% using DPS, and 64.7% in BPH, which is the opposite trend to that of the char yield described above (Figure 2-3). These results confirm that the secondary pyrolysis reactions of LG were effectively suppressed during pyrolysis of cellulose in these aromatic solvents. Because of this stabilization, the total yield of the identified products from reacted cellulose reached 76.0% for BPH, 64.6% for DPS, and 38.9% for DPB.

Formation of 5-HMF in greater yields in aromatic solvents than under nitrogen (control) was an unexpected result; 5-HMF yield increased in the order of 0.0% (control) < 3.0% (DPB) < 3.3% (DPS) < 6.4% (BPH) (Table 2-2), which is again the opposite order to that observed for the char yield. Accordingly, model pyrolysis experiments of 5-HMF (10 mg) were conducted under nitrogen and in BPH (200 mg) (280 °C/10 min). As shown in Figure 2-11, 5-HMF with an expected bp of 291.5 ± 30 °C (Scifinder, 2014) formed solid carbonized products under nitrogen prior to evaporation from the bottom of the reactor. Nevertheless, fairly pure 5-HMF was recovered by extraction with D_2O. These results indicate that 5-HMF was effectively converted into D_2O-insoluble carbonized materials in the liquid (molten) phase under nitrogen, whereas the gaseous 5-HMF was stable against thermal degradation. Fukutome et al. (Fukutome et al., 2014) obtained

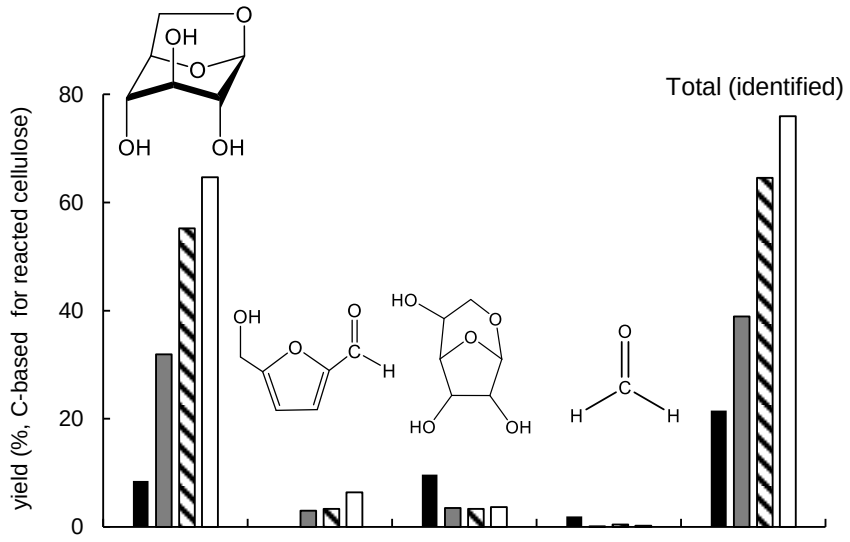

Figure 2-10. Yields (%, C-based for reacted cellulose) of LG, 5- HMF, AGF, and formaldehyde from cellulose pyrolysis under N_2 at 280 °C. Heating period: 60 min for BPH, DPS, and DPB; 58 min for the control. : BPH, : DPS, : DPB, : control.

Table 2-2. Yields of pyrolysis products from cellulose under N_2 at 280 °C. Heating period: 60 min for BPH, DPS, and DPB; 58 min for the control. LG: levoglucosan, 5-HMF: 5-hydroxymethylfurfural, AGF: 1,6-anhydro-β-d-glucofuranose, FA: formaldehyde, AA: acetaldehyde, FcOH: formic acid, AcOH: acetic acid, GA: glycolaldehyde.

	LG	5-HMF	AGF	FA	AA	FcOH	AcOH	GA	total
BPH	5.99	0.46	0.34	0.022	0.019	0.030	0.018	0.043	6.92
	(64.7)	(6.4)	(3.7)	(0.21)	(0.25)	(0.19)	(0.17)	(0.42)	(76.0)
DPS	5.82	0.27	0.35	0.049	0.018	0.020	0.035	0.197	6.76
	(55.2)	(3.3)	(3.3)	(0.42)	(0.22)	(0.11)	(0.30)	(1.69)	(64.6)
DPB	4.32	0.31	0.48	0.015	0.016	0.012	0.021	0.012	5.19
	(31.9)	(3.0)	(3.5)	(0.10)	(0.15)	(0.05)	(0.14)	(0.08)	(38.9)
Control	1.07	0.0	1.22	0.267	0.033	0.107	0.041	0.044	2.78
	(8.5)	(0.0)	(9.7)	(1.92)	(0.32)	(0.50)	(0.29)	(0.31)	(21.5)

mg (%, C-based for rreacted cellulose)

similar results using a closed ampoule reactor at higher pyrolysis temperatures. Almost no recovery of 5-HMF (0.0%) from cellulose under the control pyrolysis conditions also suggests that mass transfer would be obstructed inside the cell wall because of its lamellar structure; that is, 5-HMF may be completely converted prior to removal from the cell wall in the control experiment.

Formation of solid carbonized materials from 5-HMF was effectively prevented in BPH (Figure 2-11). This stabilization can explain the formation of 5-HMF in greater yields during pyrolysis of cellulose in aromatic solvents than under nitrogen. Although the stabilization mechanism is unknown at present, dispersion in aromatic solvent inhibits the contact of 5-HMF molecules, which is required for char formation, because carbonization from 5-HMF occurred only in the molten phase.

Carbonization mechanisms via 5-HMF and furfural have been proposed for pyrolysis of cellulose (Pastorova et al., 1994) and starch (Zhang et al., 2002) and hydrothermal carbonization of carbohydrates (Baccile et al., 2009; Falco et al., 2011; Titirici et al., 2008). In this mechanism, these furanic compounds polymerize first to form polyfurans that subsequently rearrange into polybenzenes (solid carbonized materials). Considering this information, we hypothesize that 5-HMF is an important reactive precursor for the formation of solid carbonized materials from cellulose under control pyrolysis conditions (Figure 2-12). The inverse correlation of 5-HMF yield with char yield from cellulose pyrolysis in aromatic solvents and under nitrogen also supports this hypothesis.

Although obvious signals were identified in the ^{1}H NMR spectrum (Figure 2-9), the yield of formaldehyde under the control pyrolysis conditions was only 1.92% (C-based for reacted cellulose), and decreased to the range of 0.10%–0.42% in aromatic solvents (Table 2-2). Because formaldehyde (bp −19 °C) is a gaseous compound under normal conditions, its presence is expected to originate from chemical bonding with other materials such as unreacted cellulose and pyrolysis products; unbound formaldehyde must evaporate from the mixture after pyrolysis prior to extraction.

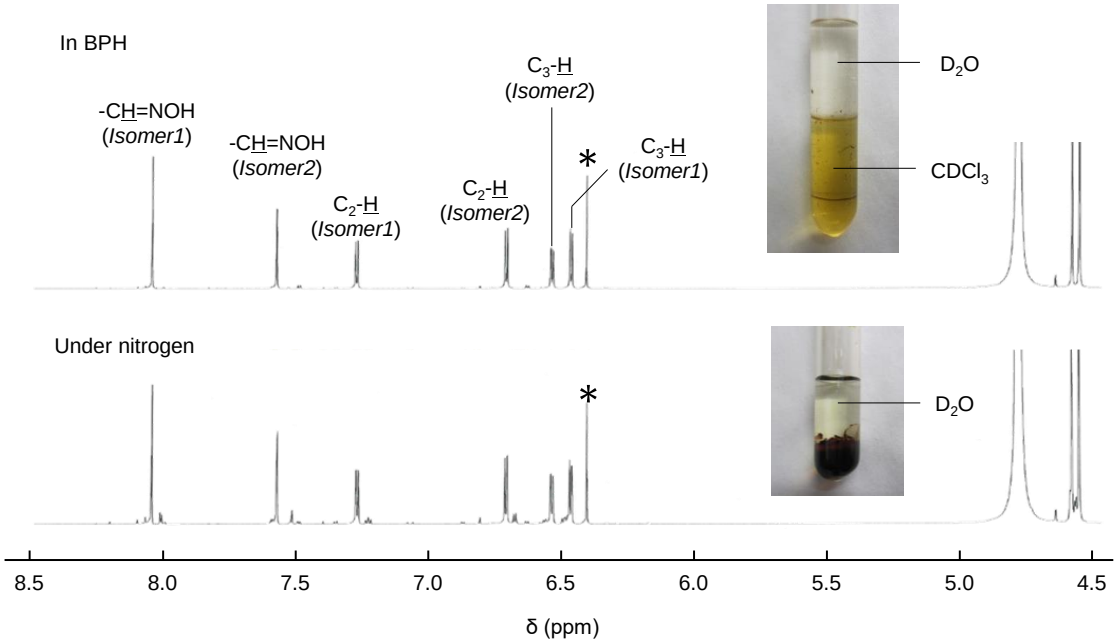

Figure 2-11. ^{1}H NMR spectra of D_2O-soluble portions obtained after pyrolysis of 5-HMF under N_2 at 280 °C, along with photographs of the pyrolysis mixtures extracted with D_2O (control) and $D_2O/CDCl_3$ (in BPH). Heating period: 10 min for BPH; 8 min for the control. The signal assigned to maleic acid (internal standard) is indicated by an asterisk.

2.3.4 Cellulose pyrolysis mechanisms in aromatic solvent

Cellulose has a heterogeneous cell wall structure consisting of microfibrils that contain cellulose I crystallites (Elazzouzi-Hafraoui et al., 2008; Nishiyama, 2009; Nishiyama et al., 2003). Because the leveling-off DP of a cellulose sample corresponds to the length of its cellulose crystallites, the DP decrease observed as the first event in cellulose pyrolysis is considered to occur at the crystallite interface (Broido et al., 1973; Elazzouzi-Hafraoui et al., 2008; Halpern and Patai, 1969; Nelson and Tripp, 1953; Nishiyama, 2009; Nishiyama et al., 2003; Rowland and Roberts, 1972; F Shafizadeh and Bradbury, 1979). The resulting cellulose crystallites are subsequently thermally degraded from the surface, so the internal molecules are believed to be stable (Kawamoto and Saka, 2006; Kim et al., 2001; Zickler et al., 2007). Reducing ends are reported to form during this decrease of DP (Matsuoka et al., 2014), which exhibit much greater pyrolytic

reactivity than that of other repeating glucose units (Matsuoka et al., 2011a, 2011b, 2014). Thermal decomposition of the reducing ends inside the cell wall has been discussed in terms of the activation mechanism of cellulose; i.e., “active cellulose” formation (Matsuoka et al., 2014), although there have been still controversial for the nature of active cellulose (O. Boutin et al., 1998; Olivier Boutin et al., 2002).

A cross-sectional image of the part of a cell wall is illustrated in Figure 2-12. Numerous cellulose crystallites with a width of 6 nm are arranged in the cell wall (Elazzouzi-Hafraoui et al., 2008), which has a width of several micrometers (Figure 1-4). Because of the heterogeneous cell wall structure, mass transfer of the pyrolysis products formed between crystallites is expected to be strongly hindered in the cell wall, which

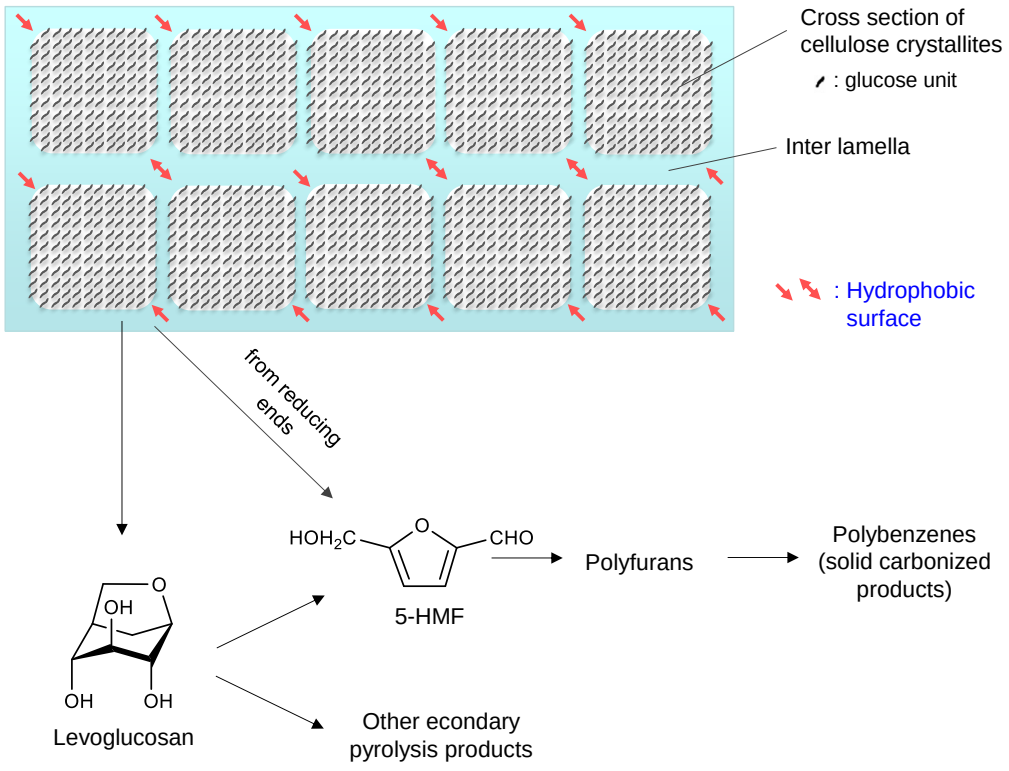

Figure 2-12. Cross-section image of the part of the cell wall of cellulose, comprising cellulose crystallites and lamellar ultrastructure, along with the proposed roles of 5-HMF and LG in cellulose carbonization.

would allow extensive secondary pyrolysis reactions to occur prior to removal from the cell wall through evaporation. When pyrolysis is carried out in aromatic solvent, the solvent can penetrate into the space between crystallites to stabilize cellulose and its degradation products against thermal degradation. Thus, the stabilization efficiency depended on the chemical structure of the aromatic solvent because of their different accessibilities to the cellulose crystallite surface.

Most of the crystallite surface is covered by the hydroxyl groups of glucose units in cellulose, which makes the crystallite surface hydrophilic (Figure 1-3) (Elazzouzi-Hafraoui et al., 2008). Shoji et al. (2017) discussed the effectiveness of the inhibition of char formation from cellulose under fast pyrolysis conditions in terms of this hydrophilic character and the polarity of the aromatic solvent. Aromatic solvents bearing polar substituents can access the hydrophilic surface more effectively than solvents with less polar ones. Consequently, the greater stabilization effect of BPH for cellulose pyrolysis than that of the other solvents in the present study can be explained by its polar >C=O substituent, which facilitates its access to cellulose crystallites. Bulky DPB would be less effective than BPH and DPS at reaching the cellulose crystallites, which leads to its smaller influence on cellulose pyrolysis.

The molecular mechanisms of cellulose stabilization have not been fully clarified, but complexation of aromatic solvents to molecules on the crystallite surface (Figure 2-13A) is proposed based on the literature information. Thermal depolymerization of cellulose is considered to occur through heterolytic cleavage of the glycosidic C1–O bonds (Kawamoto, 2016; Matsuoka et al., 2014). The intramolecular C3–OH···O5 hydrogen bonding inhibits electron donation from the O5 lone pair to C1, which stabilizes cellulose against depolymerization (Kawamoto, 2016; Matsuoka et al., 2016). Complexation of aromatic solvent molecules to the hydrophobic crystallite surface would inhibit the conformational mobility required to rupture these hydrogen bonds. In addition, hydrogen bond-mediated proton donation to C1–O by other molecules that catalyze the rupture of glycosidic bonds would also be blocked by this complexation. The CH/π interactions between hydrophobic faces of pyranose rings in carbohydrates and aromatic

substances are well documented (Asensio et al., 2013; Hudson et al., 2015; María et al., 2005; Nishiyama, 2009). Although the contribution of the hydrophobic surface is quite small for the proposed cross section of the cellulose crystallites (Figure 2-12) (Elazzouzi-Hafraoui et al., 2008), cleavage of the glycosidic bonds is expected to occur from this surface. In the enzymatic depolymerization of cellulose by cellulase, cellulase complexation on this hydrophobic surface has been clearly demonstrated to occur prior to cellulose depolymerization (Ding et al., 2012; Liu et al., 2011).

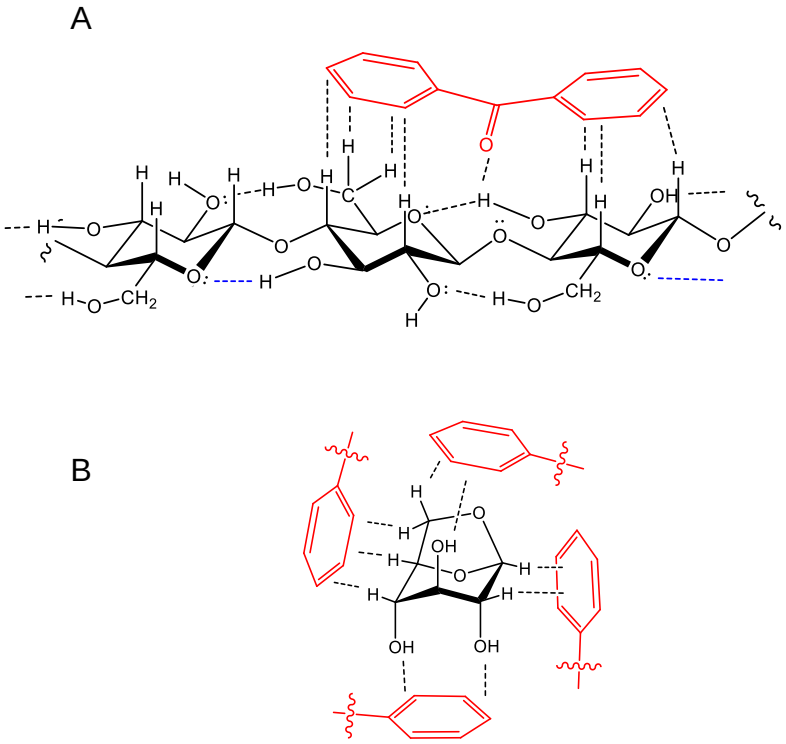

Figure 2-13. A proposed mechanism for stabilization of cellulose against thermal degradation by complexation of aromatic solvent molecules with cellulose crystallite surface molecules (A), along with the previously proposed mechanism for stabilization of LG (B).

The increased yield of LG in aromatic solvents compared with that under nitrogen can be reasonably explained by the solvation of LG with aromatic solvent molecules through CH/π and OH/π interactions, as reported in our previous papers

(Figure 11B) (Hosoya et al., 2006; Kawamoto et al., 2014). This solvation inhibits the proton donation to LG molecules through intermolecular hydrogen bonding, which can act as acid and base catalysts for LG thermal degradation.

Aromatic solvent would also affect the pyrolytic reactions of cellulose reducing ends and related secondary reactions. A number of papers (Gardiner, 1966; Katō, 1967; Mettler et al., 2012; Patwardhan et al., 2009; Sanders et al., 2003) have reported evidence for the selective formation of 5-HMF, furfural, and AGF, all of which have five-membered rings, from the reducing ends of oligo- and polysaccharides. This is reasonable because the transformation from pyranose to furanose and furan rings is facilitated by the chain structures of the reducing ends. Accordingly, from the present experimental results, we tentatively propose that 5-HMF formed from cellulose reducing ends leads to char formation (Figure 2-12), and this is inhibited in aromatic solvent through stabilizing the 5-HMF by solvation. Further systematic studies are necessary to confirm this hypothesis.

Finally, the char morphology observed during pyrolysis in DPS and BPH is discussed in terms of the hierarchical structure of the cellulose cell wall. The cross section of wood cell walls is proposed to have a lamellar structure (Fahlén and Salmén, 2002; Fratzl, 2003; Lichtenegger et al., 1999; Rafsanjani et al., 2014; Ruel et al., 1978). Fahlén and Salmén (2002) observed a concentric lamellar structure for the S2 layer of spruce (*Picea abies*) tracheids by atomic force microscopy and scanning electron microscopy. Lichtenegger et al. (1999) obtained a complete image with a helical arrangement of cellulose fibrils in the S2 layer of spruce tracheids with position-resolved synchrotron X-ray microdiffractometry. These lamellar structures have also been discussed from the viewpoint of cellulose biosynthesis, in which a complex of cellulose synthases (terminal complex) located in the cell membrane synthesizes a bundle of cellulose molecules, corresponding to the crystallite size, and then microfibrils are deposited in layers in the cell wall (Emons and Mulder, 2000).

The very large film-like char obtained from cellulose pyrolysis in DPS after hydrolysis of unreacted cellulose (Figure 2-6) can be reasonably explained by assuming the scrolling of char films contained in pyrolyzed cotton cells. If lamellar structures exist

in the cotton cell wall, DPS can penetrate into the space between each layer, where the primary pyrolysis and secondary reactions including char formation would be prevented (Figure 2-12). However, more closely packed crystallites inside the layer would be difficult for DPS to access, resulting in the formation of large scrolled char films (Figure 2-14). The smaller films obtained in BPH, which has greater accessibility to cellulose crystallite than DPS, can be explained by the penetration of BPH inside the layers of the scrolls. Further extensive studies on both pyrolysis and cellulose ultrastructure are necessary to confirm the above hypothesis, because this is the first time that a very large char film has been obtained from cellulose pyrolysis.

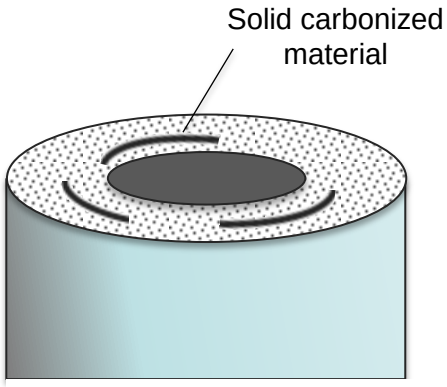

Figure 2-14. A proposed image of the formation of scrolls of char film in the cell wall of cellulose during pyrolysis in DPS.

2.4 Conclusions

Careful investigation of the products obtained from pyrolysis of cellulose (Whatman No. 42 filter paper) in aromatic solvents at 280 °C revealed the following conclusions:

(1) The pyrolytic reactivity of cellulose was decreased in aromatic solvent compared with that under nitrogen (control), and the efficiency displayed the order of BPH > DPS > DPB > control.

(2) The char yield obtained after hydrolysis of unreacted cellulose decreased with the opposite trend to that of cellulose reactivity (control > DPB > DPS > BPH). In particular, the char yield in BPH bearing a polar >C=O group was lower than the detectable level.

(3) Yields of LG and 5-HMF dramatically increased in the aromatic solvents compared with those under nitrogen.

(4) Complexation of aromatic solvent molecules with surface cellulose molecules of the crystallites explains their stabilization against thermal degradation.

(5) Solid char formation from 5-HMF was inhibited in the aromatic solvents, although the molten 5-HMF readily formed char.

(6) A large char film was formed from pyrolysis of cellulose in DPS, which suggested the formation of a scrolled char film in the pyrolyzed cellulose. Based on these results, a carbonization mechanism via 5-HMF in the lamellar cell wall ultrastructure was proposed.

(7) This study provides insight into the molecular-based cellulose pyrolysis mechanisms and efficient and selective thermochemical production of bio-based materials and chemicals.

Chapter 3

Carbonization of cellulose cell wall evaluated with ultraviolet microscopy

3.1 Introduction

Cellulose is the major component of the cell walls of plants. Thermochemical conversion technologies such as pyrolysis are promising ways to convert cellulose into renewable fuels, chemicals, and materials. Carbonization is a pyrolysis process that provides charcoal efficiently. Promoting carbonization produces more solid products as charcoal, while suppressing the reactions those produce more liquid or gaseous products such as bio-oil or biogas. Understanding the mechanism of carbonization allows for better control of pyrolysis reactions for practical application.

The carbonization mechanism of cellulose has been studied using various methods including infrared (IR) spectroscopy (Julien et al., 1991; Pastorova et al., 1994; Sekiguchi et al., 1983; Tang and Bacon, 1964a), elemental analysis (Tang and Bacon, 1964a), solid ^{13}C-NMR (Pastorova et al., 1994; Sekiguchi et al., 1983; Sekiguchi and Shafizadeh, 1984; Soares et al., 2001) and pyrolysis-gas chromatography-mass spectrometry (Py-GC/MS) (Pastorova et al., 1994). In IR analysis, characteristic signals appear at 1600 and 1700 cm^{-1} as the cellulose carbonization proceeds. These signals are assigned to conjugated unsaturated C=C bonds such as benzene rings and carbonyl groups (C=O), respectively, and are associated with dehydration reactions.(Julien et al., 1991; Pastorova et al., 1994; Sekiguchi et al., 1983; Tang and Bacon, 1964a)

Dehydration is the main reaction in cellulose carbonization, especially at relatively low pyrolysis temperatures (< 280 °C) (Degroot et al., 1988; Kashiwagi and

Nambu, 1992; Scheirs et al., 2001; Tang and Bacon, 1964b). Based on the van Krevelen diagram, which plots the H/C ratio versus O/C ratio of cellulose char, Tang and Bacon (1964b) determined that dehydration is the main reaction in the pyrolysis of cellulose at 200–280 °C. Scheirs et al. (2001) showed that dehydration of Whatman cellulose occurred from 220 °C to 350 °C, and that the total amount of water remaining was 14.3% (w/w) (Scheirs et al., 2001).

The solid carbonized product, the final product of dehydration, has been reported to contain benzene rings (Pastorova et al., 1994; Sekiguchi et al., 1983; Sekiguchi and Shafizadeh, 1984; Fred Shafizadeh and Sekiguchi, 1983; Smith and Howard, 1937; Soares et al., 2001). Smith and Howard (1937) reported that benzenecarboxylic acids were obtained from cellulose char by alkaline permanganate oxidation and that the benzene ring structures were formed at temperatures above 200 °C by slow pyrolysis. Under fast pyrolysis conditions, Shafizadeh and Sekiguchi (1983) reported that benzene ring structures developed at 350–400 °C to form stable char based on the results of permanganate oxidation and solid ^{13}C-NMR analysis.

Pastorova et al. analyzed cellulose chars prepared at different pyrolysis temperatures using Py-GC/MS (Pastorova et al., 1994). Based on the fragment structure, they reported that as carbonization progressed, the chemical structure of char changed from carbohydrate → furan → benzene. Furanoic compounds such as furfural and 5-HMF have subsequently been proposed as important intermediates in the hydrothermal carbonization of reducing sugars (Baccile et al., 2009; Falco et al., 2011; Titirici et al., 2008). In our previous paper, a negative relationship was observed between the yield of 5-HMF and solid carbonized product (cellulose char hydrolysis residue) in the pyrolysis of cellulose in nitrogen and various aromatic solvents, which can stabilize thermal degradation products (intermediates) by forming OH–π hydrogen bonds and breaking intermolecular hydrogen bonding (Nomura et al., 2017). These results indicate that 5-HMF is an important intermediate in cellulose carbonization under pyrolysis conditions.

These carbonization reactions proceed in cell walls composed of innumerable cellulose crystallites. For example, a single cotton fiber cell with a cross-sectional width

of approximately 10–20 μm (Thibodeaux and Evans, 1986; Xu et al., 1993; Xu and Huang, 2004) contains a very large number of cellulose crystallites (cross-section: 6 nm × 6 nm) (Elazzouzi-Hafraoui et al., 2008). Cellulose is consequently a heterogeneous material on the nanoscale. It has been reported that in pyrolysis, the molecules inside the crystallites are stable and the pyrolysis proceeds from the surface of crystallites (Kawamoto and Saka, 2006; Kim et al., 2001; Zickler et al., 2007). However, there is no information available on whether carbonization in the cellulose cell wall (several μm in width of cross-section) proceeds uniformly or non-uniformly.

For this purpose, there is a way to use a UV microscope with a resolution of several hundred nm. Cellulose char is frequently analyzed using optical microscopy (Haas et al., 2009) and scanning electron microscopy (SEM) (Gani and Naruse, 2007; Sørensen et al., 2000), but the resolution of the optical microscope is not sufficient to observe the inside of the cell wall due to the intrinsic low resolution. Although the resolution of SEM is high, only the shape of the char is observed, and no inference can be made about how the carbonization progresses. The analysis method with UV is not the best way to analyze the chemical structure of char because of the poor resolution and less information from the UV absorptivity. By using UV microscopy, however, we can investigate the homogeneity of cellulose cell wall pyrolysis, which was validated in this article.

Using the UV microscope with the resolution of several hundred nm, the distribution of lignin within the walls of wood cells has been clearly evaluated (Fergus et al., 1969; Fukazawa and Imagawa, 1981; Musha and Goring, 1975; Saka et al., 1982). In this work, we used UV microscopy to study pyrolyzed cotton cellulose fibers. Cotton cellulose is essentially free of UV-absorbing functional groups, whereas the carbonized products with benzene and furan structures absorb UV rays. The distributions of these products can therefore be observed in cross-sections of cell walls using UV microscopy. The mechanism by which aromatic solvents suppress carbonization is also discussed by using three aromatic solvents reported in our previous study (Nomura et al., 2017) (*Chapter 2*), focusing on the action inside the cell wall.

3.2 Materials and Methods

3.2.1 Materials

Whatman No. 42 filter paper (Whatman PLC, UK, cotton) was used as a cellulose sample. DPS, DPB and BPH were purchased from Tokyo Chemical Industry Co., Ltd. (Tokyo, Japan), Wako Pure Chemical Industries, Ltd. (Osaka, Japan), and Nacalai Tesque, Inc. (Kyoto, Japan), respectively, and used without purification. DPS is a thioether derivative. BPH has a carbonyl substituent that increases its reactivity with the hydrophilic surface of cellulose crystallites. Although DPB and BPH are solids at room temperature, they melted during the heating process. These solvents were stable under the pyrolysis conditions used in this study.

The UV spectra of furans and benzenes were measured using a UV-1800 spectrophotometer (Shimadzu Co., Japan). Furan (Nacalai Tesque Inc, Kyoto, Japan), 5-HMF (Tokyo Chemical Industry Co.), and dibenzofuran (Tokyo Chemical Industry Co.) were used as model furans. Benzene (Nacalai Tesque Inc), naphthalene (Nacalai Tesque Inc), and anthracene (Nacalai Tesque Inc) were used as model aromatic compounds.

3.2.2 Pyrolysis

Cellulose (38 mg dry basis) was placed in a Pyrex glass tube reactor (internal diameter 8.0 mm, wall thickness 1.0 mm, length 300 mm) that was connected to a nitrogen bag through a three-way tap. After the air inside the reactor was replaced with nitrogen (99.99%) using an aspirator, the reactor was inserted into a muffle furnace preheated to 280 °C. After heating for 58 min, the reactor was removed from the furnace and immediately cooled by a flow of air. The residue was first washed with chloroform (5 mL, five times) and subsequently with methanol (5 mL, five times), and then dried in an oven at 105 °C for 24 h.

Pyrolysis experiments in aromatic solvents were conducted in a similar manner. Cellulose was heated with aromatic solvent (400 mg) for 60 min because the presence of the aromatic solvent necessitated an additional 2 minutes of heating. This was determined from direct temperature measurements made with a fine thermocouple (0.25 mm in diameter, type K, Shinnetsu Co., Ltd., Ibaraki, Japan).

Chemical analyses of the solutes in each solvent and the residues have been described in our previous paper (Nomura et al., 2017).

3.2.3 Microscope observations

Cellulose carbonization in cotton cell walls was observed using UV microscopy. Each residue was embedded in epoxy resin, and the samples were cut into 0.5 μm thick sections using a diamond knife mounted on a Leica Reichert Supernova Microtome (Buffalo Grove, IL, USA). The sections were placed on quartz slides, mounted with glycerin, and covered with a quartz coverslip before examination with an MSP-800 system (Carl Zeiss, Oberkochen, Germany) with a specified filter at 280 nm ± 5 nm. The morphological regions of each fraction were analyzed on a UV microspectrophotometer using photometric point-by-point measurements (spot size: 1 × 1 μm).

3.2.4 Py-GC/MS observations of the hydrolyzed residue of pyrolyzed cellulose

Cellulose pyrolyzed under nitrogen was hydrolyzed by acid hydrolysis. Aqueous H_2SO_4 (72 wt%, 0.1 mL) was added to the residue and the mixture was then heated at 30 °C for 60 min with frequent agitation with a glass rod. The mixture was diluted with water (2.8 mL) and then heated in an autoclave at 121 °C for 60 min. After washing with distilled water and drying, the hydrolyzed residue (solid hydrolyzed products) was analyzed using a portable Curie-point injector (JCI-22, Japan Analytical Industry, Tokyo, Japan) coupled to a Shimadzu-2010 Plus gas chromatograph (Shimadzu Co., Kyoto, Japan) and a Shimadzu QP 2010 Ultra mass spectrometer (Shimadzu Co., Kyoto, Japan).

The hydrolyzed residue was pyrolyzed at 723 °C for 5 s. The instrument conditions were as follows: Agilent CPSil 8CB column (length: 30 m, diameter: 0.25 mm, Agilent Technologies, Santa Clara, CA, USA); 250 °C injector temperature; 1: 50 split ratio; helium carrier gas (1.0 mL min^{-1}). The column temperature was initially set at 50 °C for 3 min, after which it was ramped at 6 °C min^{-1} to 200 °C and 30 °C min^{-1} to 300 °C, before being held constant at 300 °C for 5 min. The MS scan parameters included a scan range of 35–600 m/z and a scan interval of 0.3 s.

3.3 Results and Discussion

3.3.1 Cellulose carbonization in cell wall under nitrogen

Figure 3-1 shows the UV photomicrographs and the absorption spectra of the cross sections of the cotton-cellulose fibers before and after pyrolysis under nitrogen. The original cellulose has no UV absorption, while the cellulose after pyrolysis absorbs UV light, and the cross section is clearly observed in the photomicrograph. The furan and benzene structures formed in the cell wall absorb UV light as discussed below. The UV absorption of the cellulose char was homogeneous within the cell wall, indicating that the carbonization reaction of cellulose occurred homogeneously within the cell wall.

The UV spectrum of the cellulose char (Figure 3-1) has a peak at 250 nm and the absorbance gradually decreases with increasing wavelength up to around 500 nm. The UV spectra of the model compounds (i.e., furan, 5-HMF, and dibenzofuran (model furans) and benzene, naphthalene and anthracene (model aromatics)) are shown in Figure 3-2 for comparison. These model compounds have UV absorption peaks at around 200–300 nm, similar to cellulose char. As the conjugated system becomes larger (benzene → naphthalene → anthracene), the peak wavelength tends to shift towards the long-wavelength region (Rieger and Müllen, 2010). Cellulose char absorbs UV up to 500 nm, indicating that polycyclic benzene- and furan-rings are present in the cellulose char.

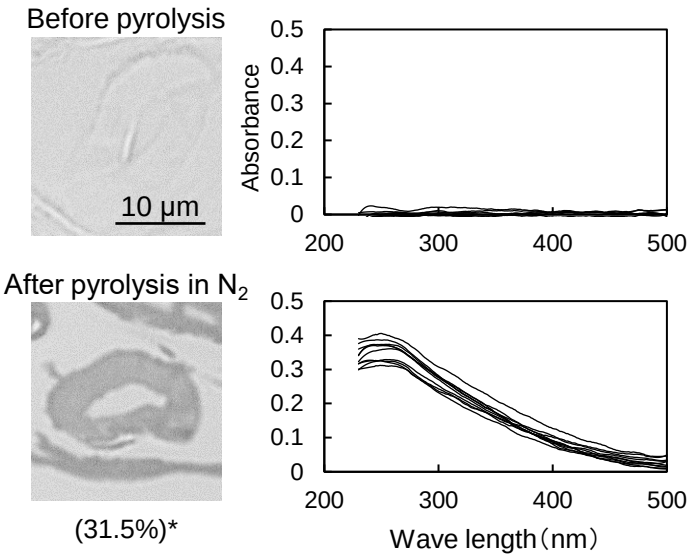

Figure 3-1. Change in the UV photomicrograph (280 nm) and UV absorption spectrum of the cross sections of cotton cellulose fiber after pyrolysis in nitrogen at 280 °C for 58 min. *Recovery rate of cellulose (cellulose base). The UV spectra were measured at ten spots selected from the cross section in the picture in a random manner excluding the edge.

When the cellulose char was hydrolyzed, the remaining cellulose was removed, and a dark brown hydrolysis residue was obtained. Figure 3-3 shows the pyrograms obtained by Py-GC/MS (764 °C/5 s) analysis of cellulose, cellulose char, and the hydrolysis residue. The chemical structure assigned to each peak in the mass spectrum is shown in Figure 3-4. Anhydrosugars such as LG are the major products from cellulose and cellulose char. These products may be formed directly by cellulose pyrolysis. Furans, benzenes, and benzofurans were clearly observed in the pyrogram of thehydrolysis residue. Pastorova et al. also reported that cellulose char obtained by pyrolysis at 270 °C and 290 °C contained furans and benzenes detected by Py-GC/MS analysis (Pastorova et al., 1994). In their study, however, large amounts of cellulose remained unreacted and it is unclear whether the furans and benzenes occurred in the solid carbonized products or in unreacted cellulose in the char. In the present study, most of the cellulose (content: 49%

in cellulose char) was removed by hydrolysis before Py-GC/MS analysis. Consequently, our results indicate that the solid carbonized products in cellulose char prepared at 280 °C contained furan and benzene rings that absorb UV light.

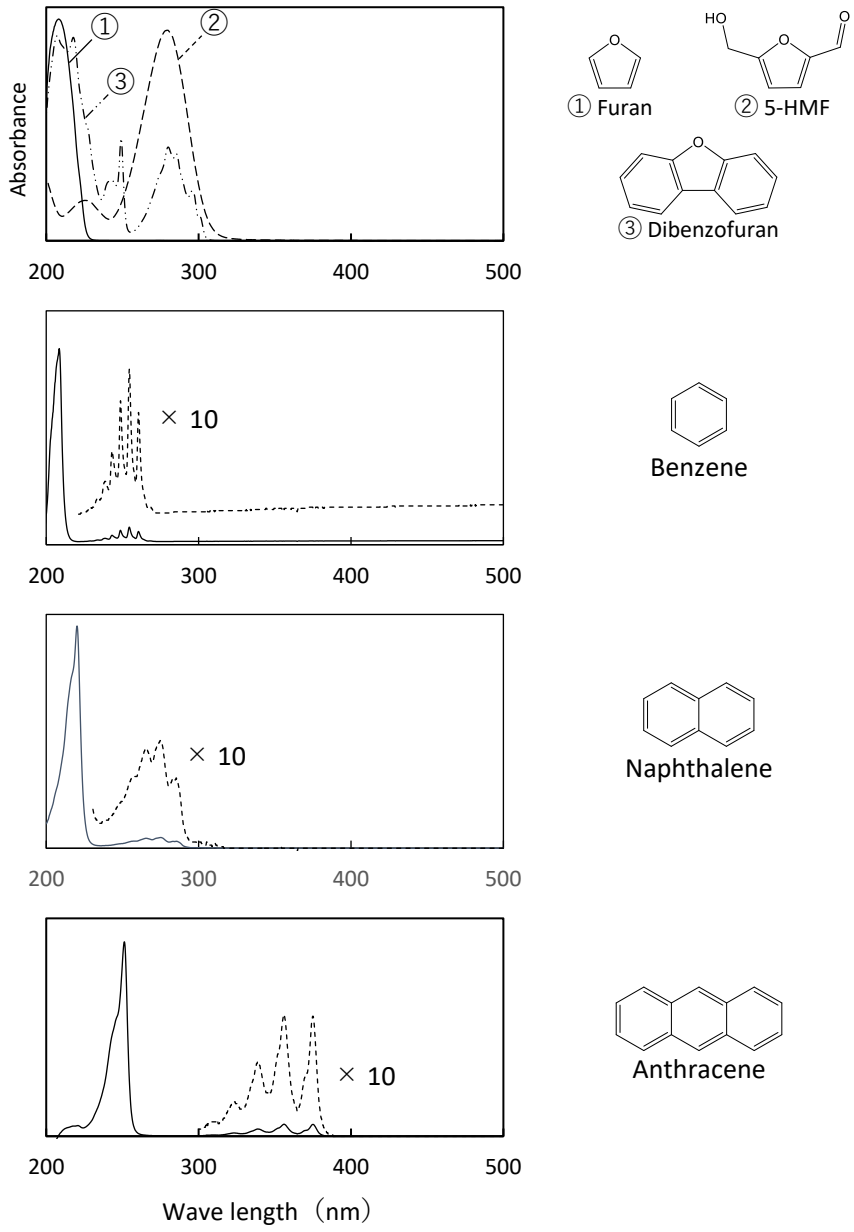

Figure 3-2. UV absorption spectra of model compounds furan, 5-HMF, dibenzofuran, benzene, naphthalene, and anthracene shown for comparison with the spectra of cellulose char.

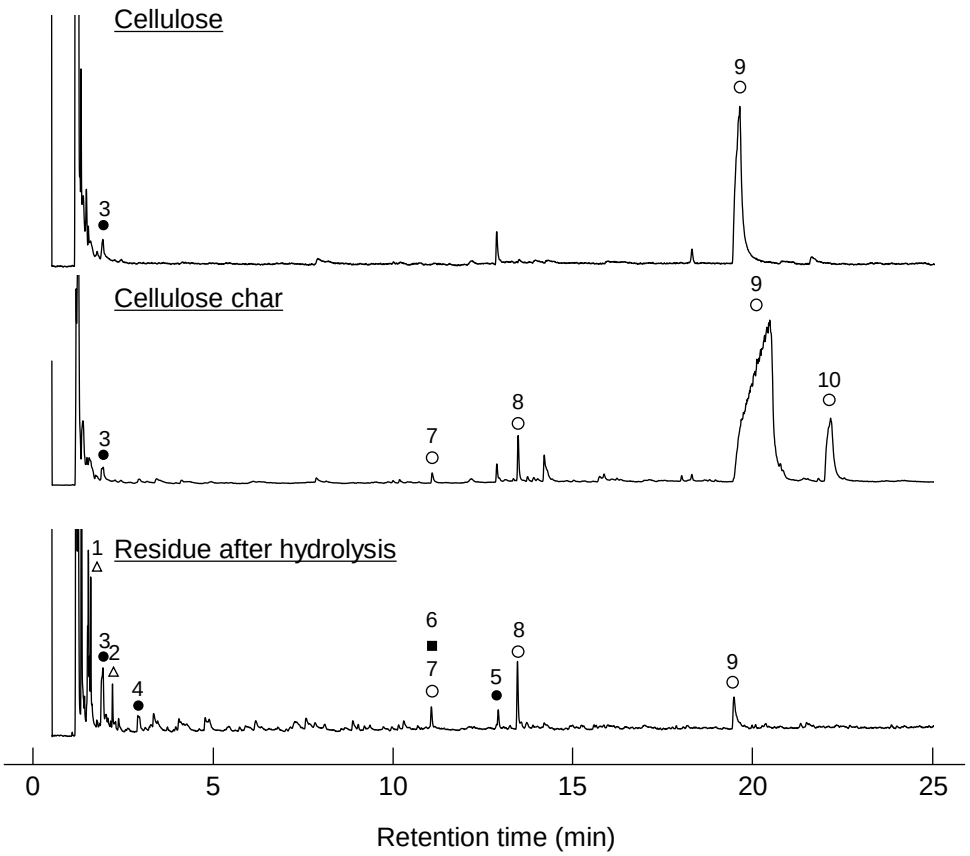

Figure 3-3. Pyrograms obtained by Py-GC/MS (764 °C / 5 s) analysis of cellulose, cellulose char, and its hydrolysis residue.

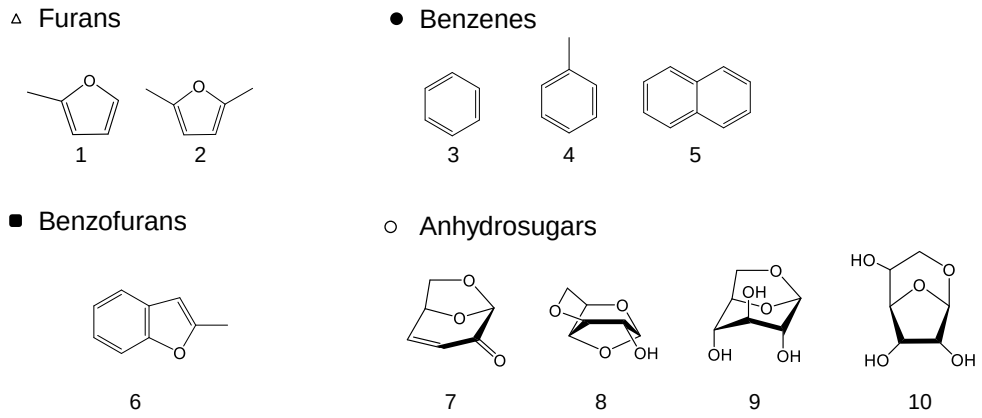

Figure 3-4. Chemical structures of the products identified by Py-GC/MS (764 °C/5 s) analysis of cellulose, cellulose char, and its hydrolysis residue (BPH, DPS, and DPB) at 280 °C for 60 min.

3.3.2 Influence of aromatic solvent

Figure 3-5 shows the UV micrographs and spectra of the cross sections of cellulose fiber pyrolyzed in aromatic solvents. The UV absorptivity of cellulose pyrolyzed in aromatic solvent is lower than that of cellulose pyrolyzed under nitrogen, and decreases in the order N_2 > DPB > DPS > BPH, which is the same order as the yield of the hydrolysis residue of char (Figure 3-6). As the yield of hydrolysis residue (%, char basis) decreases, so does the UV absorbance at 280 nm. These results confirm that the UV absorption is caused by the solid carbonized products formed in cellulose char.

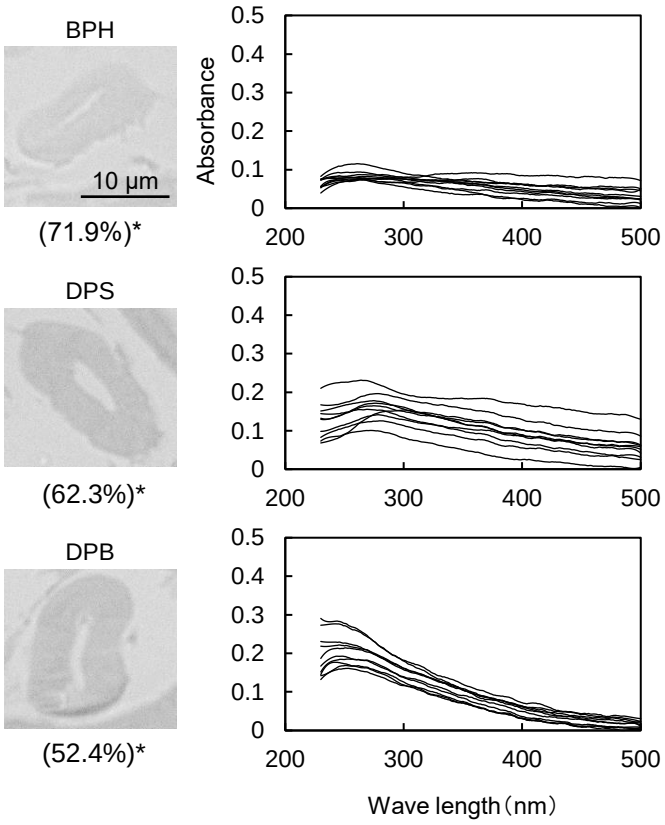

Figure 3-5. UV photomicrographs (280 nm) and UV absorption spectra of the cross sections of cotton cellulose fiber pyrolyzed in aromatic solvents (BPH, DPS and DPB) at 280 °C for 60 min. *Recovery rate of cellulose (cellulose base). The UV spectra were measured at ten spots selected from the cross section in the picture in a random manner excluding the edge.

The UV absorptivity was homogeneous within the cross section of the cellulose fiber after pyrolysis in aromatic solvents, suggesting that the aromatic solvents penetrated into the cell wall volume and effectively inhibited the carbonization reaction. Because the shapes of the UV spectra (Figure 3-5), which have absorption maxima at 250 nm, are very similar to those of cellulose pyrolyzed under nitrogen, similar carbonization reactions must take place under nitrogen and in the aromatic solvent, though the frequency of these reactions is lower in the aromatic solvent. As shown in Figure 2-7 in *Chapter 2*, the IR spectra of hydrolysis residue obtained under nitrogen and in aromatic solvent were similar (Nomura et al., 2017).

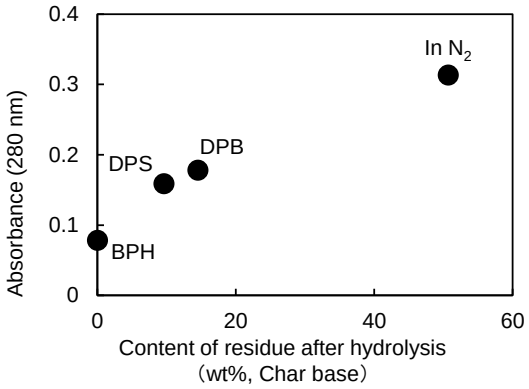

Figure 3-6. Correlation between UV absorbance at 280 nm and yield of char hydrolysis residue.

3.3.3 Carbonization mechanism of cellulose fiber

Figure 3-7 compares the UV absorbance at 280 nm in the radial direction of the cell wall. The photographs with a wider field of view are also shown in Figure 3-8. Although the variation of the UV absorbance is not small, the cellulose char prepared under nitrogen tends to exhibit greater absorptivity at the surface than in the interior of the cell wall, suggesting that carbonization occurs more efficiently at the surface under nitrogen. By contrast, the absorbance was more homogeneous when pyrolysis was conducted in aromatic solvents.

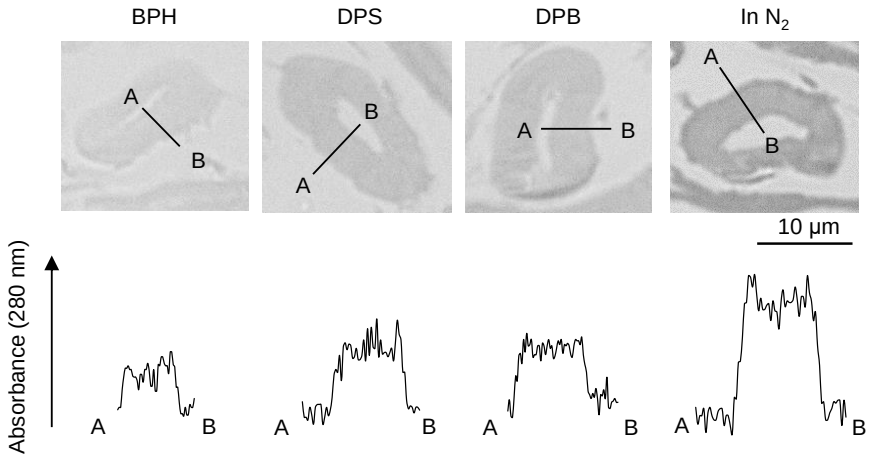

Figure 3-7. UV absorbance distribution at 280 nm along the cell wall thickness after pyrolysis of cellulose in nitrogen and aromatic solvents at 280 °C.

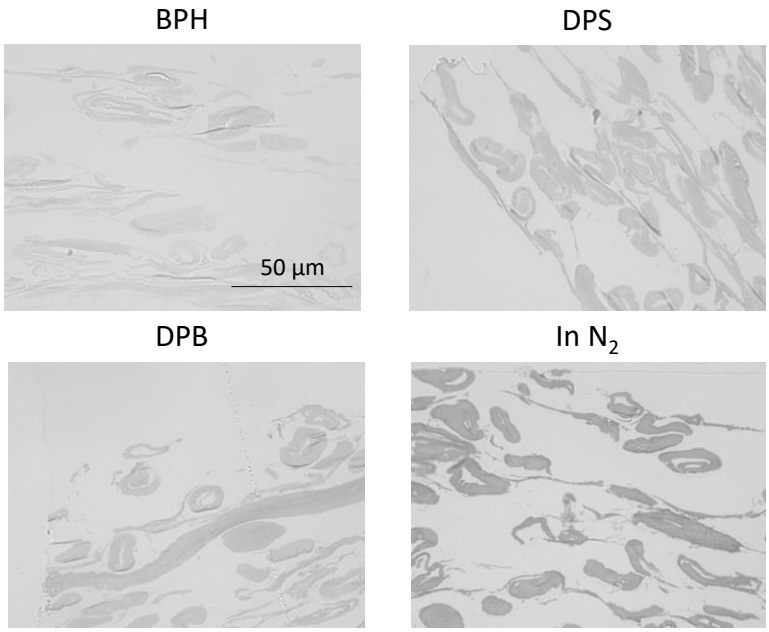

Figure 3-8. A wider field of UV microscopic image (280 nm) of pyrolyzed cellulose in nitrogen and aromatic solvents at 280 °C

Figure 3-9 (not to scale) illustrates the carbonization mechanism of cellulose cell walls. As described previously, the cell walls are hundreds of microcrystals thick. X-ray diffraction analyses of cellulose pyrolysis indicated that cellulose molecules inside the crystallites are stable and that thermal degradation begins with surface molecules

(Kawamoto and Saka, 2006; Kim et al., 2001; Zickler et al., 2007). It is also known that there is an induction period before weight loss starts during the isothermal heating of cellulose (Bradbury et al., 1979; Broido and Nelson, 1975; Matsuoka et al., 2014). The formation of "active cellulose" has been proposed as an initiation step to explain the induction period(Bradbury et al., 1979). Because the induction period was extended by removal of the cellulose reducing end by $NaBH_4$ reduction or thermal glycosylation with glycerin, it has been proposed that pyrolysis of the reactive reducing end on the crystal surface initiates the thermal decomposition of cellulose (Matsuoka et al., 2014). Nucleation kinetic models have been proposed for such heterogeneous pyrolysis of cellulose (Capart et al., 2004; Dollimore and Holt, 1973; Mamleev et al., 2007; Reynolds and Burnham, 1997).

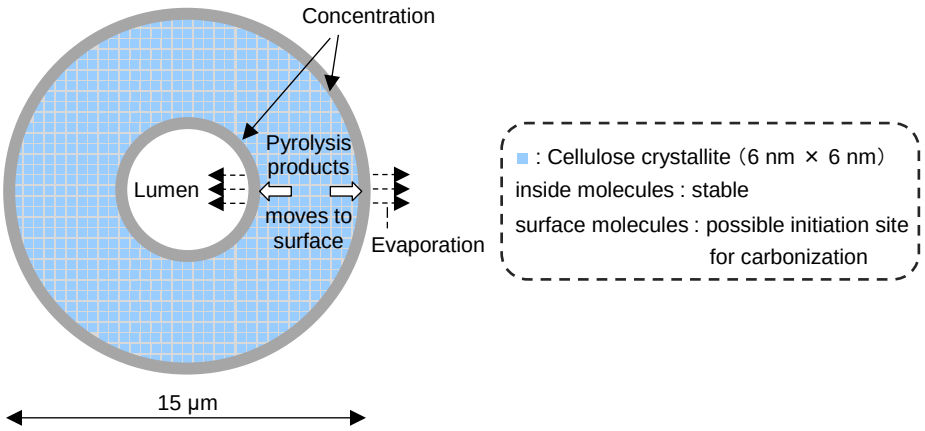

Figure 3-9. Progress of pyrolysis in cell wall cross section of cotton cellulose fiber in nitrogen to account for accumulation of carbonized products on the surface.

Liquid LG (melting point: 183 °C, boiling point: 385 °C ref. (Shoji et al., 2014)) is generated at the surfaces of crystallites inside the cell wall, moves to the cell wall surface, and then evaporates at 280 °C. This increases the concentration of LG at the surface of the cell wall in a manner similar to the higher concentration of pigment that accumulates at the edges when paper soaked in aqueous pigment is dried at ambient temperature. During transport to the surface, LG undergoes a secondary pyrolysis reaction,

producing solid carbonized products inside and at the edges of the cell wall (Fukutome et al., 2015; Kawamoto et al., 2003). The behavior of 5-HMF, another intermediate in the formation of solid carbonized product, is similar except that it has higher secondary pyrolysis reactivity than LG (Nomura et al., 2017) (*Chapter 2*).

When pyrolyzed in aromatic solvents, solvent penetrates into the cell wall and inhibits the formation of solid carbonized product (Figure 3-10). The thermal degradation products dissolve in the solvent and are removed from the cell wall. Because no evaporation is involved, intermediates do not accumulate on the cell wall surface, resulting in homogeneous UV absorbance in the cell wall. Variations in the efficiency of aromatic solvents depend on the ability of the solvent to penetrate the cell wall. Cell wall cellulose molecules that are inaccessible to aromatic solvents decompose in the same way as they do when pyrolyzed under nitrogen. The homogeneity in UV absorbance also suggests that the inaccessible parts of the cell wall are distributed in clusters smaller than the resolution of the UV microscope (280 nm).

The results reported in this work show that controlling the pyrolysis of cellulose and other lignocellulosic biomass requires that cell wall nanostructures derived from cellulose crystallites be taken into account.

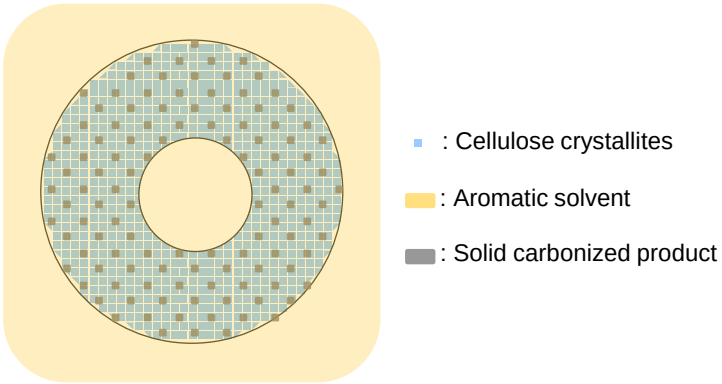

Figure 3-10. Proposed formation mechanism of carbonized product in cell walls composed of nanocrystallites and the influence of aromatic solvent.

3.4 Conclusions

Pyrolysis of cotton cellulose under nitrogen or in aromatic solvents at 280 °C was investigated with UV microscopy. The following conclusions were reached.

(1) Cross sections of cell walls of cellulose char absorb UV because of the presence of furan and benzene rings in the solid carbonized products.

(2) UV absorbance is uniform inside the cell wall except for the surface, where the UV absorbance tends to be stronger. This indicates that the carbonization occurs uniformly inside the cell wall within the resolution of the UV microscope used (280 nm). However, carbonization occurs more strongly at the surface of the cell wall volumen.

(3) A mechanism for the carbonization of cellulose cell walls composed of nano-sized microcrystals has been proposed. The LG and 5-HMF play important roles as intermediates in cellulose carbonization.

(4) Aromatic solvents uniformly inhibit the formation of solid carbonized product within the cell wall during pyrolysis, probably by inhibiting the secondary pyrolysis reactions of LG and 5-HMF via complex formation. The inaccessible part of the cell wall is carbonized and distributed in the cell wall within the resolution of UV microscope (280 nm).

(5) The characteristic pyrolysis behavior of cellulose cell wall originating from the nature of nano-sized composites of the crystallites is presented. This must be considered to understand and control pyrolysis reactions of cellulose and other lignocellulosic biomass.

Chapter 4

Hydroxymethylfurfural as an intermediate of cellulose carbonization

4.1 Introduction

Cellulose is among the most abundant renewable polymeric organic chemicals on earth. Therefore, the development of efficient conversion methods to expand cellulose use and help establish a sustainable society is important. Thermochemical conversion technologies, such as pyrolysis, gasification, and carbonization, are potential methods. In such thermochemical conversion techniques, the composition of the final products depends on the progress of the secondary reactions of the primary pyrolysis products from cellulose. Reactions that form solid carbonized products are particularly important. Promoting these reactions results in more efficient production of charcoal, which can also be used as biochar for carbon capture and storage to mitigate global warming. However, inhibiting the reactions that form solid carbonized products leads to the efficient production of bio-oil, which can be used to produce liquid fuels and industrial chemicals. Therefore, elucidating the molecular mechanism of carbonization in cellulose pyrolysis is important for reaction control.

As shown in *Chapter 3*, changes in the chemical structure of cellulose char have been investigated in various analytical methods. Based on the results, carbonization of cellulose could be summarized as a reaction that finally produces benzene-ring structures by a dehydration reaction. However, the details of its molecular mechanism have not been clear.

Pastrova et al. have indicated the roles of furan-type intermediates in benzene ring formation during cellulose pyrolysis (Pastorova et al., 1994). The authors

characterized cellulose chars prepared at different temperatures using Py-GC/MS. Although LG was the major product detected from cellulose char prepared at 250 °C, by increasing the pyrolysis temperature of char preparation, the major compounds changed to furans and benzenes in the temperature range of 270–350 °C and to benzenes above 350 °C, which has also been supported by solid ^{13}C NMR. Based on these results, they concluded that the chemical structure of cellulose char changes from cellulose → furan→ benzene types with the progress of carbonization. However, no further studies have been reported on the mechanism of cellulose carbonization.

In the hydrothermal carbonization of reducing sugars, furfural and 5-HMF have been suggested as intermediates in the formation of solid carbonized products, known as hydrothermal char (Baccile et al., 2009; Falco et al., 2011; Titirici et al., 2008; Zandvoort et al., 2013). However, the treatment conditions are different, and the reducing sugars used for treatment are different from cellulose, which is a crystalline polysaccharide. Accordingly, direct evidence is needed to determine whether furfural and 5-HMF are involved in cellulose carbonization.

We recently reported the negative relationship between the yields of 5-HMF and solid carbonized products in cellulose pyrolysis under nitrogen or in various aromatic solvents (Nomura et al., 2017) (*Chapter 2*). Aromatic solvents were used to stabilize the cellulose-derived primary pyrolysis products, such as LG, by forming OH–p hydrogen bonds, which inhibit the formation of intermolecular hydrogen bonds that act as acid and base catalysts during pyrolysis (Hosoya et al., 2006; Nomura et al., 2017). For example, when cellulose was pyrolyzed in BPH at 280 °C for 60 min, the yield of 5-HMF increased from 0.0 wt% (under N_2) to 6.4 wt%, while that of solid carbonized products, obtained as the hydrolysis residue, was decreased from 50.7 wt% (under N_2) to 0.0 wt%. Although any 5-HMF was not detected under N_2, 5-HMF was thought to decompose into carbonized products rather than evaporate at 280 °C, which is below the estimated boiling point, 291.5 ± 30.0 °C (Scifinder). In pyrolysis of cellulose, 5-HMF is known to be produced (Gardiner, 1966; Katō and Komorita, 1968). We do not believe that the functional groups of aromatic solvents, namely the benzene ring, ether oxygen, and

carbonyl (in the case of BPH), greatly influenced the formation of 5-HMF during the pyrolysis of cellulose. From these results, we hypothesized that solid carbonized products were formed via 5-HMF in cellulose pyrolysis.

In the present study, to test our hypothesis, the pyrolytic reactivity of 5-HMF was evaluated by comparing the chemical structures in the resulting char with those in cellulose char using IR, acid titration, and Py-GC/MS. Finally, a mechanism for cellulose carbonization via 5-HMF was proposed and discussed in terms of the crystalline nature of cellulose.

4.2 Materials and Methods

4.2.1 Materials

The 5-HMF (>95.0%, GC) and dimethyl sulfone ($DMSO_2$,>99.0%, GC) was purchased from Tokyo Chemical Industry, Tokyo, Japan. Before experiments, water was removed from 5-HMF by freeze-drying. Whatman No. 42 (Whatman PLC, UK, cotton) filter paper was used as a cellulose sample which was cut into small sheets (7 x 7 mm). Glycerol (>99.5%, GC), Na_2CO_3 (>99.5%, titration) and $NaHCO_3$ (99.5%, titration) were purchased from Nacalai Tesque, Inc., Kyoto, Japan, and used without purification. Aqueous NaOH solution (47-53%, titration) and aqueous HCl solution (35-37%, titration) were purchased from Wako Pure Chemical Industries, Ltd. (Osaka, Japan) and used without purification.

4.2.2 In situ IR measurement

The 5-HMF or cellulose was heated using a GladiATR system (Pike Technologies, WI, USA) at a heating rate of 10 °C/min under nitrogen, and IR spectra were recorded at 25 °C intervals in the temperature range of 50–280 °C. The temperature was held for 1 min at each interval to measure the IR spectra. ATR-FTIR spectra were

recorded by attaching GladiATR to Shimadzu IR Affinity-1 spectrometer (Shimadzu Co., Kyoto, Japan). The sample chamber in GladiATR was continuously purged with dry nitrogen (99.99%) at a flow rate of 500 mL/min. A total of 45 scans over the range between 400 and 4000 cm^{-1} were collected with a resolution of 4 cm^{-1} (PIKECalc Software, Pike Technologies, Madison, Wisconsin USA).

4.2.3 Pyrolysis of 5-HMF and cellulose

5-HMF (500 mg) was placed in a Pyrex glass tube reactor (inner diameter, 8.0 mm; wall thickness, 1.0 mm; length, 300 mm). The reactor was purged with nitrogen (99.99%), and then the bottom three-quarters of the reactor were inserted into a muffle furnace preheated at 280 °C through a small hole at the top. After heat treatment for 10–40 min, the reactor was removed from the furnace and immediately cooled with air flow. The solid product (char) was washed with water to remove the non-carbonized soluble pyrolysis products and then dried in an oven at 105 °C for 24 h. The obtained char was analyzed by Fourier-transform IR spectrometry using a Shimadzu IR Affinity-1 spectrometer in attenuated total reflection mode. A total of 45 scans over the range between 400 and 4000 cm^{-1} were collected with a resolution of 4 cm^{-1}. Similar procedures were performed in the presence of glycerol and for cellulose. Although the experimental results were not statistically evaluated, the reproducibility is confirmed by conducting each experiment twice.

To study the condensation reaction of 5-HMF, the pyrolysis mixture was extracted with acetone, and the soluble portion was analyzed by GPC, GC/MS, and NMR. GPC analysis was performed using an LC-20A system (Shimadzu Co., Kyoto, Japan) under the following conditions: Column, Shodex KF-801 (Showa Denko KK, Tokyo, Japan); column temperature, 40 °C; eluent, tetrahydrofuran (THF); flow rate, 1.0 mL/min; detection wavelength, 254 nm. Before analysis, the soluble portion was evaporated with a rotary evaporator, and resulting residue was dissolved in THF (1 mL). GC/MS analysis (QP2010 Ultra, Shimadzu Co.) was conducted under the following conditions: Column,

Agilent CPSil 8CB (length, 30 m; diameter, 0.25 mm, Agilent Technologies, Santa Clara, CA, USA); thickness of the column liquid phase, 0.25 μm); injector temperature, 250 °C; split ratio, 1:50; column temperature, 50 °C for 5 min, then increased to 300 °C at 20 °C/min, and held at 300 °C for 3 min; carrier gas, hydrogen (72.5 mL/min). MS analysis was conducted under the following conditions: an ion source temperature, 200 °C; ionization mode, EI; a filament voltage, 70 eV; emission current, 60 μA; mass range, m/z 35-500. In the GC/MS analysis, 1 μL of acetone solution was injected. ^{1}H and ^{13}C NMR spectra were recorded in $CDCl_3$ (Euriso-Top, Paris, France, 0.03% tetramethylsilane (TMS), 99.80% D) using a Bruker AC-400 spectrometer (Bruker, MA, USA) with tetramethylsilane as an internal standard. Chemical shifts and coupling constants (*J*) are given in δ (ppm) and Hz, respectively. Component quantification was conducted using dimethyl sulfone ($DMSO_2$) as an internal standard. The concentration of $DMSO_2$ in $CDCl_3$ was 6.86 g/L. The ^{1}H-NMR and ^{13}C-NMR spectra were measured with the following parameters: 30° pulse, relaxation delay of 1.0 s (^{1}H-NMR) and 2.0 s (^{13}C-NMR). The peak integration was conducted manually. The pyrolysis products were separated using preparative TLC on silica gel plates (Kieselgel 60 F254, Merck, Darmstadt, Germany).

4.2.4 Py-GC/MS analysis

Py-GC/MS analysis of the 5-HMF char and cellulose char was conducted using a portable Curie-point injector (JCI-22, Japan Analytical Industry Co., Ltd., Tokyo, Japan) coupled with GCMS (QP2010 Ultra, Shimadzu Co.). The char was rapidly heated to 764 °C, and the temperature was held for 5 s. The GC/MS conditions were set as follows: Column, Agilent CPSil 8CB (length, 30 m; diameter, 0.25 mm, Agilent Technologies, Santa Clara, CA, USA); injector temperature, 250 °C; split ratio, 1:50; column temperature, 50 °C for 3 min, increased to 200 °C at 6 °C/min, then to 300 °C at 30 °C/min, and held at 300 °C for 5 min; carrier gas, helium. The same MS analysis conditions used in GC/MS analysis were applied for Py-GC/MS.

4.2.5 Boehm titration

Acidic groups on the char surface were determined using a Boehm titration. The char (50 mg) was added to 0.1 N NaOH, 0.05 N Na_2CO_3, or 0.1 N $NaHCO_3$ aqueous solution (50 mL). The concentrations of these solutions were confirmed by titration. The vial was sealed and shaken for 24 h. The solution (10 mL) was pipetted and excess base was titrated with 0.1 N HCl. The number of acidic sites was quantified, assuming that NaOH neutralized carboxyl, lactone, and phenol groups, Na_2CO_3 neutralized carboxyl and lactone groups, and $NaHCO_3$ neutralized only carboxyl groups. The potentiometric titrator (AT-510, KEM, Japan) was used for titration.

4.3 Results and Discussion

4.3.1 In situ IR mesurement

Figure 4-1 shows some examples of IR spectra of cellulose and 5-HMF obtained by in situ measurement using a GladiATR system at a heating rate of 10 °C/min. This system allowed continuous monitoring of the spectrum during heating, which enabled identification of the temperature range in which the spectrum changed. The cellulose spectrum began to change at 280 °C, with signals characteristic of cellulose carbonization appearing at 1600 cm^{-1} (C=C) and 1700 cm^{-1} (C=O). Furthermore, the hydroxyl group signal (3000–3500 cm^{-1}) gradually shifted toward a higher wavenumber with increasing temperature, attributed to hydrogen bond cleavage (Agarwal et al., 2011; Kokot et al., 2002; Watanabe et al., 2006). After heating for 60 min at 280 °C, the shape of the OH signal changed to be characteristic of carboxyl groups (Silverstein et al., 1986).

When 5-HMF was heated, the signal assigned to OH groups (3000–3500 cm^{-1}) disappeared completely at around 170 °C, which indicates that the OH group in 5-HMF was removed in this temperature range. When the temperature was raised further, the OH signal reappeared at 225 °C, but the shape was now characteristic of carboxyl groups. As

observed in cellulose, the signals at 1600 and 1700 cm^{-1} were broad, but those assigned to the furan ring (1670 cm^{-1}) and aldehyde group (1700 cm^{-1}) of 5-HMF were retained, even after heating at 280 °C for 60 min. Therefore, 5-HMF underwent similar structural changes to cellulose, as reflected in the IR spectra, although 5-HMF showed slower conversion.

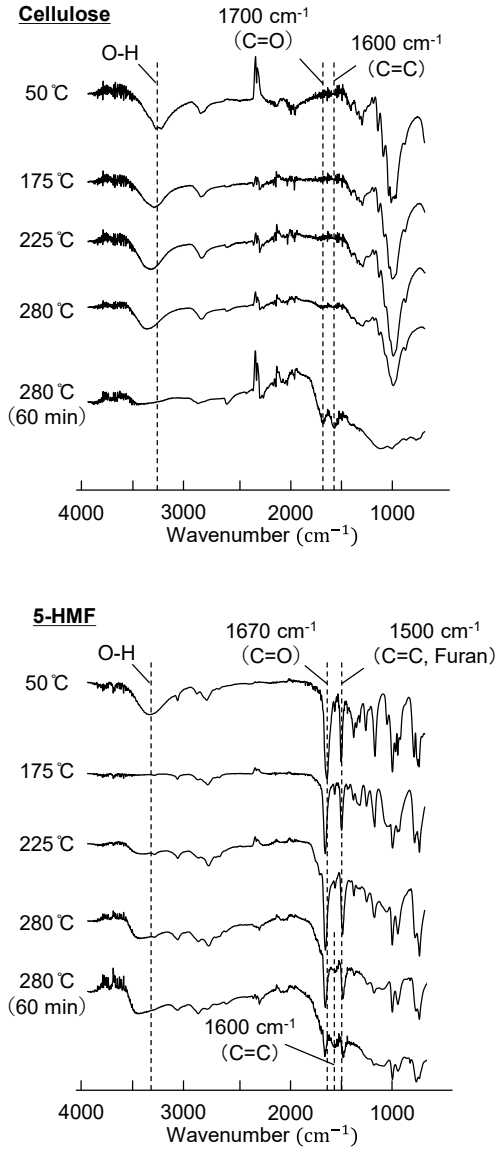

Figure 4-1. Examples of spectra from in situ IR measurement of cellulose and 5-HMF under nitrogen.

4.3.2 Thermal polymerization of 5-HMF

As in situ IR measurements indicated OH group removal from 5-HMF at around 170 °C, polymerization reactions were expected to occur. 5-HMF is a potential feedstock for the production of renewable plastics, but most related studies have utilized 5-HMF derivatives, such as 2,5-bis(hydroxymethyl)furan and 2,5-furandicarboxylic acid (Chheda and Dumesic, 2007; Keskiväli et al., 2017; West et al., 2008; Wrigstedt et al., 2017). Accordingly, information on the polymerization of 5-HMF by heating is limited (Chambel et al., 1998). Therefore, the polymerization behavior of 5-HMF was evaluated at 280 °C.

The heat-treatment product of 5-HMF was extracted with acetone to separate soluble and residual constituents. The residue was obtained as a glassy material and was insoluble in other solvents, such as methanol, tetrahydrofuran, DMSO, and chloroform, which indicated a highly condensed product. Gel-permeation chromatography (GPC) of the acetone-soluble portions (Figure 4-2), conducted after heating at 280 °C for 10 and 30 min heating, exhibited two large signals corresponding to unreacted 5-HMF and a

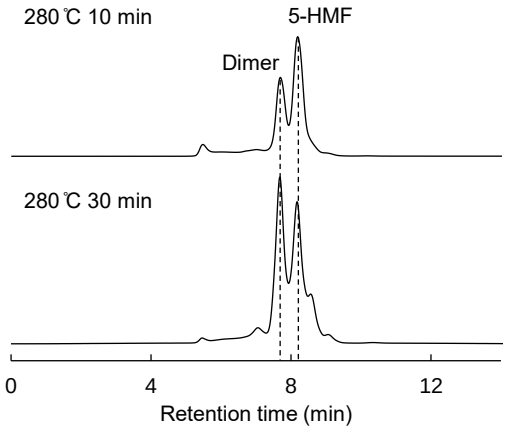

Figure 4-2. GPC chromatograms of acetone-soluble portions of 5-HMF pyrolysis mixtures (280 °C, 10 and 30 min).

dimer. This was confirmed by GC/MS analysis (Figure 4-3). Using thin layer chromatography (TLC; solvent system, ethyl acetate/hexane = 1:2), a 5- HMF dimer, 5,5'(oxy-bis(methylene))bis-2-furfural (**11**), was isolated and identified by ^{1}H NMR, ^{13}C NMR, and GC/MS (Figure 4-4). Dimer **12** has been reported from treating 5-HMF under acidic conditions (Amarasekara et al., 2019; Casanova et al., 2010; Tschiersky and Baltes, 1989) or by heating at 210 °C (Chambel et al., 1998).

Figure 4-5 shows the effect of the heating period on the yields of dimer **11**, insoluble residue (char), and unreacted 5-HMF. At 10 min, no char was detected, but the amount of 5-HMF was reduced by about half and dimer **11** was produced in a 17.9 wt% yield. This indicated that dimer **11** was formed initially, and then char was generated. When extended to 30 min, char was produced in 61.3 wt% yield, but the principle components detected in the GPC chromatogram were dimer **11** and unreacted 5-HMF (Figure 4-2). Therefore, the polymerization of 5-HMF proceeded quickly to give insoluble char, and small amounts of polymerization products that were soluble in acetone, except for dimer **11**, although the role of the dimer is currently unknown. In situ IR measurement of 5-HMF Figure 4-1) showed that unreacted 5-HMF completely disappeared at 175 °C. Unreacted 5-HMF (estimated boiling point, 291.5 ± 30.0 °C) (Scifinder) was removed by evaporation during in situ IR measurements, because the polymerization reactivity of 5-HMF at 175 °C was lower according to the results in Figure 4-5.

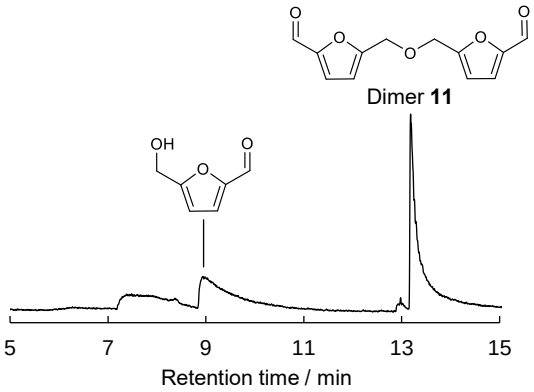

Figure 4-3. Total-ion chromatogram of acetone-soluble portion of 5-HMF pyrolysis mixture (280 °C, 30 min).

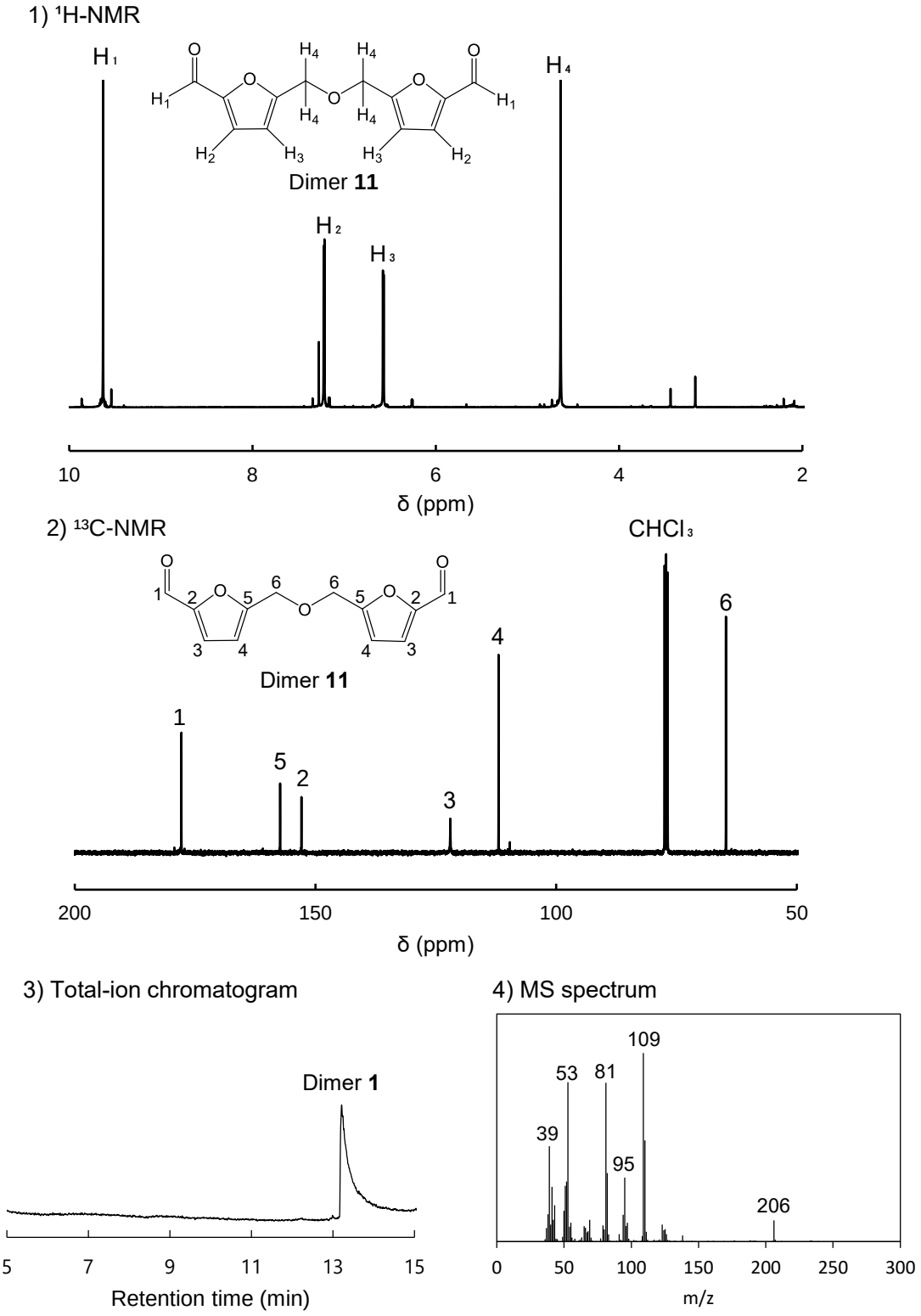

Figure 4-4. A) [1]H-NMR spectrum, B) [13]C-NMR spectrum, C) total-ion chromatogram and D) MS spectrum of 5,5'(oxy-bis(methylene))bis-2-furfural (Dimer **11**)

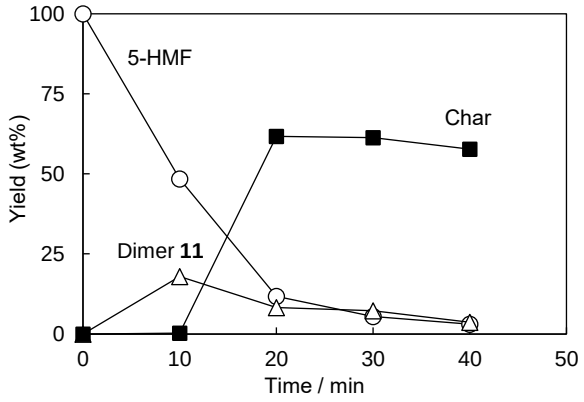

Figure 4-5. Time-course change of pyrolysis products from 5-HMF at 280 °C.
○ : 5-HMF, △ : dimer **11**, ■ : char

Next, glycerol was used as a model compound for cellulose-derived pyrolysis products that were expected to coexist with 5-HMF in cellulose pyrolysis as discussed later. Accordingly, the polymerization reactivity of 5-HMF in the presence of glycerol was investigated at 280 °C. The heat-treated mixture of 5-HMF (200 mg) and glycerol (200 mg) was separated using a binary solvent system of water and ethyl acetate. The resulting water-soluble portion was separated by TLC using 5% MeOH/$CHCl_3$ and subsequently 7% MeOH/$CHCl_3$ (five times) to give coupling product 5-[(2,3-dihydroxypropyoxy)methyl]-2-furaldehyde (**12**) in 14.4 mol% yield. No glassy solid products were produced in the presence of glycerol, which indicates that the polymerization of 5-HMF was inhibited by glycerol.

The ^{1}H NMR spectrum of the coupling product is shown in Figure 4-6 and compared with that of the acetate derivative (also see Figure 4-7). The protons assigned to the aldehyde (H_1, 9.62 ppm) and furan ring (H_2, 7.22; H_3, 6.55 ppm) were observed, along with protons assigned to the glycerol moiety at 3.5–4.0 ppm, which confirms that this was the coupling product of glycerol and 5-HMF. Acetylation caused the signals for H_6, H_7, and H_8 to be shifted downfield because of the influence of electron-withdrawing acetyl groups, while the effect on the chemical shifts of signals assigned to H_4 and H_5 was small. These results indicated the coupling position between glycerol and 5-HMF

moieties in compound **12**. ^{13}C NMR, GC/MS, and UV spectra of compound **12** are shown in Figure 4-8, as compound **12** has not been reported previously. These results indicated that 5-HMF combined with other cellulose-derived products containing hydroxy groups during cellulose pyrolysis.

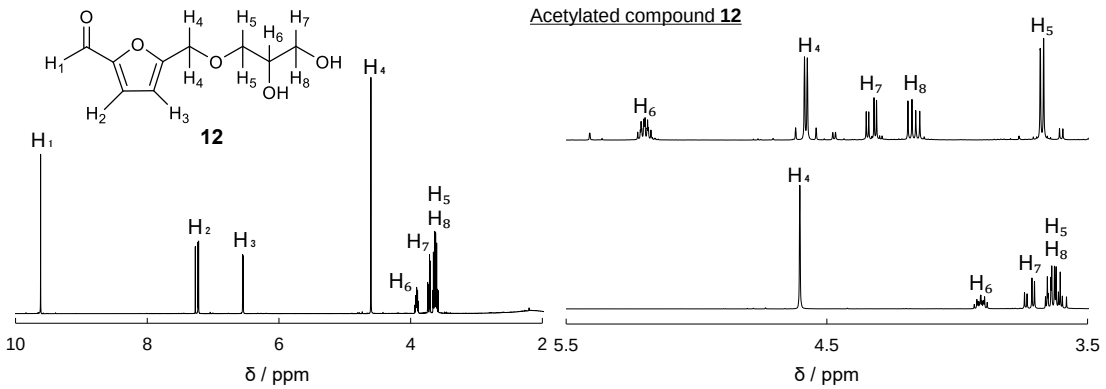

Figure 4-6. ^{1}H NMR spectrum of compound **12** obtained from the pyrolysis of 5-HMF and glycerol at 280 °C for 20 min, as compared with the spectrum of acetylated compound **12**.

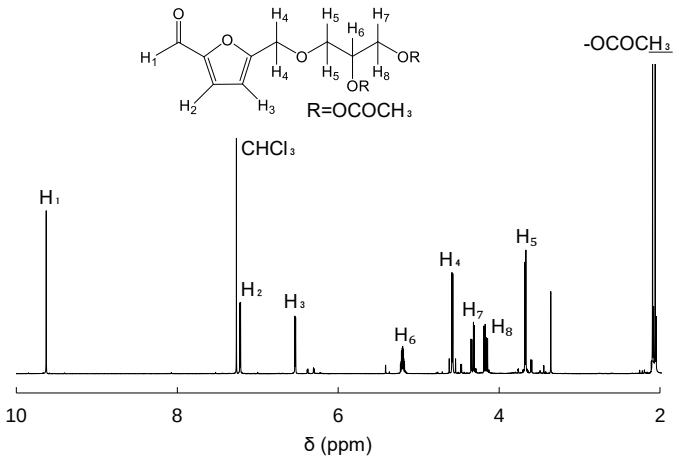

Figure 4-7. ^{1}H-NMR spectrum of compound 1**2** after acetylation

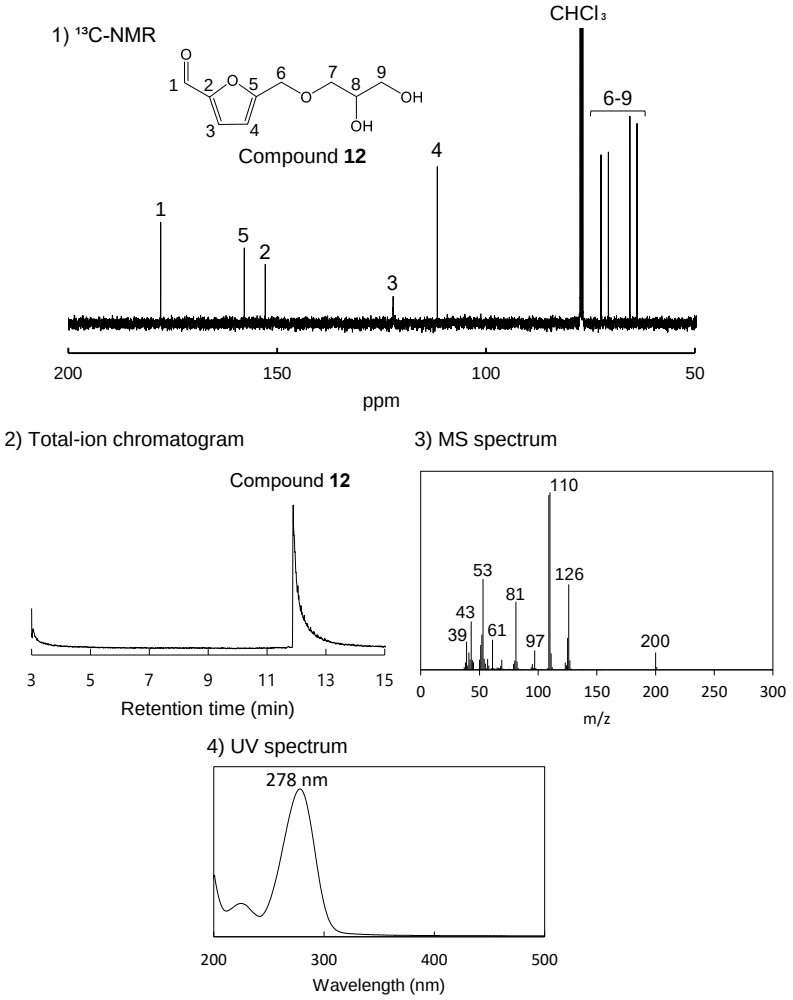

Figure 4-8. A) ^{13}C-NMR spectrum, B) total-ion chromatogram, C) MS spectrum and D) UV spectrum of compound **12**

Polymerization, dimerization, and coupling reactions between glycerol and 5-HMF would occur via the mechanisms shown in Figure 4-9. The OH group on 5-HMF is removed, assisted by electron donation from the oxygen in the furan ring. The resulting oxonium intermediate is attacked by the hydroxyl groups of 5-HMF and glycerol to form dimer **11** and glycerol-adduct **12**, respectively. In the absence of glycerol, the homopolymer of 5-HMF (5-HMF char) formed as a glassy solid substance through nucleophilic addition of 5-HMF, containing several nucleophilic sites, to the oxonium intermediate.

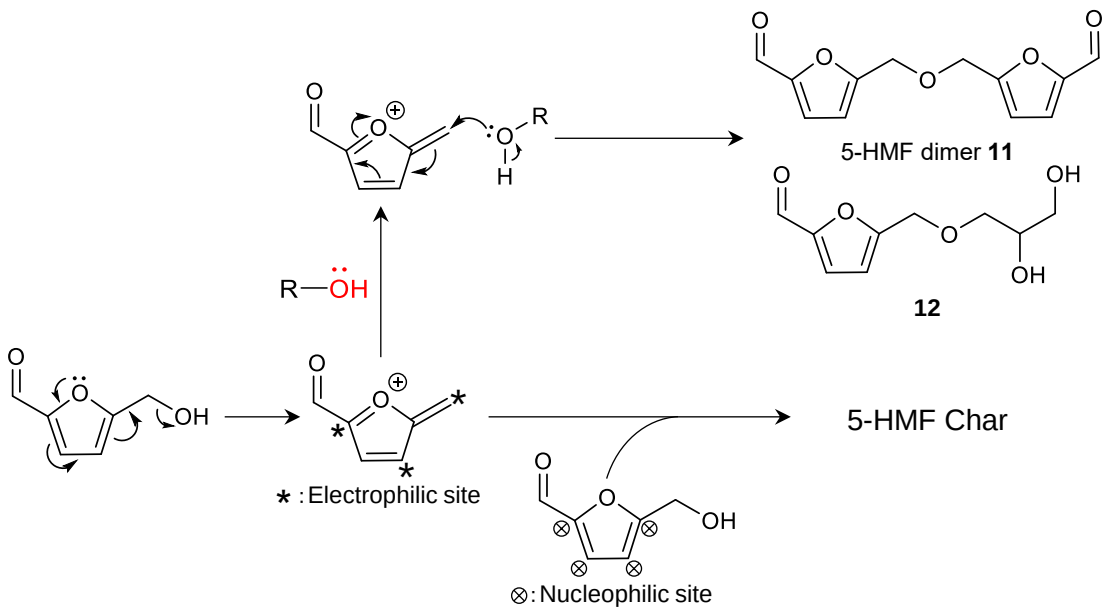

Figure 4-9. Proposed condensation mechanisms of 5-HMF during heat treatment.

4.3.3 Conversion of 5-HMF in the presence of glycerol

In actual cellulose pyrolysis, 5-HMF coexists with other pyrolysis products, including carbohydrates, such as LG, oligosaccharides, and anhydro-oligosaccharides, fragmentation products, and water. Therefore, the influence of these coexisting materials on the carbonization of 5-HMF must be considered. However, when these compounds are mixed with 5-HMF, it is difficult to determine which lead to the formation of carbonized products. Therefore, glycerol and water were selected to be mixed with 5-HMF to obtain reaction conditions closer to that of actual cellulose. Glycerol contains three hydroxyl groups, but was stable at 280 °C.

A mixture of 5-HMF (500 mg) and glycerol (4.0 g) was heated at 280 °C for 60 min, and solid char was obtained by washing with water and then oven-drying. Figure 4-10 shows the appearance and IR spectrum of the resulting char, which was compared with those prepared from cellulose and pure 5-HMF. The char produced in the presence of glycerol is denoted as 5-HMF char (glycerol). By mixing with glycerol, the signals assigned to 5-HMF moieties disappear completely, with two signals appearing at 1600

and 1700 cm^{-1}, which are characteristic of cellulose carbonization. These results indicated that the carbonization reactions of 5-HMF moieties dispersed in the 5-HMF char (glycerol) proceeded efficiently, in contrast to the previously described hard glassy 5-HMF char.

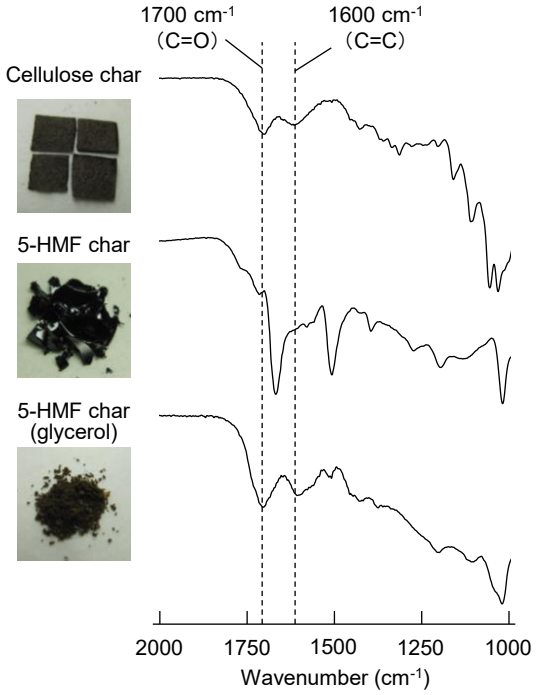

Figure 4-10. IR spectra of char fractions obtained from the pyrolysis of cellulose and 5-HMF at 280 °C for 60 min.

4.3.4 Acidic group determination

Table 4-1 summarizes the results of acidic group titration performed using the Boehm method. This allowed carboxylic acids, phenolic acids, and lactones (carboxyesters) to be quantified separately according to the alkalinity of the solution used for neutralization. Although the relative compositions were different, carboxylic acids, lactones, and phenols were detected in certain amounts from cellulose char and 5-HMF char (glycerol). Consequently, the formation of these functional groups, which are characteristic of cellulose carbonization (Cheng et al., 2006; Chun et al., 2004; Fidel et

al., 2013; Kang et al., 2012; Saha et al., 2019), also occurred by heating 5-HMF in the presence of glycerol.

The formation of carboxylic acids and esters was also confirmed by changes in the IR spectrum caused by neutralization (Figure 4-11). The signal at 1700 cm^{-1}, assigned to carboxyl (COOH) and lactone (–COO–) groups, showed reduced intensity, while signals appeared at 1375 and 1550 cm^{-1}, assigned to carboxylate (COO^{-}) groups.

The IR spectrum of the 5-HMF char (Figure 4-1) prepared from pure 5-HMF

Table 4-1. Contents of acidic groups in cellulose and 5-HMF char.

(mmol/g)

	Carboxylic acid	Lactone	Phenol
Cellulose char	0.556	0.177	2.68
5-HMF char	nd	nd	nd
5-HMF char (glycerol)	0.104	0.273	0.169

nd: not detected

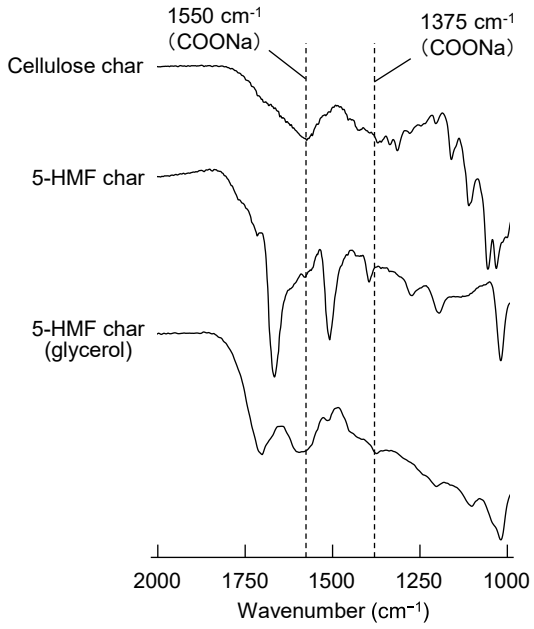

Figure 4-11. IR spectra of cellulose char and 5-HMF char (280 °C, 30 min) after alkali treatment.

contained signals that indicated the formation of carboxylic acids, but these groups could not be titrated (Table 4-1). The IR spectrum also did not change under treatment with alkaline solution (Figure 4-11). These results indicated that alkaline solution might not be able to penetrate inside the glassy 5-HMF char.

4.3.5 Py-GC/MS analysis

The chemical structure of char obtained from 5-HMF was evaluated by Py-GC/MS analysis, which was performed at 764 °C with a solid heating period of 5 s. Substructures formed in the char were expected to be released and identified using this method. Figures 4-12 and 4-13 show the total-ion chromatograms (pyrograms) and chemical structures of the compounds identified, respectively.

When a mixture of 5-HMF and glycerol was directly analyzed by Py-GC/MS without prepyrolysis, large signals of 5-HMF and glycerol were observed, along with a relatively small peak assigned to methylfurfural (**13**). Therefore, most 5-HMF and glycerol evaporated without suffering thermal degradation, although methylfurfural was formed by cleavage of the C–OH bond in 5-HMF through Py-GC/MS analysis.

In the pyrogram of 5-HMF char, the large 5-HMF signal disappeared and methylfuran (**1**) and dimethylfuran (**2**) were produced as furanic compounds, along with methylfurfural (**13**). This indicated that 5-HMF reacted to form other furan-type structures. The formation of benzene-type (benzene (**3**), toluene (**4**), and naphthalene (**5**)) and benzofuran-type (methylbenzofuran (**6**)) compounds indicated that benzene rings were formed in the 5-HMF char, as these types of product were not detected in the pyrogram of 5-HMF + glycerol (untreated).

By adding glycerol, the number of products detected in the pyrogram increased, and methylfurfural (**13**), observed as a large signal in the 5-HMF char, disappeared completely. These results confirmed that carbonization reactions of 5-HMF proceeded efficiently by dilution with glycerol. The formation of furanic compounds **14**–**18** also confirmed that condensation reactions of 5-HMF occurred. Indene (**21**) and phenol (**19**

and **22**) were also detected, which are known to be substructures of carbonized products from cellulose (Pastorova et al., 1994). Phenol formation was consistent with the acid titration results.

4.3.6 Role of 5-HMF in cellulose carbonization mechanism

Natural cellulose is a cellular substance with a cell wall several micrometers thick that is an aggregate of hundreds of crystallites (6 × 6 nm, in cross section (Elazzouzi-Hafraoui et al., 2008)). Based on X-ray diffraction analysis (Kawamoto and Saka, 2006; Kim et al., 2001; Zickler et al., 2007), the thermal degradation of cellulose crystallites is thought to begin with surface molecules, while the internal molecules are stable. Furthermore, thermal degradation of cellulose was reported to be delayed significantly by removing the reducing end through $NaBH_4$ reduction or thermal glycosylation with glycerol (Matsuoka et al., 2011a, 2011b, 2014). Consequently, on a nanoscale, the thermal degradation of cellulose proceeds heterogeneously in the cell wall volume, although our previous work on observing cellulose carbonization using UV microscopy showed that cellulose carbonization progressed uniformly within the cell wall volume at a resolution of 280 nm (Nomura et al., 2020). These results indicated that pyrolysis begins heterogeneously, but with the area evenly distributed within cell wall. Accordingly, a carbonization reaction mechanism was proposed, as shown in Figure 4-14.

The first event when heating cellulose is a decrease in the degree of polymerization (DP) to around 200, which corresponds to the size of cellulose crystallites in the length direction (Broido, Javier-Son, Ouano, Barrall, et al., 1973; F Shafizadeh and Bradbury, 1979). The reducing end of the cellulose crystallite then decomposes, because it is more reactive to thermal decomposition than other repeating and non-reducing end groups (Matsuoka et al., 2011b, 2014). Our previous report (Matsuoka et al., 2014) indicated that this process initiates the thermal degradation of cellulose by forming pyrolysis products at the crystallite interface. 5-HMF is among these pyrolysis products, and its formation is reasonably attributed to the reducing ends via the chain structure,

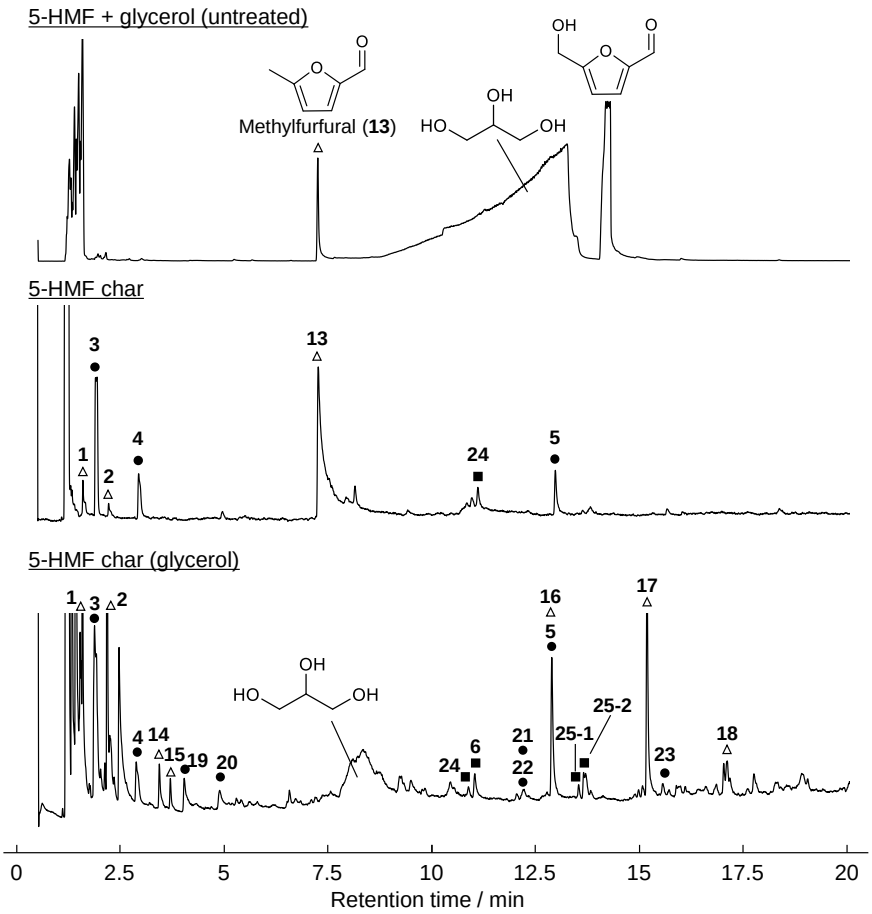

Figure 4-12. Pyrograms obtained by Py-GC/MS analysis (764 °C, 5 s) of 5-HMF char obtained by pyrolysis at 280 °C for 60 min.

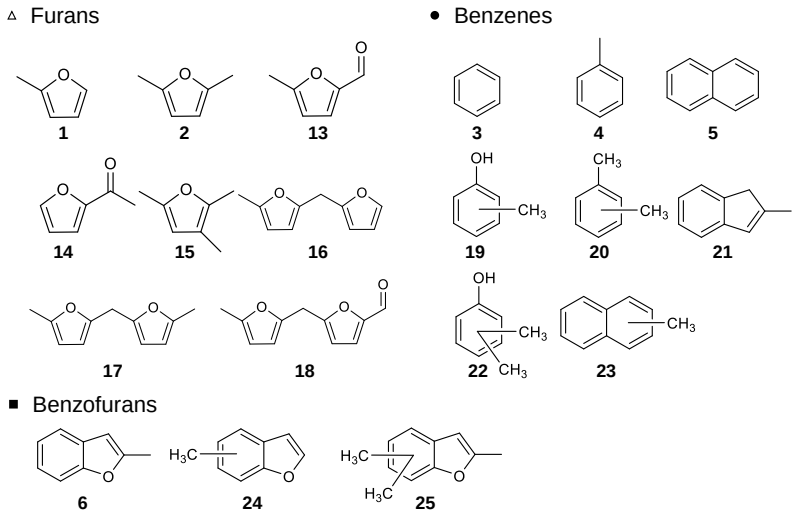

Figure 4-13. Chemical structures of products identified in Py-GC/MS analysis (764 °C, 5 s) of 5-HMF char obtained by pyrolysis at 280 °C for 60 min.

which is efficiently dehydrated via six-membered transition states.(Fukutome et al., 2016; Nimlos et al., 2006) This pathway produces 2 mol of water that hydrolyzes cellulose, generating new reducing ends.(Matsuoka et al., 2014) Therefore, as these reactions proceed, the thermal degradation of cellulose accelerates exponentially.

The present experimental results indicated that the 5-HMF produced was diluted by other degradation products, with their coupling reaction inhibiting formation of a stable homopolymer. Under such conditions, the 5-HMF moiety is efficiently converted into benzene, benzofuran, and indene-type structures, reported as substructures of solid carbonized products.(Julien et al., 1991; Nomura et al., 2020; Pastorova et al., 1994; Sekiguchi and Shafizadeh, 1984; Fred Shafizadeh and Sekiguchi, 1983; Smith and Howard, 1937; Soares et al., 2001)

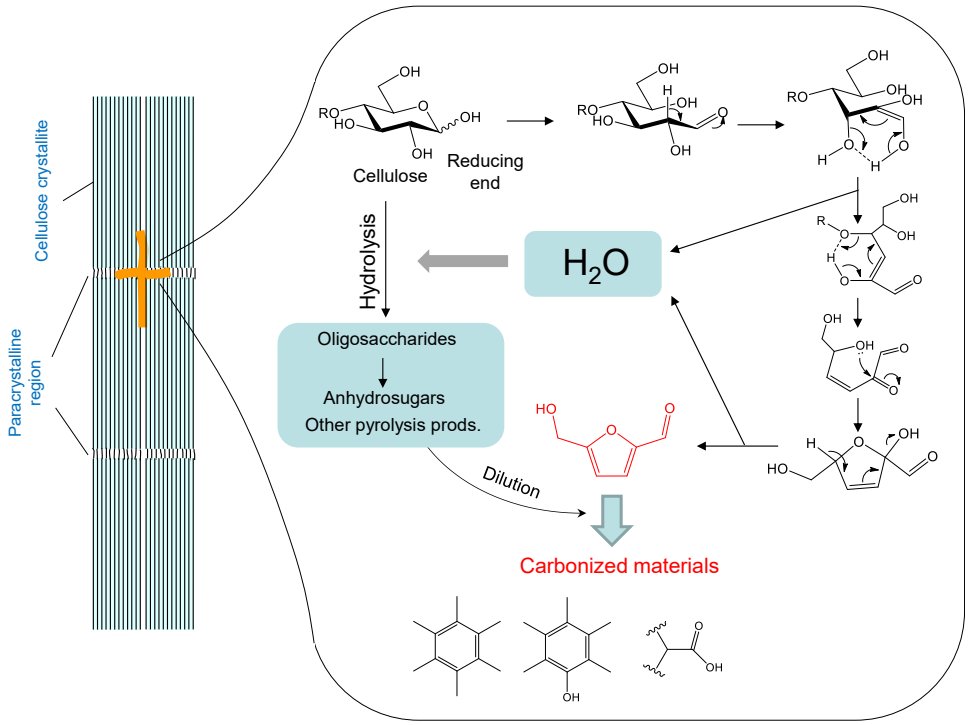

Figure 4-14. Proposed cellulose carbonization mechanism focusing on the cell wall ultrastructure and role of 5-HMF.

Acidic groups, such as carboxylic acids and phenols, are also produced. These acidic groups accelerate cellulose carbonization by catalyzing hydrolysis and dehydration reactions. Consequently, to suppress carbonization, the initial reactions caused by degradation of the reducing end should be prevented. The use of aromatic solvents to effectively suppress the secondary pyrolysis reaction caused suppression of the cellulose carbonization by up to 30% conversion, but control was difficult once carbonization had started.(Nomura et al., 2017)

4.4 Conclusions

The pyrolysis reactivity of 5-HMF was investigated to determine its role in cellulose carbonization. We found that 5-HMF was converted to stable glassy materials by hydroxyl group removal, while subsequent carbonization reactions were very slow. Furthermore, pyrolysis of 5-HMF in the presence of glycerol, a model of coexisting pyrolysis products, gave the coupling product in a certain yield, which indicates that 5-HMF formed during cellulose pyrolysis binded with other coexisting products, such as anhydrosugars and oligosaccharides. Additionally, upon pyrolysis with glycerol, the 5-HMF moiety was converted to benzene, benzofuran, and indene-type structures, along with carboxylic acids, phenols, and carboxyesters. These are characteristic structures of carbonized cellulose, which suggests that 5-HMF is an intermediate in cellulose carbonization. Finally, a cellulose carbonization mechanism was proposed and discussed, focusing on the ultrastructure of the cellulose cell wall. Reducing ends might have an important role in the formation of 5-HMF. The carbonization reaction might be accelerated by the action of water and acidic groups generated during carbonization.

Chapter 5

Benzene-ring structure formation via 5-HMF in cellulose carbonization

5.1 Introduction

Chemically and physically stable cellulosic biomass resources are efficiently decomposed by pyrolysis technologies. The pyrolysis products, bio-char, bio-oil and bio-gas, are expected to be used as fuel and chemical sources. However, the low product selectivity limits the practical application of thermochemical conversion technologies. Therefore, it is important to understand and control the pyrolysis reactions. For example, promoting carbonization reactions improves the selectivity of bio-char. On the other hand, the yields of bio-oil or bio-gas can be increased by suppressing carbonization reaction. In present article, we focus the carbonization reaction of cellulose.

In *Chapter 2*, cellulose (Whatman No.42 filter paper) was pyrolyzed in various aromatic solvents at 280 °C. The carbonization of cellulose was markedly suppressed, and the yields of LG and 5-HMF increased considerably. Interestingly, a negative correlation was found between the yields of 5-HMF and char. This fact implies that 5-HMF has a crucial role in the cellulose carbonization.

Furthermore, the solid carbonized product from 5-HMF was studied by using FT-IR, Py-GC/MS and acid titration analysis in *Chapter 4*. From these results, we proposed cellulose carbonization mechanism via 5-HMF (Chapter 4). In this Chapter, benzene ring formation mechanism was investigated by conducting pyrolysis of $^{13}C-$ labeled 5-HMF and ^{13}C-labeled glucose. Based on the obtained results, the carbonization mechanism of cellulose via 5-HMF is discussed.

5.2 Materials and methods

5.2.1 Materials

5-HMF (>95.0%, GC) was purchased from Tokyo Chemical Industry (Tokyo, Japan). Before experiments, water was removed from 5-HMF by freeze-drying. D-[1-^{13}C] glucose, D-[2-^{13}C] glucose, D-[6-^{13}C] glucose (>99.8%, HPLC), glycerol (>98.0%, GC) and Acetonitrile (>99.0%, GC) were purchased from Nacalai Tesque, Inc. (Kyoto, Japan) and used without purification. 1-butyl-3-methylimidazolium chloride (>98.0%, HPLC) and 12-molybdophosphoric acid were purchased from Wako Pure Chemical Industries, LTD (Osaka, Japan).

The ^{13}C-labeled 5-HMF was synthesized from the corresponding ^{13}C-labeled glucose according to the previous literature (Chidambaram and Bell, 2010). Acetonitrile (0.79 g) was mixed with 1-butyl-3-methylimidazolium chloride (2.0 g) at 60 °C. ^{13}C-labeled Glucose (180 mg) was then added to this solution and stirred until completely dissolved. Finally, 12-molybdophosphoric acid (18 mg) was introduced. The flask was sealed and heated to 120 °C. Reaction was continued for 3 h, the sample was cooled to room temperature, and 2 ml of water was added. The sample was neutralized with 0.0233 mmol of sodium carbonate and extracted with 5 × 10 ml of ethyl acetate and treated with excess sodium sulfate (Na_2SO_4) to remove the water. Using thin layer chromatography (TLC; 5 % MeOH/$CHCl_3$), the ^{13}C-labeled 5-HMF was isolated and identified.

5.2.2 Pyrolysis

The mixture of ^{13}C-labeled 5-HMF (5 mg) and glycerol (40 mg), or ^{13}C-labeled glucose (5 mg) was placed in a Pyrex glass tube ample (internal diameter 15.0 mm, wall thickness 1.75 mm, length 50 mm). The air inside the reactor was replaced with nitrogen (99.99%) before sealing the ample. The ample was inserted into a muffle furnace preheated to 280 °C. After heat treatment for 60 min, the reactor was taken out from the

furnace and immediately cooled with airflow. The residue (char) was washed with water, then dried in an oven at 105 °C for 24 h.

5.2.3 Py-GC/MS analysis

Py-GC/MS analysis of the 5-HMF char and glucose char was conducted using a portable Curie-point injector (JCI-22, Japan Analytical Industry, Tokyo, Japan) coupled with a gas chromatography-mass spectrometry (GCMS-QP2010 Ultra, Shimadzu Co., Kyoto Japan). The char was rapidly heated to 764 °C, and the temperature was held for 5 s. The GC/MS conditions were set as follows: column; Agilent CPSil 8CB (length: 30 m, diameter: 0.25 mm, Agilent Technologies, Santa Clara, CA, USA), injector temperature; 250 °C, split ratio; 1:50, column temperature; 50 °C (3 min), 6 °C/min to 200 °C, 30 °C/min to 300 °C, 300 °C (5 min), carrier gas; helium, flow rate; 1.0 mL/min. Unlabeled and ^{13}C-labeled glucose was analyzed by Py-GC/MS analysis for 15 seconds at 280 °C heated with the portable Curie point injector.

5.3 Results and discussion

5.3.1 Py-GC/MS analysis of glucose

Unlabeled and ^{13}C-labeled glucose was analyzed by Py-GC/MS analysis for 15 seconds at 280 °C heated with the portable Curie point injector. Figure 5-1 shows the total-ion chromatograms (pyrograms) of the pyrolysis products from glucose. The major products were furfural and 5-HMF. Since glucose is a reducing sugar, conversion to furans via chain structure would proceed easily.

The mass spectra of furfural and 5-HMF from unlabeled glucose, D-[1-^{13}C] glucose, D-[2-^{13}C] glucose and D-[6-^{13}C] glucose is shown in Figure 5-2. From unlabeled glucose, 5-HMF (m/z=126) and furfural (m/z=96) were detected. Fragment ion at m/z=97 was observed in the MS spectrum of 5-HMF. Perez et al. reported that CHO (m/z=29)

was eliminated from the aldehyde group or hydroxymethyl group of 5-HMF to form the ion at m/z=97 (Perez Locas and Yaylayan, 2008). The fragment ion at m/z=67 was obtained from furfural, which was due to the elimination of aldehyde group. In the mass spectra of 5-HMF and furfural produced from D-[2-^{13}C] glucose, the m/z of all fragment ions is increased to +1. This indicates that 5-HMF incorporates the C-2 of glucose into furan ring. The furfural at m/z=97 was generated from D-[1-^{13}C] glucose. In addition, the m/z of fragment ion of furfural from D-[1-^{13}C] glucose was 67, which is same to the furfural from unlabeled glucose. These results indicate that C-1 of glucose was incorporated into the aldehyde group of furfural and 5-HMF. The furfural (m/z=96), which include no ^{13}C, was obtained from D- [6-^{13}C] glucose. On the other hand, the m/z of 5-HMF from D- [6-^{13}C] glucose was 127, which indicates the 5-HMF include one ^{13}C. Therefore, 5-HMF incorporates the C-6 of glucose into the hydroxymethyl group. During the fragmentation of 5-HMF, the aldehyde group was released more easily compared to hydroxymethyl group. The ratio at m/z=97 and 98 was reversed between 1-C and 6-C labeled glucoses (Perez Locas and Yaylayan, 2008). Based on these results, the carbons of 5-HMF are numbered in the manner corresponding to the carbon of glucose as shown in Figure 5-3 in this dissertation.

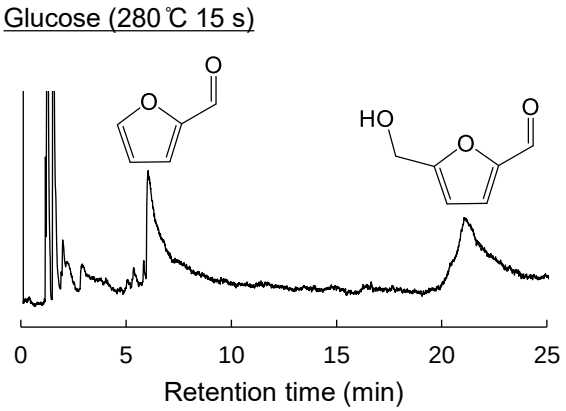

Figure 5-1. Pyrograms obtained by Py-GC/MS analysis (280 °C, 15 s) of glucose.

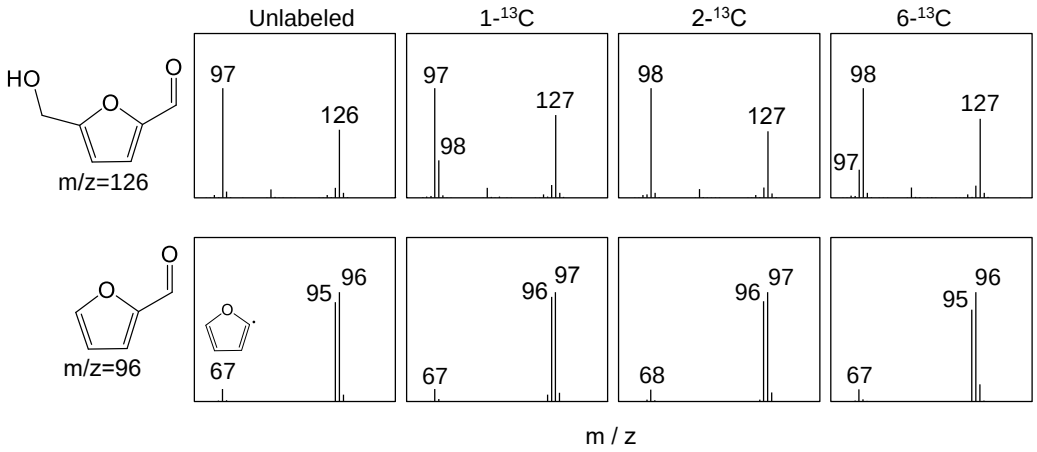

Figure 5-2. MS spectra of 5-HMF and furfural from unlabeled and labeled glucose.

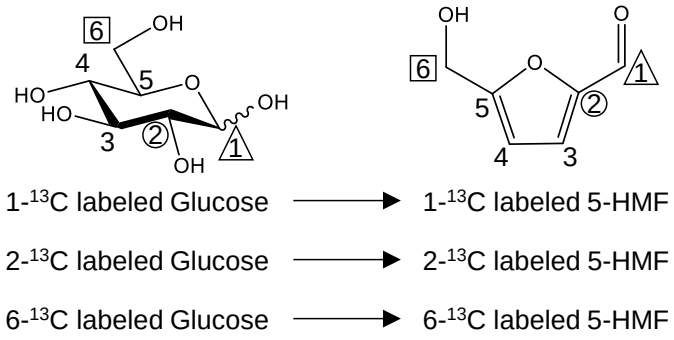

Figure 5-3. Numbering of glucose and 5-HMF in this dissertation.

5.3.2 Py-GC/MS analysis of 5-HMF char

Unlabeled and ^{13}C labeled 5-HMF or glucose were pyrolyzed at 280 °C for 60 min. The chemical structure of char obtained from 5-HMF and glucose were evaluated by Py-GC/MS analysis at 764 °C for 5 s. In this analysis, a part of the char is decomposed to obtain the products, which reflects the chemical substructure of char. Figures 5-4 and 5-5 show the pyrograms and chemical structures of the compounds identified, respectively.

Furan-, benzene- and benzofuran-type compounds were produced from both 5-HMF char and glucose char. The compounds from 5-HMF char were very similar to the results obtained in our previous study (Figures 5-4 and 5-5) (*Chapter 4*). The formation of furan-type compounds from glucose char indicates that the benzene-ring structures

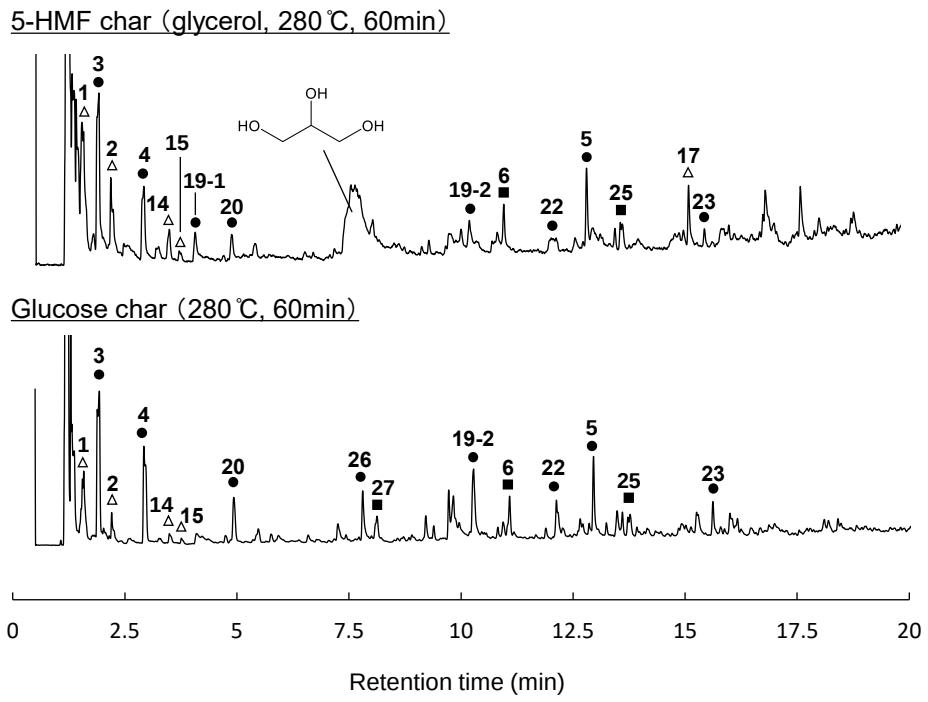

Figure 5-4. Pyrograms obtained by Py-GC/MS analysis (764 °C, 5 s) of 5-HMF char and glucose char obtained by pyrolysis at 280 °C for 60 min.

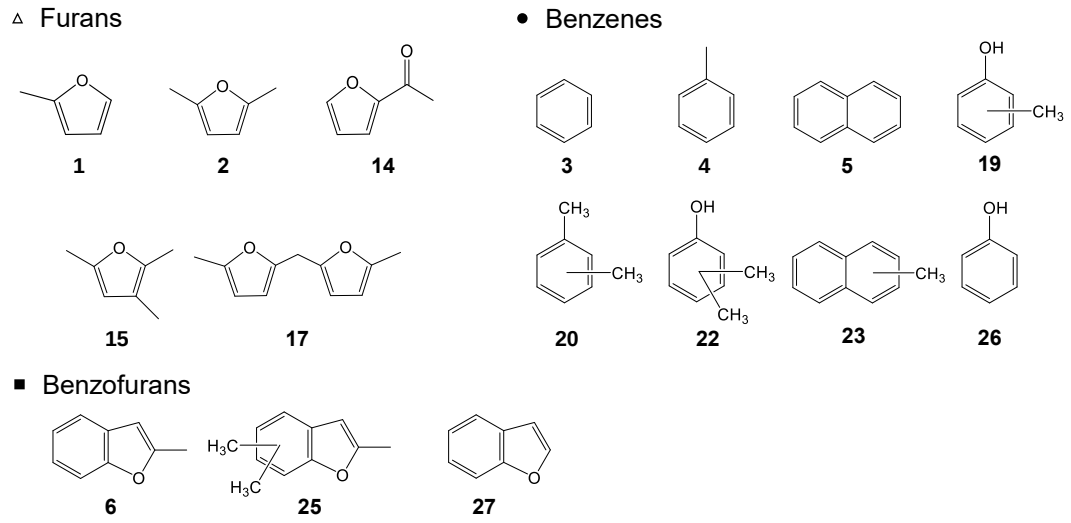

Figure 5-5. Chemical structures of products identified in Py-GC/MS analysis (764 °C, 5 s) of 5-HMF char and glucose char obtained by pyrolysis at 280 °C for 60 min.

formation via furan-rings might proceed in the case of pyrolysis of glucose. Because these pyrolysis products are also obtained from cellulose char, the 5-HMF char and glucose char could be used as a model of cellulose char (Nomura et al., 2020; Pastorova et al., 1994).

Figure 5-6 shows the MS spectra of pyrolysis products generated from 5-HMF char. From these MS spectra, ^{13}C incorporation rate of the products are calculated (Figure 5-7). In this figure, +x means the number of ^{13}C atom incorporated into the obtained products from 5-HMF char.

The peak of MS spectra of dimethylfuran (**2**), which was produced from ^{13}C-labeled 5-HMF char, was shifted +1 (m/z=96→m/z=97). This result is very similar to the MS spectra of furfural and 5-HMF shown in Figure 5-2, which indicates that most of the dimethylfuran generated from ^{13}C labeled 5-HMF char contains one ^{13}C atom (Figure 5-7). Although ^{13}C was not introduced in some cases due to the desorption of one carbon, many methylfuran (**1**) also contains one ^{13}C atom (+1). These results suggest that the furan structure contained in the 5-HMF char is directly derived from the structure of 5-HMF.

On the other hand, for benzenes (benzene (**3**), toluene (**4**) and naphthalene (**5**)), one ^{13}C incorporation rates (+1) were not high. Much of benzene (**3**) and toluene (**4**) have no ^{13}C labels. If the benzene structure was directly produced from 5-HMF, it must include only one ^{13}C. Therefore, the direct formation of benzene ring from the furan ring would not be dominant. Figure 5-8 shows the possible formation pathway of benzene-ring structure via reactive fragments, which are the model intermediate. After 5-HMF polymerization with other compounds, the furan-ring would be cleaved by addition reaction of water. Further reactions proceed, and reactive fragments thought to be produced. These fragments may contribute to the benzene-ring structure formation. Because the reactive fragments might randomly condensate to form benzene structure, the benzenes which include 0-3 ^{13}C atoms were obtained from ^{13}C labeled 5-HMF char.

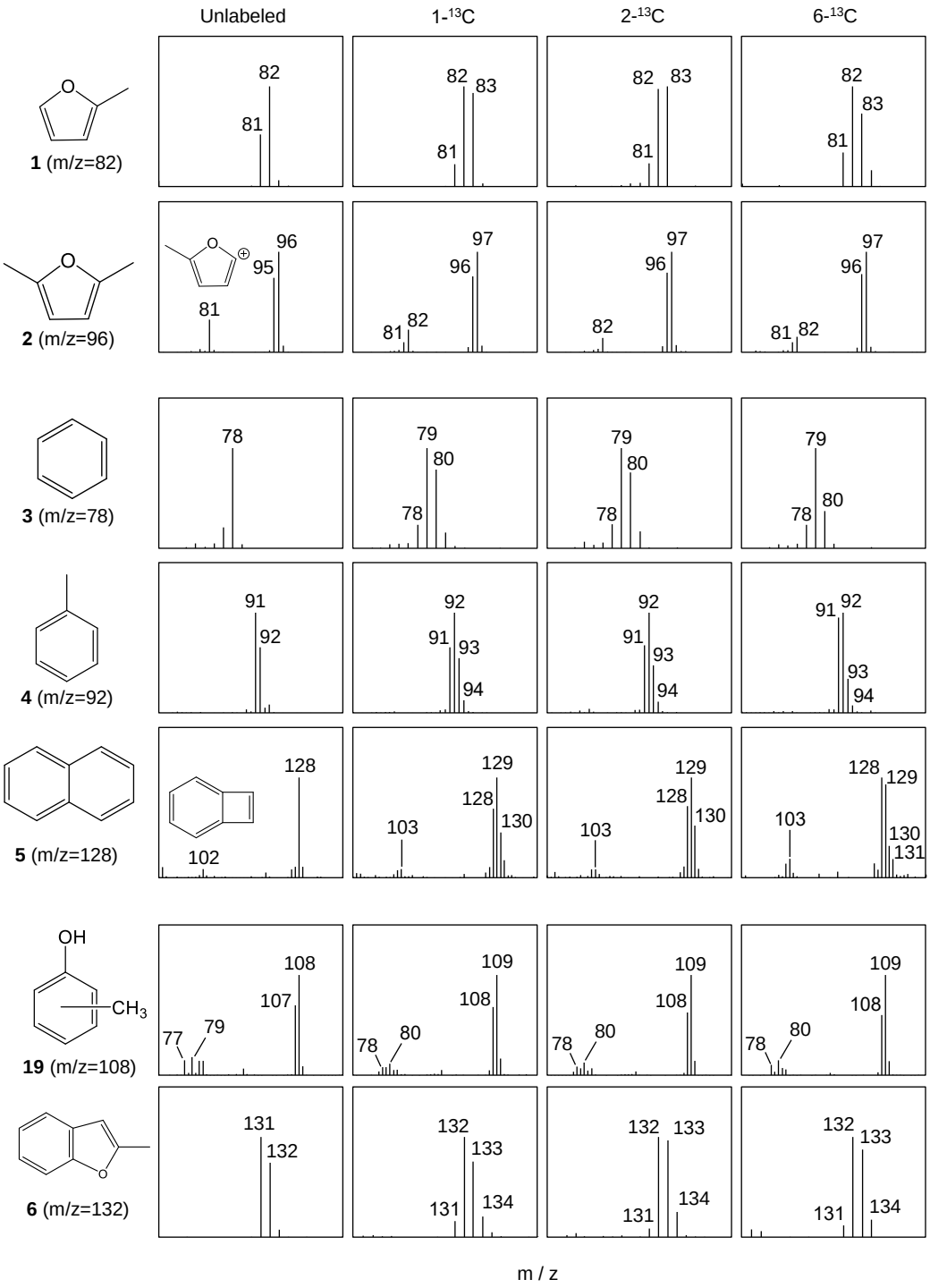

Figure 5-6. MS spectra of pyrolysis products obtained by Py-GC/MS analysis (764 °C, 5 s) of unlabeled and labeled 5-HMF char obtained by pyrolysis at 280 °C for 60 min.

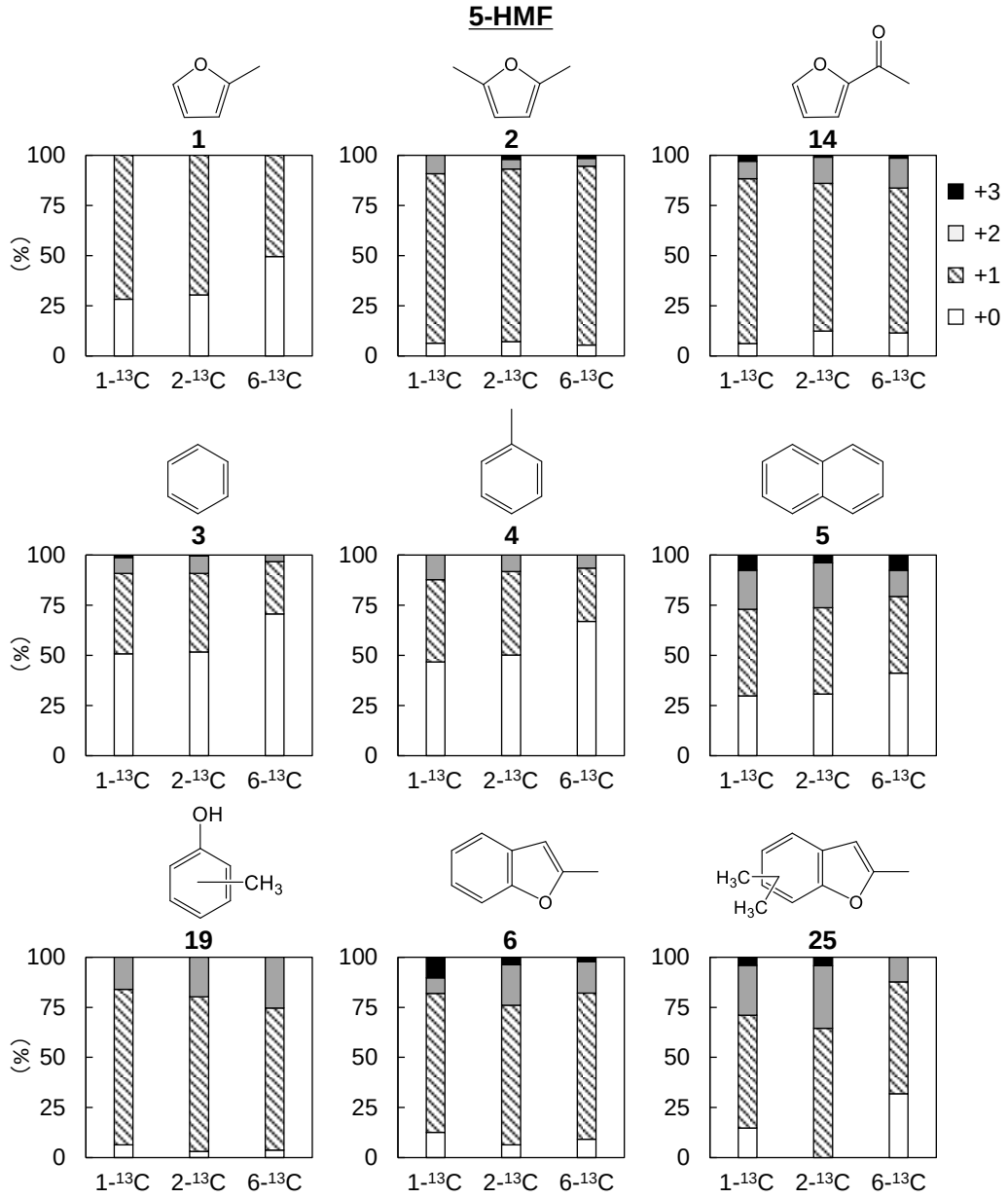

Figure 5-7. Number of ^{13}C atoms incorporated into pyrolysis products after pyrolysis of ^{13}C-labeled 5-HMFs.

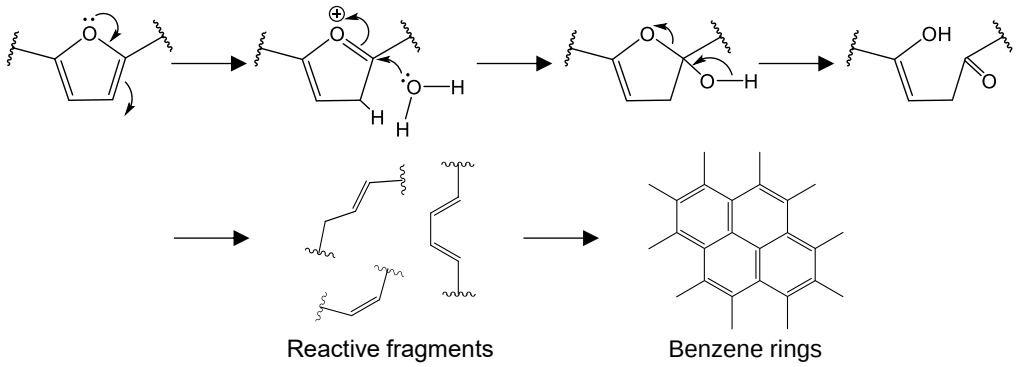

Figure 5-8. Benzene-type structure formation pathway via reactive fragments from furan ring

Many benzofurans (**6** or **25**) contain one ^{13}C atom (+1), because the furan ring of benzofurans would be directly derived from 5-HMF. Figure 5-9 shows the possible benzofurans formation pathways. Diels-Alder reaction between furan-ring and the reactive fragment produced by cleavage of furan ring might proceed. After elimination of hydrogen for benzene-ring formation, the benzofurans are thought to be produced.

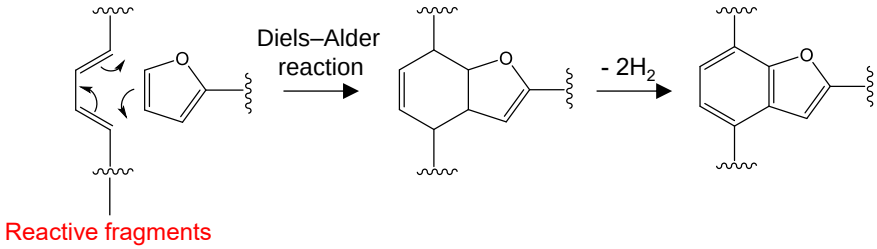

Figure 5-9. Benzofuran-type structure formation pathway.

Different from benzenes, methylphenol (**19**) mostly includes one ^{13}C (+1), suggesting that there is a direct pathway from 5-HMF or 5-HMF polymer into phenol structures. The production pathway of phenols was investigated from the MS spectra of methylphenol (**19**). Figure 5-10 shows a partial enlargement of the MS spectra of methylphnols (**19**) and its fragment ions. Unlabeled methylphenol (**19**) includes the signals at m/z=77 and 79. These fragment ions were produced by elimination of protons

and CO via 7-membered ring formation shown in Figure 5-10 (Silverstein, 1986). In this fragmentation pathway, the carbon atom connected to hydroxy group is desorbed as CO. In the MS spectra of methylphenol (**19**) from 1-^{13}C labeled 5-HMF char and 2-^{13}C labeled 5-HMF char, the fragment ions of m/z=77-80 were observed, which indicate some of ^{13}C atom was eliminated by desorption of CO. On the other hand, the fragment ions of m/z=78 and 80 were mainly observed from the methylphenol (**19**) produced from 6-^{13}C labeled 5-HMF char, which indicates the carbon from the 6th carbon of 5-HMF was not released as CO. These results suggested that the carbons of methylphenol derived from 1st and 2nd carbons of 5-HMF were connected to hydroxy group, but the carbon derived from 6th carbon of 5-HMF was not connected to hydroxy group. From these results, the mechanism of phenol production was proposed (Figure 5-11). After pushing the lone pair of electrons to remove the hydroxyl group, water reacts the 2nd carbon of 5-HMF. After opening the furan ring, the 6th carbon was connected with 1st carbon, which is assisted by the electron push of oxygen. The benzene ring is formed by a reaction that changes from the keto type to the enol type. These reactions then form phenol, which binds the hydroxyl groups to the first and second carbons, but not the hydroxyl groups to the sixth carbon. This proposal is consistent with the mass spectra shown in Figure 5-10.

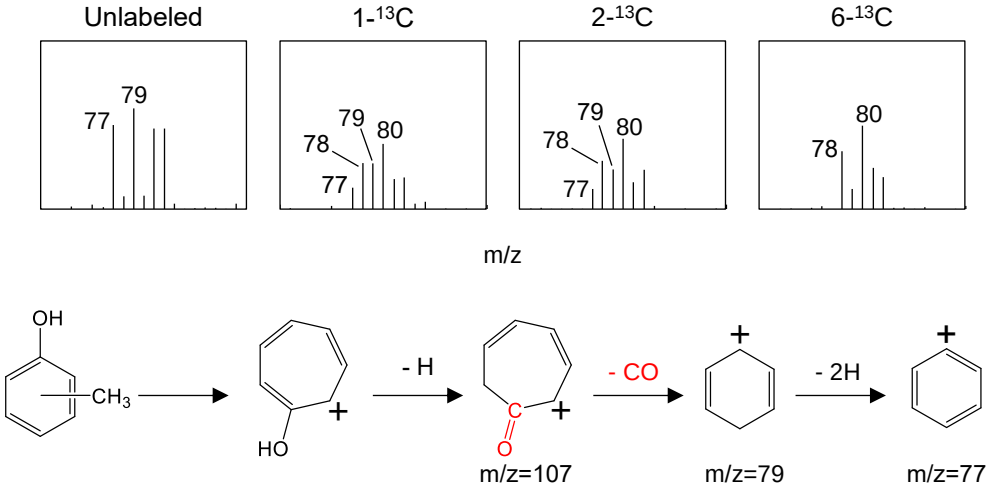

Figure 5-10. Enlarged view of MS spectra of methylphenol form 5-HMFs and the possible generating pathway of fragments.

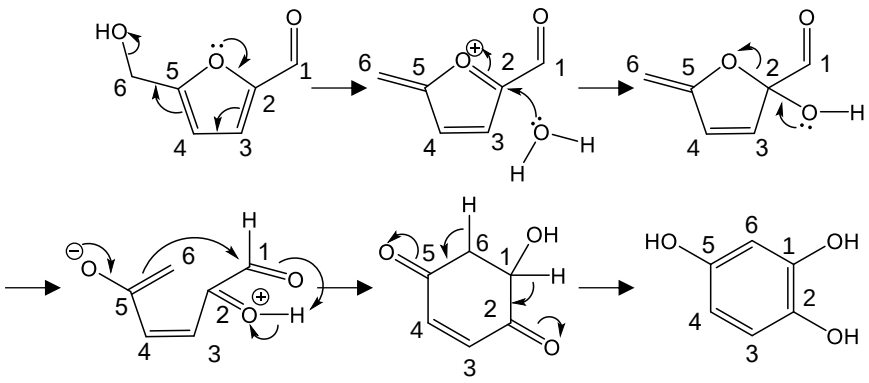

Figure 5-11. Phenol production pathway from 5-HMF.

5.3.3 Py-GC/MS analysis of glucose char

The MS spectra and ^{13}C incorporation rate of the products from unlabeled and ^{13}C labeled glucose char were shown in Figures 5-12, 5-13. As same as the results of 5-HMF, the furan-type compounds generated from ^{13}C labeled glucose char contains roughly one ^{13}C atom. This supports that the direct pathway of furan-ring formation from glucose. In addition, one ^{13}C atom incorporation rate of benzenes was not higher than that of furans. Even from glucose, the benzene-ring structures also might be produced via reactive fragments. On the other hand, one ^{13}C incorporation rate (+1) of phenols was not high, which was different from 5-HMF char. This suggest that there is another pathway for phenols production, which is not proceeded via 5-HMF. The fragments would be produced directly from glucose for generating benzene-ring structures. However, the pathways are unclear and further studies are needed.

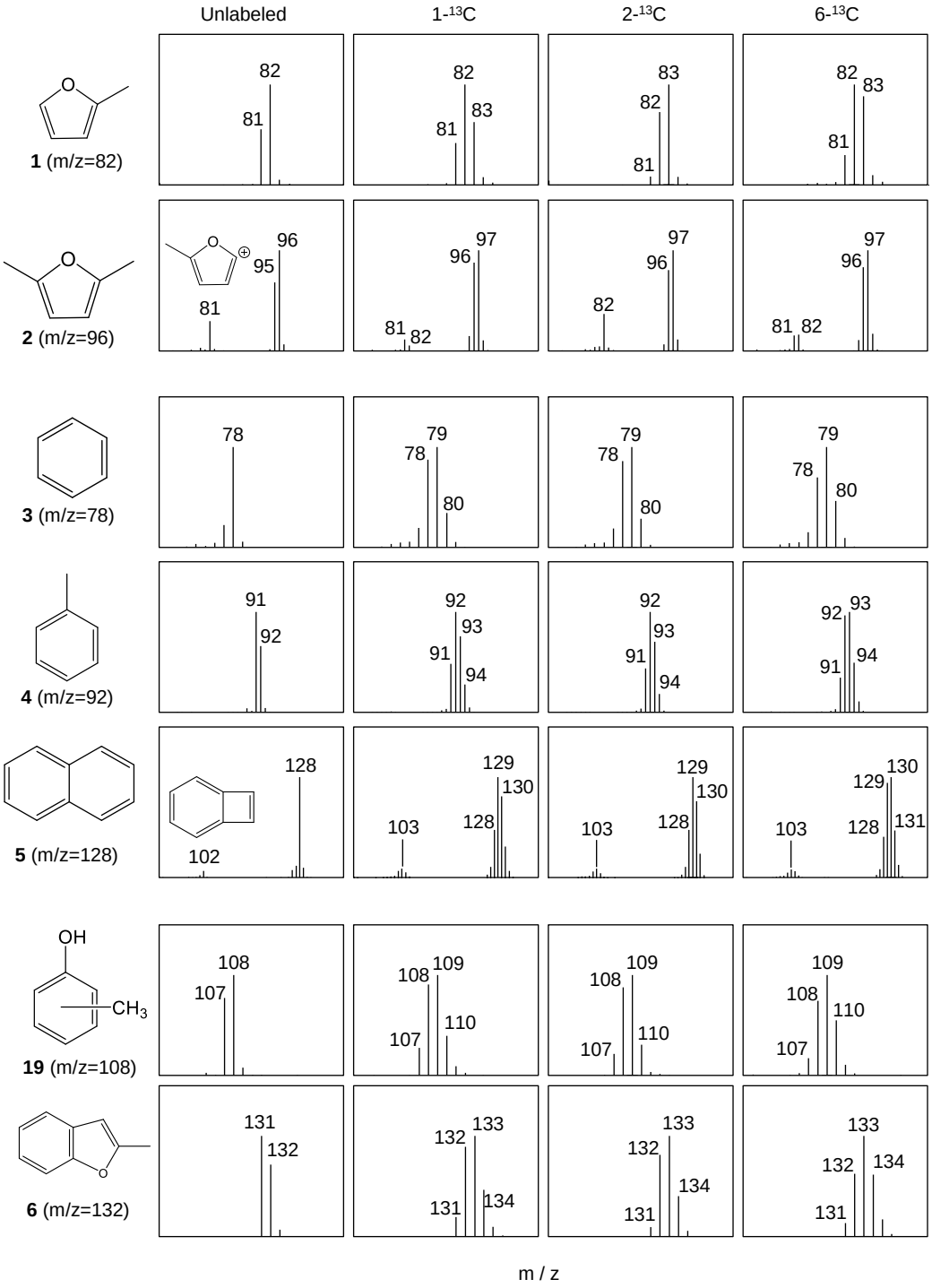

Figure 5-12. MS spectra of pyrolysis products obtained by Py-GC/MS analysis (764 °C, 5 s) of unlabeled and labeled glucose char obtained by pyrolysis at 280 °C for 60 min.

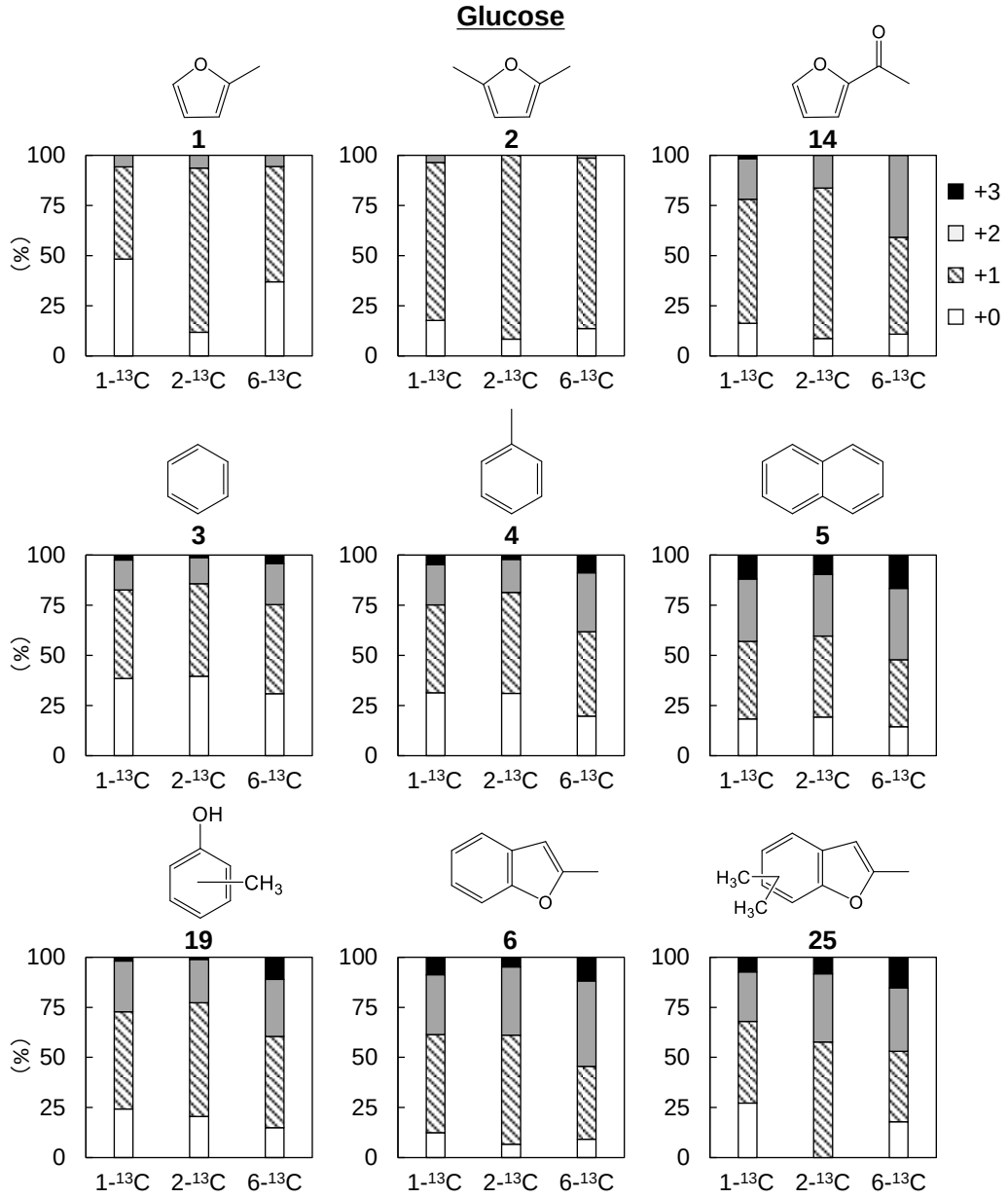

Figure 5-13. Number of ^{13}C atoms incorporated into pyrolysis products after pyrolysis of ^{13}C-labeled 5-HMFs.

5.3.4 Role of 5-HMF in benzene-ring structure formation in cellulose carbonization

Cellulose fiber consists of hundreds of cellulose crystallites (6 × 6 nm, in cross section (Elazzouzi-Hafraoui et al., 2008)). Observation of the pyrolyzed cotton cellulose using ultraviolet (UV) microscopy revealed that the carbonization reactions progressed uniformly within the cell wall at a resolution of 280 nm (Nomura et al., 2020). However, X-ray diffraction analysis of pyrolyzed cellulose showed that thermal degradation of cellulose crystallites was suggested to start with surface molecules, while the internal molecules are stable (Kawamoto and Saka, 2006; Kim et al., 2001; Zickler et al., 2007). On the other hand, the reducing end of cellulose was reported to exhibit much greater pyrolytic reactivity, because the pyrolysis reactions were delayed significantly by eliminating the reducing end through $NaBH_4$ reduction or thermal glycosylation with glycerol (Matsuoka et al., 2011a, 2011b, 2014). Consequently, thermal degradation reactions of cellulose were proceeded heterogeneously on a nanoscale. We proposed a carbonization and benzene formation mechanism as shown in Figure 5-14.

The first event in thermal decomposition of cellulose is a decrease in the DP to around 200, which produced new reducing ends (Broido, Javier-Son, Ouano, Barrall, et al., 1973; F Shafizadeh and Bradbury, 1979). From the reducing ends, pyrolysis products, such as oligosaccharides, anhydrous sugars, 5-HMF or water, are produced. Since cellulose consists of huge number of crystallites, mass transfer of the pyrolysis products formed in reducing ends is thought to be strongly inhibited in cell wall volume. Produced 5-HMF forms a polymer with other pyrolysis products (*Chapter 4*). After the polymerization, the furan-rings are thought to be opened by addition reaction of water. Because much amount of water is generated during formation of dehydration products (Scheirs et al., 2001; Tang and Bacon, 1964b), such as 5-HMF, and benzene-ring structures, the carbonization reactions accelerates exponentially. We considered the phenol-type structures are formed from the ring-opening structure of furan-rings. On the other hand, benzene- or benzofuran-type structures are produced via reactive fragments, which formed by the cleavage of ring-opening structure. Since the benzene-ring structures

are formed via furan-rings even at low temperature (280 C), cellulose was easily decomposed to carbonized products.

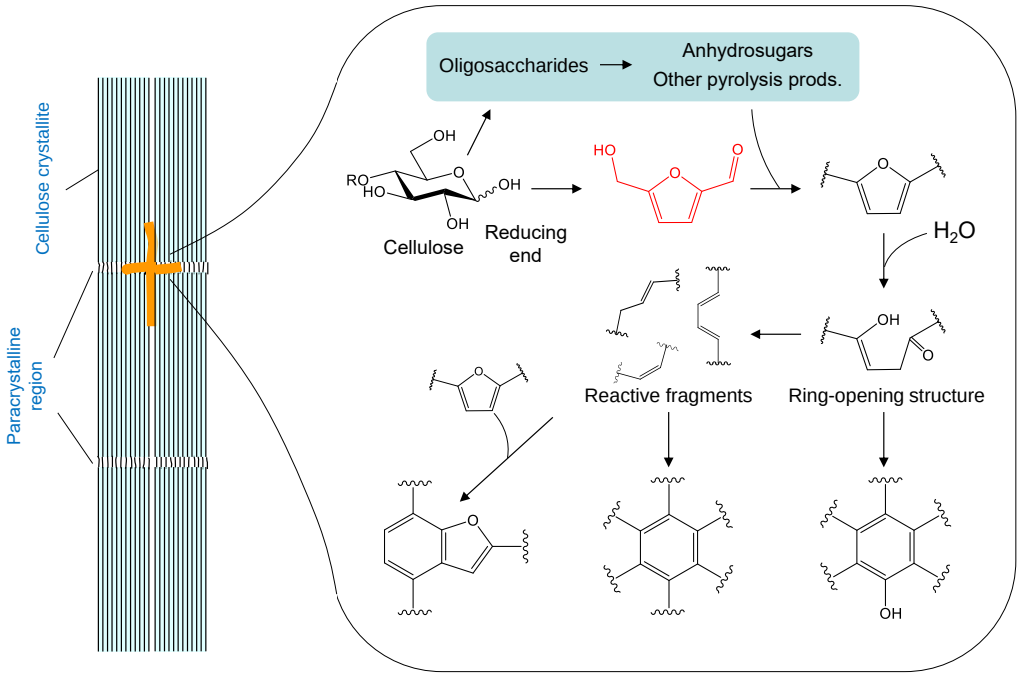

Figure 5-14. Benzen-ring formation mechanism of cellulose via 5-HMF in the reducing end of celllose crystallites.

5.4 Conclusions

The mechanism of benzene ring formation from furan ring was determined using ^{13}C-labeled 5-HMF and glucose. Following conclusions were revealed.

(1) Furan-, benzene- and benzofuran-type structures were formed during pyrolysis of glucose and 5-HMF in glycerol.

(2) Furan structures in the 5-HMF char and glucose char were directly derived from the 5-HMF or 5-HMF polymer.

(3) Phenol structures were also directly generated from 5-HMF or the polymer.

(4) Benzene-type structures were not directly produced from furan-rings. Benzene-rings were thought to be formed via reactive fragments, which was generated from 5-HMF during pyrolysis.

(5) The furan rings, derived from 5-HMF, would form the benzofuran structures with the reactive fragments.

(6) For benzene-ring structure formation via furan-rings, the ring-opening reactions by water addition are significant. At reducing end of cellulose, 5-HMF was polymerized with other pyrolysis products and converted into benzene structures assisted by water, which was generated during dehydration reactions.

Chapter 6

Fast pyrolysis of cellulose by infrared heating

6.1 Introduction

Owing to the depletion of fossil fuel resources and environmental concerns, there is currently significant interest in the use of renewable resources. Biomass has received much attention in this regard as the only renewable carbon source that can be converted into useful chemicals and fuels. Cellulosic biomass accounts for the majority of biomass resources on Earth, but the polymeric nature of these materials limits their widespread use. Accordingly, the development of efficient cellulose conversion technologies is very important. Pyrolysis conducted under oxygen-free conditions is a potentially viable approach to this goal because this technique is able to rapidly degrade stable cellulosic biomass (Jahirul et al., 2012; Uddin et al., 2018).

Fast pyrolysis is a process characterized by rapid heating to yield a mixture of liquid products, known as bio-oil, instead of char (that is, solid products) from lignocellulosic biomass (Bridgwater, 2012; Kersten and Perez, 2013; Perkins et al., 2018; Sharifzadeh et al., 2019; Venderbosch and Prins, 2010). The bio-oil produced can be utilized as a source of liquid fuels (gasoline and diesel) and bio-chemicals. Levoglucosan (LG, 1,6-anhydro-β-D-glucopyranose) is one of the major components of bio-oil obtained from cellulose (Junior et al., 2020; Kwon et al., 2007; Shafizadeh et al., 1979), and can be used as a source of various chemicals. As an example, the hydrolysis of LG gives glucose, which can be converted to ethanol, lactic acid and other products via fermentation.

It has been reported that the temperature of cellulose during fast pyrolysis is in the range of 400–450 °C, which is much higher than the value of approximately 350 °C associated with slow pyrolysis (Boutin et al., 1998; Boutin et al., 2002; Lédé et al., 2002; Shoji et al., 2014). This overheating can promote the recovery of LG, which has a boiling point of 385 °C (Shoji et al., 2014), by rapid evaporation. However, the efficient production of LG from the fast pyrolysis of cellulose requires information regarding the susceptibility of this compound to thermal degradation. Prior work has shown that LG undergoes thermal polymerization in the vicinity of 250 °C, which is much lower than the temperature required for the formation of LG during cellulose pyrolysis (Fukutome et al., 2015; Hosoya et al., 2008; Kawamoto et al., 2003; Pictet, 1918). These seemingly contradictory temperature values can be explained by the difference in LG reactivity in the molten and gas phases. In the gas phase, LG is stable up to 500–600 °C and fragments into gaseous products at higher temperatures (Fukutome et al., 2015). The greater reactivity of molten LG can be explained by hydrogen bonding between LG molecules, which act as acidic and basic catalysts (Kawamoto et al., 2013, 2014). The literature therefore indicates that the capture of gaseous LG produced by the fast pyrolysis of cellulose is very important to obtaining a high yield of this compound.

To maintain such a high cellulose degradation temperature (400–450 °C), various types of furnaces have been developed and are classified into two types depending on the heating principle (Boutin et al., 1998; Boutin et al., 2002; Bridgwater, 2012; Dauenhauer et al., 2009; Lédé et al., 1987; Luo et al., 2017; Nordin et al., 1974; Schroeter and Felix, 2005; Suzuki et al., 1983; Teixeira et al., 2011; Venderbosch and Prins, 2010; Weldekidan et al., 2018); the entrained down-flow, ablative reactor, and fluid bed types are based on the conductive heating, where biomass is heated by contact with a hot environment or hot metal surface (Bridgwater, 2012; Dauenhauer et al., 2009; Lédé et al., 1987; Luo et al., 2017; Suzuki et al., 1983; Teixeira et al., 2011; Venderbosch and Prins, 2010). The other type is based on radiation heating (Boutin et al., 1998; Boutin et al., 2002; Nordin et al., 1974; Schroeter and Felix, 2005; Weldekidan et al., 2018), and biomass is efficiently heated by adsorbing radiation such as infrared (IR) (Boutin et al.,

1998; Boutin et al., 2002), condensed solar (Weldekidan et al., 2018), and lasers (Nordin et al., 1974; Schroeter and Felix, 2005). This feature of selective heating favors the production of LG from cellulose.

The precise control of the pyrolysis temperature is vital during the production of LG, because gaseous LG is quickly converted into other products such as CO and H_2 above 600 °C (Fukutome et al., 2015). For this reason, radiation heating, which can heat materials selectively, may be superior to conductive heating. Shoji et al. (2014) reported that a furnace temperature in excess of 600 °C was necessary to obtain a cellulose degradation temperature above 400 °C so as to maintain fast pyrolysis conditions with a small amount of cellulose in a preheated furnace (Figure 1-7). Under such conditions, the secondary degradation of LG is inevitable even in the gas phase. In order to suppress the secondary decomposition of LG in the gas phase, IR heating was selected for pyrolysis of cellulose. When using radiation heating, the LG produced is efficiently cooled using a stream of nitrogen that has not been effectively heated due to insufficient IR absorption of nitrogen.

The fast pyrolysis of cellulose using radiation heating has been previously reported (Boutin et al., 1998; Boutin et al., 2002; Hopkins et al., 1984; Kwon et al., 2006; Nordin et al., 1974; Schroeter and Felix, 2005; Westerhof et al., 2016; Zeng et al., 2017), while most of the studies focus on the utilization of solar energy for pyrolysis (Hopkins et al., 1984; Zeng et al., 2017) and formation of melting substances during irradiation (Boutin et al., 1998; Boutin et al., 2002; Nordin et al., 1974; Schroeter and Felix, 2005). As for the production of LG, Suzuki et al. (Suzuki et al., 1983) reported the formation of LG and anhydro-oligocellosaccharides by irradiating CO_2 laser on cellulose, although the yields from cellulose were quite low. By using similar CO_2 laser irradiation under nitrogen flow or vacuum conditions, Kwon et al. reported that the yield of LG reached a maximum at around 25% from Whatman CF11 cellulose powder. However, the efficient production of LG from cellulose by radiation heating has not been achieved, and the thermal degradation mechanisms under the irradiation conditions have not been fully clarified.

In the present study, the production of LG from cellulose by IR heating under a nitrogen flow was studied. After the investigation of the effects of the experimental parameters on the product yield, the thermal degradation mechanism at the surface where IR is absorbed was evaluated.

6.2 Materials and Methods

6.2.1 Cellulose samples

Whatman No. 42 cotton filter paper (Whatman PLC, UK, pore size : 2.5 μm) and microcrystalline cellulose powder (Avicel PH-101, Asahi Kasei Corp., Tokyo, Japan) were used in the pyrolysis trials. These materials were employed as received without further purification. The Whatman filter paper was cut into 1.0 × 4.3 cm pieces weighing 30 mg (dry) before use.

6.2.2 Pyrolysis and product analysis

Figure 6-1 shows a diagram of the experimental set-up, in which an IR image furnace (RHL-E45N, Advance Riko, Kanagawa, Japan) was used to heat the cellulose. A quartz tube (internal diameter 30 mm, length 495 mm) was set inside a cylindrical furnace and the IR radiation was focused on the center of the furnace. During trials with the Whatman cellulose sheets, each sample was placed on a stainless steel mesh situated at the center of the reactor. In the case of the Avicel cellulose trials, a quartz boat (length 35 mm, width 10 mm, height 6 mm, AS ONE Corporation, Osaka, Japan) containing the sample was placed on the mesh and then inserted into the reactor. A sampling bag made of Tedlar® (5 L) containing methanol (30 mL) was attached to the outlet of the reactor tube to collect the volatile products, and the air inside the reactor system was replaced with nitrogen before each trial by purging with a nitrogen flow (5 L/min) for 5 min. The nitrogen in the sample bag was released from the vent before pyrolysis trial, and the

process time was sufficiently short to accommodate the whole volume of injected nitrogen. The nitrogen in the sample bag was released from the vent before pyrolysis, and the process time was sufficiently short to accommodate the whole volume of injected nitrogen. After the nitrogen flow was adjusted to the designated value (from 1 to 10 L/min), the cellulose was heated using an IR output energy in the range of 0.5 to 4.0 kW.

During the pyrolysis, a colorless (white) mist escaped from the reactor and was captured in the sampling bag, where it collected on the inner walls after standing for 30 min (Figure 6-2). A 5.0 mL quantity of neon gas was added to the sample bag as an internal standard, after which the contents were analyzed by micro gas chromatography (GC, CP-4900, Varian Inc., Palo Alto, CA, USA). The chromatographic conditions included a 10 m MS5 A column, Ar as the carrier gas, a column temperature of 100 °C, a column pressure of 170 kPa and a thermal conductivity detector (TCD). Using these conditions, the compounds analyzed (and their retention times) were Ne (25.7 s), H_2 (27.0 s), O_2 (35.8 s), CH_4 (60.9 s) and CO (79.8 s). A second channel on the instrument included a 10 m PoraPLOT Q column with He as the carrier gas, a column temperature of 80 °C, a column pressure of 190 kPa and a TCD. The associated analytes (and retention times) were CO_2 (19.3 s), C_2H_4 (22.6 s), C_2H_6 (25.3 s) and C_3H_6 (53.5 s).

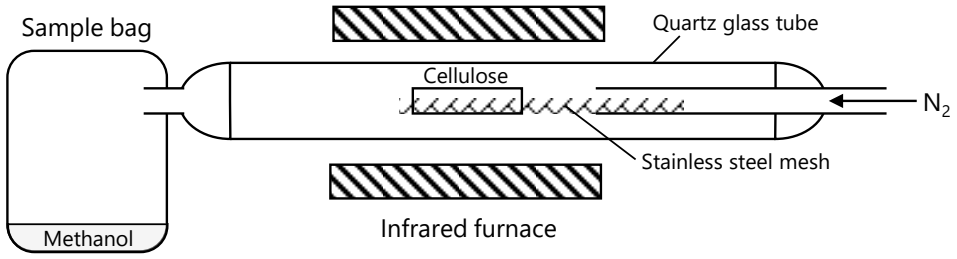

Figure 6-1. The fast pyrolysis system incorporating an infrared image furnace used in this study.

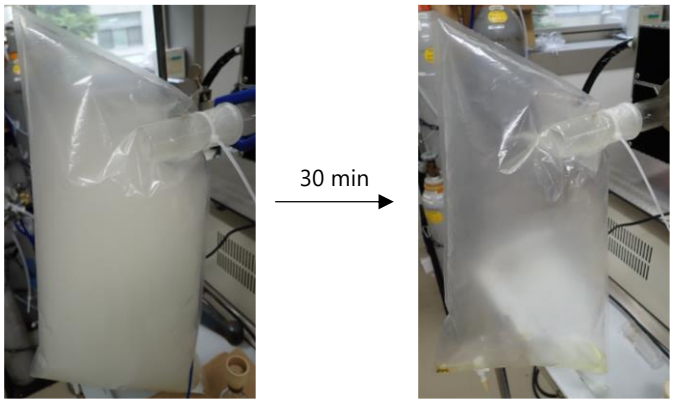

Figure 6-2. Photographic images of sample bags immediately after pyrolysis and 30 min later.

After each trial, the condensates in the sample bag and on the walls of the reactor were extracted with methanol (200 mL) after which the methanol was evaporated under vacuum. A Bruker AC-400 (400 MHz) spectrometer (Bruker, MA, USA) was subsequently used to acquire a ^{1}H nuclear magnetic resonance (NMR) spectrum of the resulting material in DMSO-d_6 (0.7 mL), containing maleic acid as an internal standard and hydroxylamine hydrochloride (NH_2OH•HCl, 10 mg) for the *in situ* derivatization of aldehydes and ketones in the product mixture to the corresponding oximes. The yields of the products, including LG and glycolaldehyde (GA), were determined by comparing the peak areas of the characteristic signals of these compounds with that of the internal standard. The methanol, DMSO-d_6, maleic acid and hydroxylamine hydrochloride were purchased from Nacalai Tesque, Inc. (Kyoto, Japan) and used without purification.

The solid residue remaining on the stainless steel mesh was weighed and the result is referred to as the char mass herein. The mass of the solid carbonized materials adhering to the inner surface of the sample boat was obtained from the mass loss after heating the boat in air at 600 °C for 2 h.

The temperature in the interior of the Avicel cellulose in the sample boat was monitored using a fine thermocouple (0.25 mm in diameter, type K, Shinnetsu Co., Ltd., Ibaraki, Japan) connected to a thermologger (AM-8000, Anritsu Corporation, Kanagawa, Japan). The tip of the thermocouple was embedded in the center of the sample in the depth direction.

Most of the experiments were repeated three times and the results are shown as mean values along with standard deviations.

6.3 Results and discussion

6.3.1 Effects of the experimental parameters on the product yield

The effects of the experimental parameters on the yields of LG and other products were evaluated using the Whatman cellulose to evaluate the capacity of this pyrolysis system to generate LG. The effects of modifying the position of the cellulose in the reactor (at points A, B and C in Figure 6-3), the flow rate of nitrogen and the IR power on the product yield were evaluated. Figure 6-4 summarizes the yields of LG, gas and char obtained under various conditions. Yield is not 100% in total due to the presence of unquantified products such as water. In general, a large amount of water is produced during pyrolysis of cellulose. However, the amount of water was not quantified in the present dissertation.

The position of the cellulose was expected to affect the LG yield because the residence time of the volatile products in the IR irradiation area varied depending on the position (C > B > A). We anticipated that the extent to which secondary pyrolysis reactions of the gaseous LG proceeded would be increased with increases in the residence time. However, the LG yield, which ranged from 32 % to 42 %, was not greatly changed when modifying the sample position (Figure 6-4) during the trial employing 4.0 kW radiation, 5 s irradiation and a 10 L/min nitrogen flow. These results indicate that the degree of secondary degradation of the gaseous LG in response to IR irradiation was very limited, possibly because of the minimal absorption of IR radiation by the gaseous LG and the nitrogen carrier gas. In this respect, IR heating is superior to other conductive heating methods for the production of LG via the fast pyrolysis of cellulose.

Unexpectedly, the gas yield was high (10.1 ± 5.6 %) when the cellulose was set near the outlet of the furnace (position A). The secondary degradation of gaseous LG to

permanent gases such as CO and H_2 is significant above 600 °C in conjunction with short residence times of 1–2 s similar to those in the present study (Hosoya et al., 2008), and such high temperatures could have occurred at position A. This is also supported by the gas composition as discussed later. To evaluate this possibility, the temperatures upstream and downstream of the IR furnace were measured in blank tests with and without the stainless steel mesh (Figure 6-3, 4.0 kW, 5 s irradiation, 10 L/min nitrogen flow). The temperature was found to increase by 4.7 and 25.1 °C without and with the mesh, respectively, when the nitrogen carrier gas passed through the IR irradiation zone. These increases were insufficient to promote secondary degradation of the LG, but could possibly have raised the temperature of the cellulose to promote the secondary degradation of LG at position A.

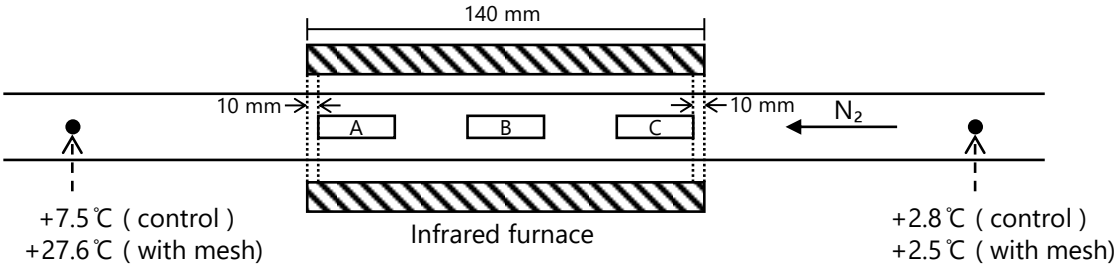

Figure 6-3. Positions (A-C) of Whatman cellulose samples in the reactor and changes in the temperatures upstream and downstream of the IR furnace were measured in blank tests with and without the stainless steel mesh (4.0 kW, 5 s irradiation, 10 L/min nitrogen flow). The values shown here are the increases relative to room temperature.

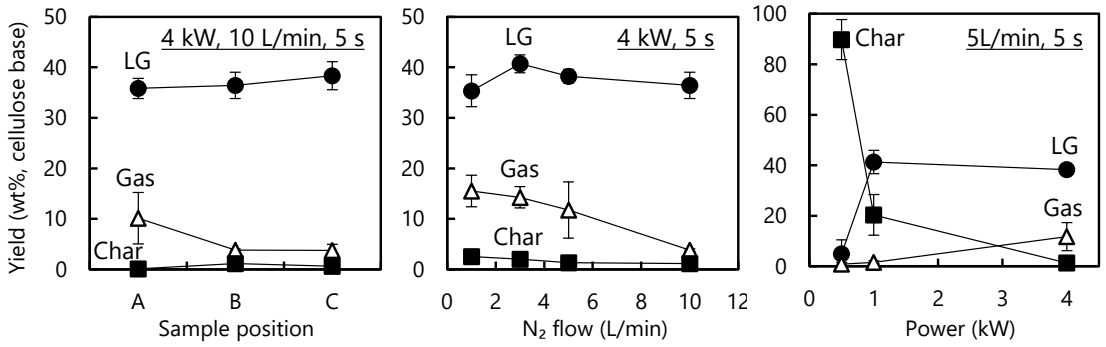

Figure 6-4. Effects of experimental parameters on the yields of LG, gas and char from the pyrolysis of Whatman cellulose.

The nitrogen flow rate was expected to affect the reaction yield by carrying volatile products to a cooler region of the apparatus such that they did not condense on the hot reactor wall where secondary degradation may occur. The flow rate could also conceivably affect the cellulose degradation temperature during the pyrolysis, because the nitrogen was not efficiently heated by the IR radiation. Four nitrogen flow rates (1.0, 3.0, 5.0 and 10.0 L/min) were assessed at a constant IR power of 4.0 kW and constant irradiation time of 5 s. The data show that the LG yield was increased with decreases in the flow rate from 10 to 5.0 L/min, which can be explained by the greater heating efficiency at lower flow rates of the cool nitrogen. The gas yields increased when the flow rate was further decreased to 3.0 and 1.0 L/min, while the LG yield was decreased at 1.0 L/min as a result of secondary degradation.

The IR power directly affected the heating efficiency of the cellulose. Consequently, the LG yield decreased significantly when the IR power was reduced from 1.0 to 0.5 kW, while the char yield was greatly increased as a result of the large amount of unreacted cellulose. Experiments with a longer irradiation time of 10 s were also conducted at 0.5 and 1.0 kW (Table 6-1). Prolonging the irradiation time increased the LG yield while lowering the char yield, and the maximum LG yield of 52.7% was obtained after 10 s of irradiation at an IR power of 1.0 kW. The three-time average under the same conditions was 47.5±3.8 %. These yields were higher than those reported in other studies using radiation heating (10-30 %) and fluidized bed (up to 40 %) (Hopkins et al., 1984; Kwon et al., 2006; Westerhof et al., 2016; Zeng et al., 2017). For example, the LG yields reported in the literature using CO_2 laser were less than 25 % (Kwon et al., 2006). The greater sweep efficiency of the nitrogen flow system in the present study may increase the LG recover at the expense of the occurrence of the secondary degradation of LG.

As shown by the numbers in parentheses, the yields of LG during the irradiation periods of 0–5s and 5–10 s were determined by assuming that the difference in the mass values of the char at 5 s and at 10 s equaled the amount of cellulose degraded during the irradiation time from 5 to 10 s. It should be noted that the estimated LG yields during the

first and last 5 s intervals were not greatly different. This result illustrates a very important aspect of IR heating that is discussed in more detail below.

These data establish that the IR power, nitrogen flow rate and sample position all affected the actual cellulose degradation temperature. When this temperature was greater than 600 °C, the LG yield decreased because of the conversion of the LG to permanent gases. The IR irradiation time was also found to have an important effect in terms of obtaining complete cellulose pyrolysis.

Table 6-1. Yields of LG, gas and char from the pyrolysis of Whatman cellulose while varying the IR power and irradiation time with a 5 L/min nitrogen flow.

Infrared power (kW)	Irradiation time (s)	Yield (wt%, cellulose base)		
		LG	Gas	Char
0.5	5	4.9 ± 5.6 (48.1 ± 1.8)*	0.9 ± 0.7	89.8 ± 7.9
	10	35.0 ± 2.7 (51.3 ± 1.3)	4.0 ± 3.3	31.7 ± 5.6
1.0	5	41.3 ± 4.6 (51.9 ± 4.1)	1.6 ± 0.6	20.4 ± 8.1
	10	47.5 ± 3.8 (48.3 ± 3.7)	4.3 ± 0.1	1.7 ± 0.8

* Figures in parentheses are estimated yields based on the amounts of cellulose that were degraded over 0–5 s and 5–10 s. The latter amount was calculated from the difference in mass between the char portions obtained at 5 s and at 10 s.

The major by-products obtained from the fast pyrolysis of cellulose under IR irradiation in this work were gaseous but the specific compounds changed depending on the pyrolysis conditions. In Figure 6-5, the molar percentages of H_2, CO and CO_2 are plotted against the gas yields from the various trials. At gas yield less than 4 %, H_2 and CO_2 were the main components, while at higher gas yields CO was produced, and the molar ratios of CO to H_2 became 1.3-2.5 along with lesser amounts of CO_2. These results are reasonably explained with gas production from the secondary degradation of gaseous LG, based on prior reports that CO and H_2 are selectively produced from LG in the gas

phase above 600 °C (Kawamoto et al., 2003). Therefore, the formation of CO appears to be a useful indicator of the appearance of cellulose degradation temperatures greater than 600 °C. It should be noted that it was challenging to measure the actual sample temperature throughout the IR irradiation process because of the nonuniform progression of the thermal degradation of the cellulose, as discussed further on.

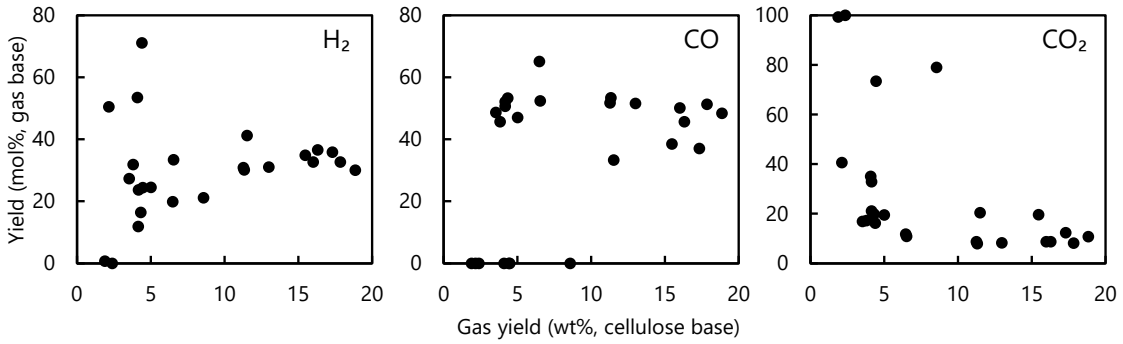

Figure 6-5. Proportions of H_2, CO and CO_2 in the gaseous products as functions of the overall gas yield from the fast pyrolysis of Whatman cellulose.

The GA was the other major by-product, and Figure 6-6 summarizes the yields of GA obtained under various fast pyrolysis conditions compared with the overall gas yields. It is apparent that there were no correlations between the yields of both products, and that the GA yield remained relatively constant as the various parameters were changed while the gas yield varied greatly. Accordingly, the formation of GA cannot be explained by the secondary degradation of LG.

In pyrolysis of cellulose, GA has been reported to form in higher temperature range than LG, and a negative correlation has been reported between the yields of these products (Piskorz et al., 1989). Therefore, there was controversy over the GA formation pathway, although literature (Banyasz et al., 2001; Piskorz et al., 1989; Piskorz et al., 1986; Richards, 1987) shows a direct formation pathway from cellulose that competes with LG formation. The observations in the present study clearly show the direct pathway of GA formation. GA is believed to form during the primary cellulose pyrolysis stage, likely via retro-Aldol type fragmentation reactions of the reducing ends of cellulose and

carbohydrate intermediates. Such reactions are favorable because stable six-membered cyclic transition states are involved (Figure 6-7). A similar mechanism has been proposed for the pyrolysis of cellobiose based on prior work using pyrolysis-GC/MS spectrometry in conjunction with ^{13}C-labeled cellobiose (Degenstein et al., 2015).

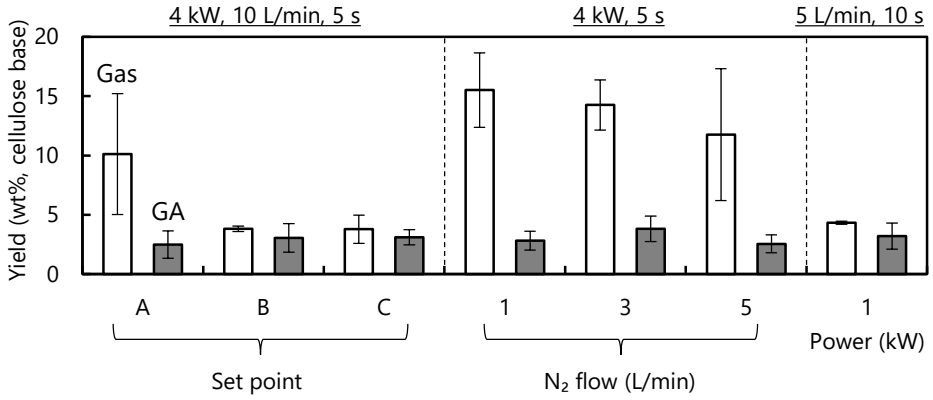

Figure 6-6. Yields of GA and overall gas yields (wt% based on amount of cellulose) from the pyrolysis of Whatman cellulose under various conditions.

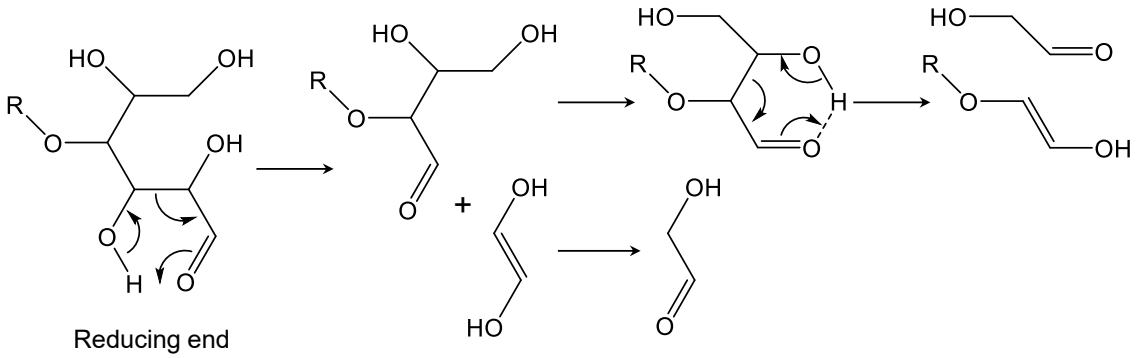

Figure 6-7. Mechanism for the formation of GA from the reducing ends of cellulose and other intermediate carbohydrates during the fast pyrolysis of cellulose.

6.3.2 Control of fast pyrolysis reaction

A high boiling point aromatic solvent, 25 mg of benzoanthraquinone (b.p. 472 °C.), was dissolved in *p*-xylene (25 mL). Whatman cellulose was impregnated with the solution. The *p*-xylene was removed by freeze drying. The obtained cellulose sample with benzoanthraquinone was pyrolyzed (1 kW, 5 L/min nitrogen flow, 30 s). As a result,

LG yield was 49.5%, and the yield did not improve. It was considered that the aromatic solvent volatilized before the thermal decomposition of cellulose proceeded, and the aromatic solvent could not affect.

Thermal discoloration and carbonization reactions of glycerol-treated cellulose, in which the reducing ends were reported to be converted into glycosides (non-reducing ends), were suppressed compared with untreated cellulose (Matsuoka et al., 2011a, 2011b). Since the reported experiment was performed by slow pyrolysis, the effect of removing the reducing end in fast pyrolysis is unknown. Therefore, glycerol-treated cellulose was heat-treated by infrared heating.

The Whatman No. 42 cellulose filter paper (30 mg × 4) and glycerol (13 g) was placed in a Pyrex glass tube reactor (internal diameter 8.0 mm, wall thickness 1.0 mm, length 300 mm) that was connected to a nitrogen bag through a three-way tap. After the air inside the reactor was replaced with nitrogen (99.99%) using an aspirator, the reactor was inserted into a muffle furnace preheated to 280 °C. After heating for 30 min, the reactor was removed from the furnace and immediately cooled by a flow of air. The glycerol-treated cellulose was washed with ion-exchanged water and dried in an oven (105 °C, overnight). The glycerol-treated cellulose (30 mg) was pyrolyzed by infrared radiation at 1.0 kW for 10 s under nitrogen flow 5.0 L / min.

Table 6-2 shows the yields of LG, GA, gas and char (wt%, cellulose base). Compared to the untreated cellulose sample, the yield of LG increased significantly to 78.2 wt%. The yield of GA decreased to 1.6 wt%. The reduction in GA yield by glycosylation of the reducing end supports the GA formation mechanism from reducing ends described in Figure 6-7. The negative correlation between the yields of LG and GA indicates that LG production reaction and the reaction from the reducing ends are competitive reactions. This result suggests that the reaction from the reducing ends also have a great influence on the thermal reactions under fast pyrolysis condition.

Table 6-2. LG, gas and char yields (wt %, cellulose base) at 0.5 or 1.0 kW, for 5 or 10 s under 5 L/,min.

		Yield (wt%, cellulose base)			
Power (kW)	Time (s)	LG	GA	Gas	Char
1.0	10	78.2	1.6	2.8	4.1

6.3.3 The mechanism for cellulose pyrolysis by infrared irradiation

Figure 6-8 presents photographic images of the char residues recovered from Whatman cellulose after applying IR irradiation at either 0.5 or 1.0 kW. A colorless (white) unreacted part clearly remained intact on the specimen after the trial at 0.5 kW, suggesting that the thermal degradation of cellulose occurred non-uniformly under such conditions. The pyrolysis in the upstream region of the nitrogen flow (the right side of the apparatus) was particularly slow, presumably due to the effect of the cool nitrogen. This tendency was also observed at the higher irradiation power of 1.0 kW after 5 s of irradiation, although the unreacted part was completely pyrolyzed by prolonging the irradiation time to 10 s. High selectivity for LG formation was also maintained under these conditions, as shown in Table 6-1.

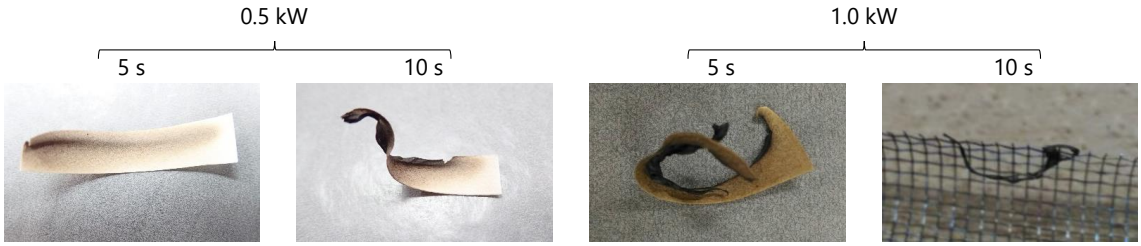

Figure 6-8. Photographic images of cellulose chars obtained under various fast pyrolysis conditions.

Figure 6-9 provides an enlarged microscopic view of the char obtained at 1.0 kW after 5 s and demonstrates the formation of a very narrow (less than 0.5 mm) film-like carbonized zone. Cellulose generates film-like char when fast pyrolysis conditions are achieved because it rapidly converts to molten intermediates prior to the evaporation of

LG and other products. On the basis of these images, it appears that the thermal degradation of the cellulose occurred within a very small area adjacent to the narrow carbonized zone, which was heated quickly owing to the efficient absorption of IR radiation (Figure 6-10). This process spread over the cellulose sheet as the irradiation time span increased. Gas formation would also occur in this small area in conjunction with the evaporation of LG as temperatures greater than 600 °C were achieved. Boutin et al. [11] reported the formation of short-lived liquid species while irradiating the surface of a cellulose pellet with a concentrated xenon lamp. However, they did not analyze LG and did not report the progression of the pyrolysis zone to the stage where cellulose was completely degraded.

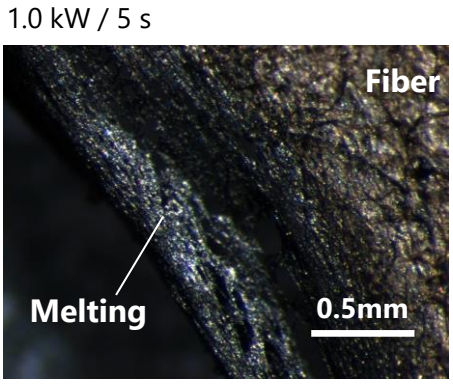

Figure 6-9. Micrographic image of the dark carbonized area of the cellulose char obtained at 1.0 kW after 5 s.

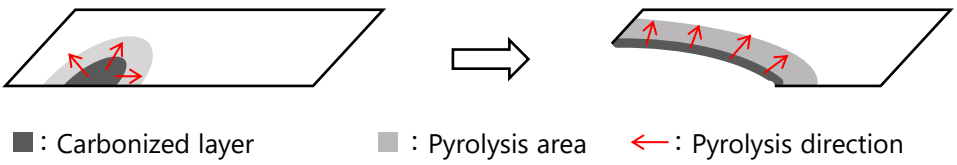

Figure 6-10. A diagram showing the process occurring during the fast pyrolysis of a Whatman cellulose sheet under IR irradiation.

The above data obtained using the Whatman cellulose sheets provide useful insights into the pyrolysis in the planar direction. To complement this information, pyrolysis behavior in the thickness direction was also examined using the Avicel cellulose

powder. In these trials, a 300 mg portion of this powder was transferred to a quartz boat and irradiated at 2.5 kW for 30 s under a 5 L/min nitrogen flow. Similar experiments using only 100 mg samples were also conducted to understand the effect of sample loading. Under these conditions, LG was obtained in 44.3% (with 100 mg samples) and 48.5% (300 mg) yields, which were comparable to those obtained from the Whatman cellulose sheets. The film-like chars seen in the images in Figure 6-11 indicate that fast pyrolysis was achieved during these experiments. It should also be noted that a high LG yield was observed when using either 100 or 300 mg samples, indicating that the sample amount did not affect the ability to perform fast pyrolysis.

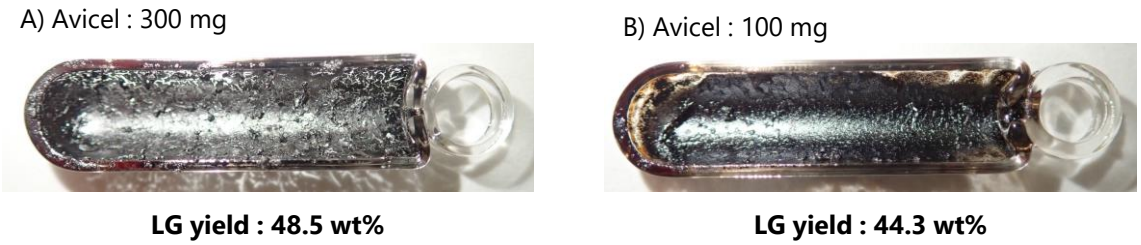

Figure 6-11. Photographic images of quartz boats after applying IR radiation to A) 300 mg and B) 100 mg Avicel cellulose samples (1 kW, 5 L/min nitrogen flow, 30 s).

The temperature in the middle of the cellulose sample in the boat was monitored using a fine thermocouple in trials with a power level of 1.0 kW, a 20 s irradiation time and a 5 L/min nitrogen flow. The irradiation time of 20 s was insufficient to completely pyrolyze the cellulose, meaning that the sample temperature during cellulose degradation could be assessed. During these trials, the bottom of the sample boat was covered with aluminum foil so that the sample only received radiation from the top. Figure 6-12 provides photographic images of the boat after the trial, along with a plot of the internal sample temperature over time. It is evident that the surface of the sample was darkened to a greater extent than the interior, based on the left half of the sample where the surface has been removed. The temperature plot demonstrates a relatively slow rate of temperature rise inside the cellulose layer. The final temperature of 250 °C at 20 s was

lower than the minimum value of 350 °C required for the efficient thermal degradation of cellulose. The brief pause in the temperature increase observed in the range of 100–150 °C is attributed to the volatilization of water. When the IR irradiation time was extended to 30 s, only a small amount of film-like char remained in the boat, as can be seen in Figure 6-11, and LG was obtained in a 50.0% yield. These results indicate that the thermal degradation of cellulose proceeded non-uniformly from the surface that received the IR radiation, as illustrated in Figure 6-13.

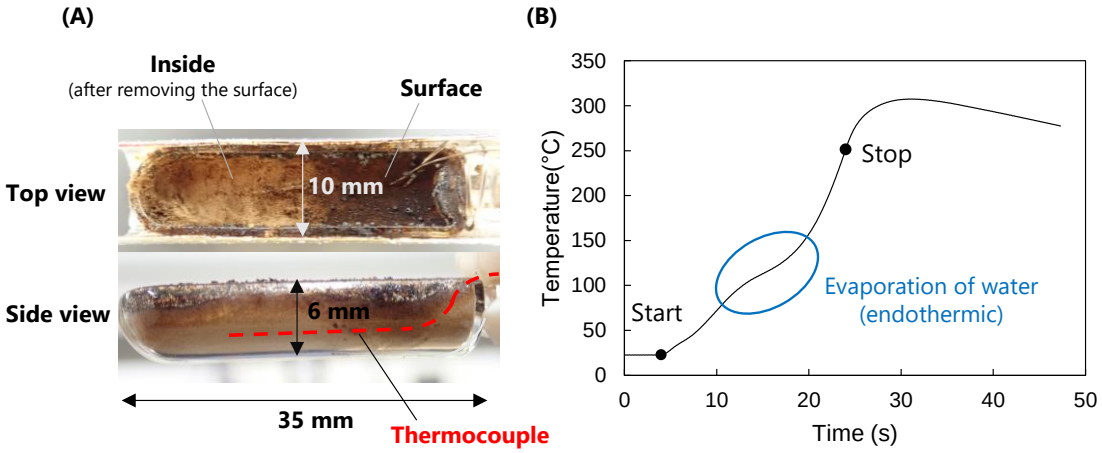

Figure 6-12. A) Photographic images of a quartz sample boat after IR irradiation for 20 s (less than the 30 s required for complete pyrolysis of Avicel cellulose) and B) the temperature inside the cellulose over time (1 kW, 5 L/min nitrogen flow).

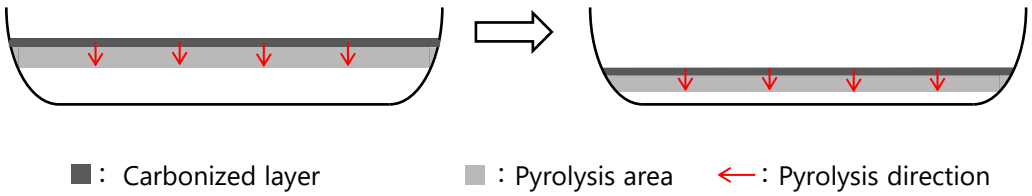

Figure 6-13. **A** diagram showing the progression of the fast pyrolysis of Avicel cellulose powder in a quartz boat in response to IR irradiation.

Figure 6-14 illustrates the heat and mass transfer processes and related events in the thin surface layer in which fast pyrolysis occurred during the IR irradiation of the Avicel

cellulose. Cellulose tends to reflect IR, so the absorption of IR radiation by the cellulose was not sufficient to raise the sample temperature rapidly to above 400 °C. However, once solid carbonized materials were produced at the surface, this region underwent fast heating as it became more efficient at absorbing the radiation. The resulting heat energy was transferred to the adjacent cellulose to promote rapid thermal degradation. The temperature of the degrading cellulose was rapidly raised to above 400 °C and liquid intermediates were generated. The evaporation of LG and other products is an endothermic process, while the formation of char is exothermic (Cho et al., n.d.; Milosavljevic et al., 1996; Mok and Antal, 1983). As a result of the greater contribution of the former endothermic process, the fast pyrolysis was overall endothermic and so required continued heat input from the carbonized layer. The heat transfer to the interior of the cellulose was relatively slow, based on the low thermal conductivity of cellulose (0.04 W/mK) (Blasi, 1994; Majumdar et al., 2010), and so only a narrow region experienced high temperatures.

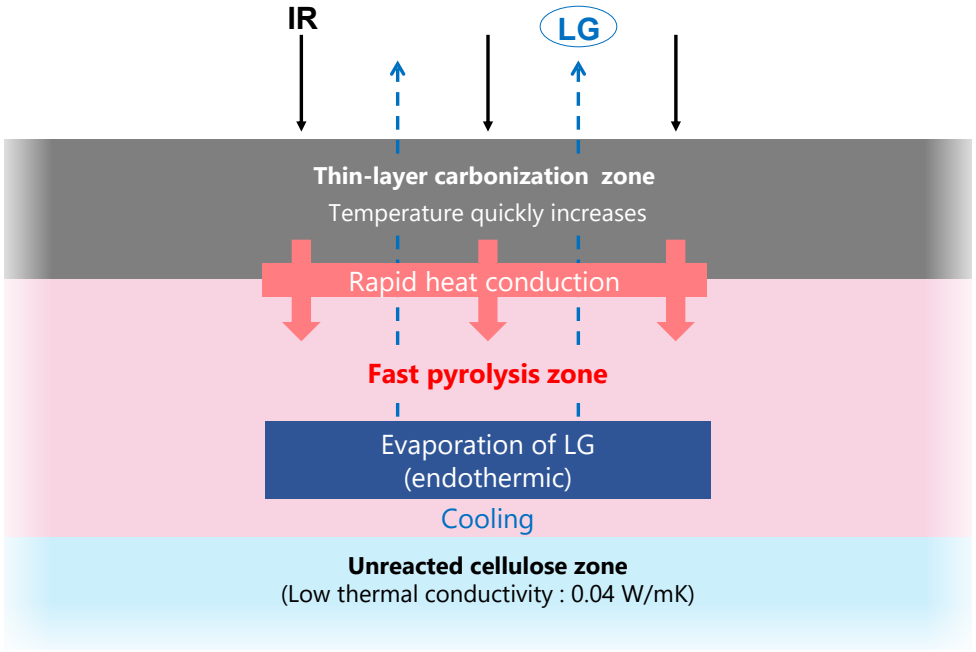

Figure 6-14. Physicochemical processes occurring in the pyrolysis zone, in which the thermal degradation of cellulose proceeds in a very narrow area near the carbonized layer.

6.4 Conclusions

The pyrolysis of cellulose using IR irradiation was studied, resulting in the following conclusions.

(1) The sample position in the IR furnace, the IR power level and the nitrogen flow rate all affected the thermal degradation of cellulose, by modifying the cellulose degradation temperature.

(2) Under the optimum conditions, LG was obtained in a 52.7 wt% yield from Whatman cellulose sheets (infrared power : 1.0 kW, nitrogen flow : 5 L/min, irradiation time : 10 s).

(3) The gas yield increased when the cellulose was overheated to above 600 °C as a result of the secondary degradation of LG. This effect could be monitored by tracking the formation of CO, although *in situ* temperature measurements were difficult due to the nonuniform progression of the cellulose thermal degradation.

(4) GA was the other major product of cellulose degradation and the yield of this compound was not correlated with the gas output, suggesting that it was not a secondary LG degradation product. GA was evidently produced during the primary cellulose pyrolysis stage via the retro-Aldol fragmentation of the reducing ends of cellulose and other intermediate carbohydrates.

(5) The thermal degradation of cellulose occurred in a non-uniform manner in response to IR irradiation, with the formation of a narrow carbonization layer. This layer was rapidly heated by efficiently absorbing IR and, in turn, heated the adjacent cellulose. This process then propagated throughout the cellulose to maintain a high LG output rate.

(6) The use of IR heating during the production of LG from cellulose offers several advantages compared with other fast pyrolysis methods based on heat conduction. The latter methods require the cellulose to be ground and heated quickly to maintain a high sample temperature, while the IR heating methods allow the use of any cellulose, regardless of size. Infrared power can also be easily controlled by changing the electric power.

(7) These results give insights into the production of biochemicals and biofuels via LG and pyrolysis-based saccharification.

Chapter 7

Hydrolysis of levoglucosan with solid acid by microwave heating

7.1 Introduction

Glucose can be converted to bioethanol or various chemical feedstocks, such as acetic acid and lactic acid, by fermentation. The production of glucose from cellulose, which is a renewable and nonedible resource, would be a huge step toward the creation of a sustainable society. Acid hydrolysis (Esteghlalian et al., 1997; Sivers and Zacchi, 1995), enzymatic saccharification (Béguin and Aubert, 1994; Duff and Murray, 1996; Sun and Cheng, 2002), and hydrothermal treatment (Ehara and Saka, 2005; Rabemanolontsoa and Saka, 2016; Sasaki et al., 1998) have been proposed as methods for cellulose treatment, but many challenges remain with these methods because crystalline cellulose is physically and chemically stable and insoluble in water. For example, typical acid hydrolysis requires a large amount of concentrated sulfuric acid (72%) to solubilize cellulose, followed by dilution with water and incubation at 121 °C to obtain glucose (Dence, 1992). A large amount of base is also necessary for neutralization. Furthermore, because hydrolysis is performed in water, considerable energy is then required to remove water from the end product.

In contrast, in cellulose pyrolysis, which is a water-free method, LG can be produced in high yield (60–70 wt% on cellulose) (Kwon et al., 2007; Shafizadeh et al., 1979). Anhydrous sugars such as LG are soluble in water and easily converted to glucose with a small amount of water. This two-step process of pyrolysis of cellulose followed by

hydrolysis with minimal water can realize a high glucose concentration and thus reduce the energy consumption for water removal after conversion.

In the literature, the use of sulfuric acid is often described for hydrolysis of anhydrous sugars (Blanco et al., 2018; Helle et al., 2007), but the use of sulfuric acid has several problems: corrosion of the reactor, and recovery or neutralization of the catalyst. In the present study, a solid acid catalyst (a cation exchange resin) was used for hydrolysis of LG. Solid catalysts have the advantage of avoiding neutralization and separation processes. Because it is commonly used as a solid acid, a cation exchange resin was used as a solid catalyst in the present study. We used microwaves as the heating method because microwaves have the advantage of fast heating rates and the ability to selectively heat reactants. In addition, we discuss the effect of microwave heating compared with heating in an oil bath (Gedye et al., 1986; Herrero et al., 2008).

7.2 Materials and Methods

Approximately 10 mg of LG (Tokyo Chemical Industry, Tokyo, Japan, purity > 99.0%) was dissolved in 50 mL of distilled water as a standard LG solution. In this dissertation, Amberlyst 15JWET (ORGANO, Tokyo, Japan) was used as the solid acid catalyst. Amberlyst 15JWET is a cation exchange resin with a sulfonyl group attached to its polystyrene structure. Wet granules of the cation exchange resin (bulk volume 20 mL) were placed in a 100-mL measuring cylinder with the standard LG solution (10 mL), and distilled water was added until the total volume reached 60 mL. According to the literature (Zhou et al., 2012), the cation exchange resin (Amberlyst) was characterized here; acidity: 4.70 mmol/g, average pore diameter : 32 nm, particle size: 90-200 μm, maximum operating temperature: 120 °C. An aliquot (1 mL) was collected to determine the initial concentration of LG by high-performance liquid chromatography (HPLC). From the above mixture, supernatant (3 mL) and the cation exchange resin (bulk volume 2 mL) were transferred to a 10-ml CEM microwave reactor vessel (internal diameter 12.0 mm, wall thickness 1.5 mm, length 90 mm) with a magnetic stirrer and sealed. The vessel was

heated in a single-mode microwave apparatus (Discover SP, CEM Corporation, NC, USA) or an oil bath. The microwave frequency of Discover SP is 2455 MHz, and we set the maximum power to 50 W. The temperature in the vessel was measured with a fiber-optical thermometer. After the treatment, the yield of glucose was determined by HPLC in mol% based on the treated LG. The HPLC analysis was performed with a Prominence chromatograph (Shimadzu Co., Kyoto, Japan) under the following conditions: column, CarboPac^{TM} PA1 (4 × 250 mm, Thermo Scientific, Waltham, MA, USA); temperature, 35 °C; eluent, 0.03 M NaOH; flow rate, 1.0 mL min^{-1}; electrochemical detector (DECADE Elite, Antec Scientific, Zoeterwoud, Netherlands).

7.3 Results and discussion

Figure 7-1 shows the glucose yield when the LG solution was treated with the cation exchange resin. The conversion of LG was almost the same as the glucose yield. In the case of microwave treatment (Figure 7-1a), the yield increased slowly at 95 °C and reached about 45 mol% after 40 min. When the temperature was increased, high glucose yields were achieved in shorter time. At 120 °C, the glucose yield reached 95.4 mol% after 30 min. Thus, hydrolysis of LG proceeded well by microwave heating under practical treatment temperatures and times. When heated in an oil bath Figure 7-1b), hydrolysis tended to be slightly faster at 95 °C and 100 °C, but hydrolysis rates at 110 °C and 120 °C were similar to those observed for microwave treatment.

To clarify the difference between microwave heating and oil bath heating, the hydrolysis rate constant, k (s^{-1}), was estimated on the assumption of a pseudo-first-order reaction. Although there were heating-up periods of 1–2 min for both cases, the reaction rates were evaluated from the slopes of the linear portion at the initial stage of the reaction, as depicted by red lines in Figure 7-1. The corresponding Arrhenius plots are shown in Figure 7-2 with activation energies (E_a, kJ/mol) and frequency factors (A, s^{-1}). As shown later, since the cation exchange resin temperature was higher than the LG solution temperature in microwave heating, the E_a and A shown in this dissertation would differ

from the actual values. However, the values are practical for hydrolysis by microwave heating. The E_a for microwave heating was higher than that for oil bath heating. The Arrhenius plots intersected at 110 °C, above which microwave heating showed a higher hydrolysis rate constant than oil bath heating. The reason behind this result was not apparent and further investigation is needed. Although there was a slight difference in hydrolysis achieved by microwave heating and oil bath heating, the hydrolysis abilities of the heating treatments were considered comparable.

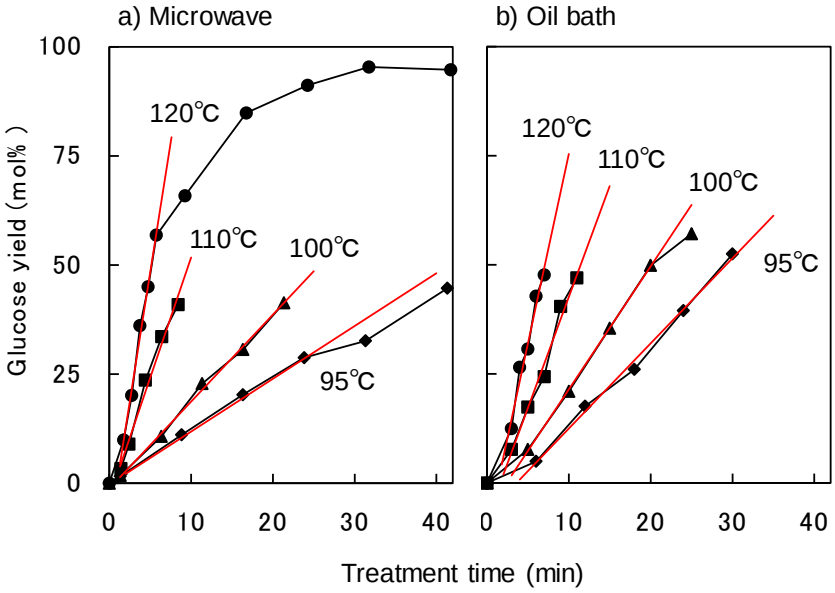

Figure 7-1. Glucose yield after hydrolysis of LG with the cation exchange resin at various temperatures.

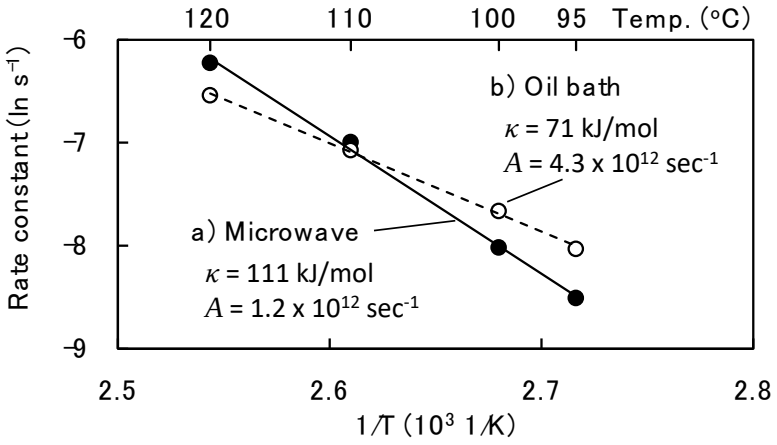

Figure 7-2. Arrhenius plots for rate constants of LG

hydrolysis with the cation exchange resin.

The experiments described above were performed with low-concentration LG solutions (~0.1 g/L). However, LG can also be obtained without the need for added water by pyrolysis of cellulose. This means that only minimal added water is required for hydrolysis. Table 7-1 shows glucose yields after hydrolysis of concentrated LG solutions. High glucose yields over 85 mol% were obtained at 100 and 200 g/L. Therefore, a high-concentration glucose solution is expected from hydrolysis of LG obtained via cellulose pyrolysis.

Table 7-1. Glucose yields from high-concentration LG solutions after microwave heating with the cation exchange resin at 120 °C for 30 min.

Concentration of LG (g/L)	100	200
Glucose yield (mol%)	86.2	90.3

To further investigate the effect of microwave heating, hydrolysis was conducted at 110 °C with different temperature measurement positions and microwave power settings, as shown in Figure 7-3. In these experiments, the temperature was measured above the the cation exchange resin region (see Figure 7-3a Upper) or inside the cation exchange resin region (see Figure 7-3b Lower). When measuring the temperature in the upper position, the glucose yield was about 40 mol%. When the measurement point was inside the cation exchange resin region, the glucose yield decreased despite using the same temperature and treatment time. This result indicates that the temperature of the cation exchange resin region was higher than the LG solution, and the cation exchange resin absorbed microwaves more easily than water.

Furthermore, as shown in Figure 7-3, at the same treatment temperature (110 °C), the glucose yield was almost constant independent of microwave power. Although the nonthermal effects of microwave treatment have been reported (Gedye et al., 1986), the effect of temperature is thought to be dominant in the hydrolysis of LG with the cation exchange resin, and the effect of microwave energy itself was not evident.

To investigate the absorption of microwaves by the cation exchange resin, a constant microwave power (10 W) was supplied to (a) the cation exchange resin and water, (b) polystyrene and water, and (c) water only, and changes in temperature were measured (Figure 7-4). the cation exchange resin has sulfonyl groups (-SO_3H) as acid sites on a polystyrene backbone. The temperature of the cation exchange resin reached the highest values, while the cases of polystyrene–water and water only were almost the same. Therefore, as shown in Figure 7-5, the sulfonyl group in the cation exchange resin is thought to preferentially absorb microwaves more than polystyrene and water, which increases the local temperature.

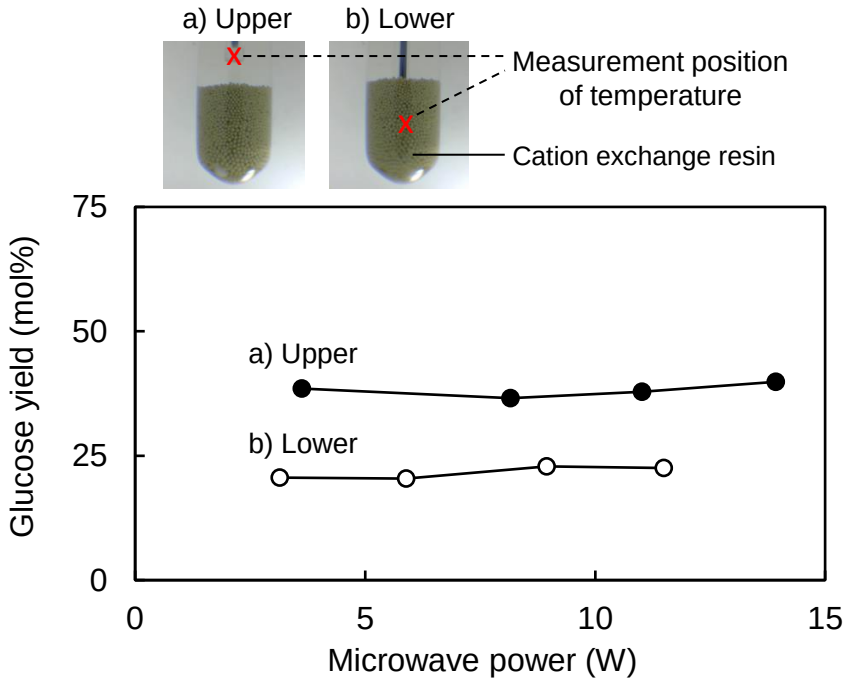

Figure 7-3. Hydrolysis of LG at 110 °C for 7 min with different temperature measurement positions and microwave powers. Red crosses show measurement positions.

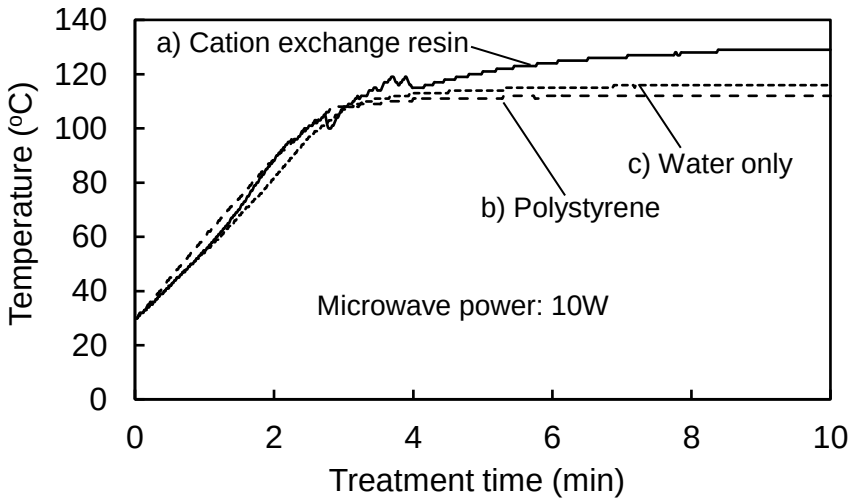

Figure 7-4. Microwave heating at 10 W for a) Cation exchange resin and water, b) polystyrene and water, and c) water only.

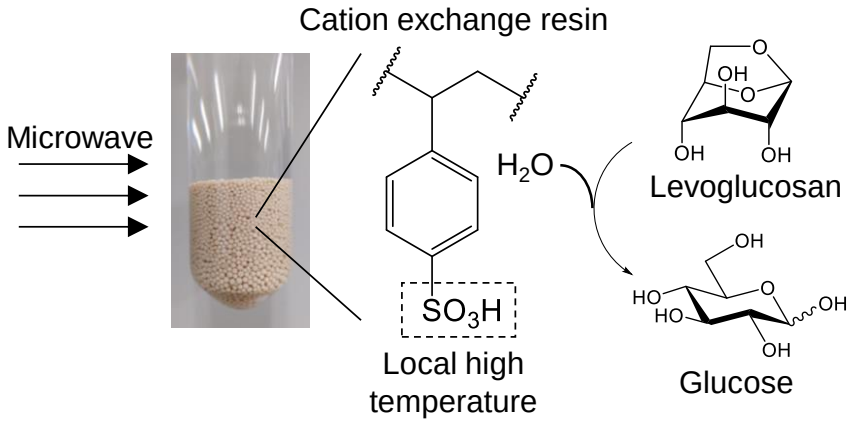

Figure 7-5. Hydrolysis of LG with microwave heating and the cation exchange resin.

Finally, the pyrolysis product from cellulose was tried to be hydrolyzed by microwave heating with the cation exchange resin. Avicel cellulose was used as the cellulose sample, and the cellulose sample was pyrolyzed by an infrared gold image furnace (*Chapter 6*). Avicel cellulose (300 mg × 2) was heat treated, and the obtained pyrolysis product was extracted with methanol (200 mL). After removing methanol with an evaporator, water (3.5 mL) and the cation exchange resin (2.0 mL) were added to the

pyrolysis product. The supernatant (0.5 mL) was collected after stirring well and analyzed by HPLC. The LG concentration of pyrolysis product was 57.2 g/L. The pyrolysis product solution was treated with microwave at 120 °C for 30 min. The solution after hydrolysis was analyzed in same method. As a result, the glucose concentration was found to be 68.3 g/L. The yield was 107.3 mol% (LG base). The molar yield of glucose exceeds 100 mol%, because the pyrolysis product would contain anhydrous sugars other than LG, and the anhydrous sugars were thought to be also converted into glucose by hydrolysis. From these results, anhydrosugars in actual cellulose pyrolysis products were found to be hydrolyzed into glucose by solid acid and microwave.

Table 7-2. Glucose yields from pyrolysis product after microwave heating with cation exchange resin at 120 °C for 30 min.

Concentration of LG (g/L)	57.2
Glucose yield (mol%)	107. 3

7.4 Conclusions

The hydrolysis of LG with microwave treatment and solid acid (cation exchange resin) revealed:

(1) LG was hydrolyzed into glucose in high yield (95.4 mol%) at 120 °C for 30 min.

(2) The activation energy of hydrolysis with microwave treatment was estimated to be 111 kJ/mol.

(3) LG was hydrolyzed efficiently in high yield, even from high-concentration LG solutions.

(4) The temperature measurement position affected the glucose yield because the temperature around the cation exchange resin region was higher than in the LG solution.

(5) Sulfonyl groups in the cation exchange resin absorbed microwaves more readily than polystyrene or water.

(6) Pyrolysis product from cellulose could be converted into glucose with microwave treatment and solid acid.

Chapter 8

Concluding Remarks

In this dissertation, we tried to increase the yield of LG from cellulose by suppressing the carbonization. In addition, the cellulose carbonization mechanism was investigated. The following conclusions are obtained. Details of the background are shown in *Chapter 1*.

In aromatic solvents, LG is stabilized up to 350 °C. Therefore, cellulose was pyrolyzed at 280 °C in aromatic solvents (*Chapter 2*). Cellulose was pyrolyzed at 280 °C in aromatic solvents. The pyrolysis reactivity of cellulose was reduced in aromatic solvents compared to under nitrogen. The char yield after hydrolysis of unreacted cellulose decreased in the opposite tendency to the cellulose reactivity. The suppression of the secondary reactions of the products dramatically increased the yield of LG and 5-HMF in aromatic solvents. In particular, the effect of BPH having a polar >C=O group was high. BPH was thought to be more accessible to the hydrophilic surface of cellulose crystallites.

To investigate the effect of aromatic solvents in the cell wall volume, the cellulose pyrolyzed under nitrogen or in aromatic solvents at 280 °C was observed with UV microscopy (*Chapter 3*). Cross sections of cell walls of cellulose char absorbed UV because of the presence of furan and benzene rings in the solid carbonized products. UV absorbance was uniform inside the cell wall. This indicates the carbonization proceeded uniformly inside the cell wall. Aromatic solvents uniformly inhibited the formation of solid carbonized product within the cell wall. However, the inaccessible part of the cell wall volume was carbonized and distributed in the cell wall volume within the resolution of UV microscope (280 nm).

Based on the studies of cellulose pyrolysis in aromatic solvents and under nitrogen (*Chapter 2*), we found there is negative correlation between 5-HMF yield and solid carbonized products. The pyrolysis reactivity of 5-HMF was investigated to determine its role in cellulose carbonization in *Chapter 4*. We found that 5-HMF was converted to stable glassy materials by hydroxyl group removal, while subsequent carbonization reactions were very slow. Furthermore, pyrolysis of 5-HMF in the presence of glycerol, a model of coexisting pyrolysis products, gave the coupling product in a certain yield, which indicates that 5-HMF formed during cellulose pyrolysis binded with other coexisting products, such as anhydrosugars and oligosaccharides. Additionally, upon pyrolysis with glycerol, the 5-HMF moiety was converted to benzene, benzofuran, and indene-type structures, along with carboxylic acids, phenols, and carboxyesters. These are characteristic structures of carbonized cellulose, which suggests that 5-HMF is an intermediate in cellulose carbonization. Reducing ends might have an important role in the formation of 5-HMF. The carbonization reaction might be accelerated by the action of water and acidic groups generated during carbonization.

The formation of benzene-ring structures via 5-HMF was investigated using ^{13}C label (*Chapter 5*). Phenol structures were also directly generated from 5-HMF or the polymer. However, the benzene-type structures were not directly produced from furan-rings. The intermediates, such as reactive fragments, would be formed, and the benzene-ring structure would be produced via the reactive fragments. For benzene-ring structure formation via furan-rings, the ring-opening reactions by water addition are significant. At reducing end of cellulose, 5-HMF was polymerized with other pyrolysis products and converted into benzene structures assisted by water generated during dehydration reactions.

Carbonization reactions proceeded between cellulose crystallites, which were inaccessible with aromatic solvents. Therefore, cellulose was heat-treated under fast pyrolysis conditions in which the crystallites melted instantly in *Chapter 6*. Infrared radiation was used for the heat-treatment under nitrogen flow. The maximum yield of LG was 52.7 %. There was a correlation between the gas yield and CO production; CO was

suggested to be the secondary pyrolysis product of LG. The yield of GA was almost constant regardless of the conditions. This indicates that GA was formed directly from the reducing end of cellulose in fast pyrolysis. The infrared radiation was easily absorbed by the carbonized and colored areas. Therefore, the pyrolysis proceeded heterogeneously. The heating rate of inside cellulose was found to be slow by using thermocouple measurements. Fast pyrolysis of cellulose proceeds only at the surface area and the internal cellulose pyrolysis is slower in infrared heating. This would be due to the short lifetime of liquid cellulose at high temperatures (< 1s), the low thermal conductivity of cellulose (0.04 W/mK) and the level off of the temperature by LG evaporation.

Since the aromatic solvent volatilized before starting of pyrolysis of cellulose, the yield of LG did not improve under the infrared heating condition when an aromatic solvent was added. On the other hand, the yield of LG was greatly increased from the glycerol treated cellulose. In fast pyrolysis of the glycerol treated cellulose, the pathway of slow pyrolysis would be inhibited.

In fast pyrolysis by infrared heating, LG was efficiently produced from cellulose (*Chapter 6*). For expanding the use of LG, the hydrolysis with microwave treatment and solid acid (a cation exchange resin) was investigated in *Chapter 7*. LG was hydrolyzed into glucose in high yield (95.4 mol%) at 120 °C for 30 min. The activation energy of hydrolysis with microwave treatment was estimated to be 111 kJ/mol. LG was hydrolyzed efficiently in high yield, even from high-concentration LG solutions. The temperature measurement position affected the glucose yield because the temperature around the cation exchange resin region was higher than in the LG solution. Sulfonyl groups in the cation exchange resin absorbed microwaves more readily than polystyrene or water. Pyrolysis product from cellulose could be converted into glucose with microwave treatment and solid acid.

These lines of information guide the development of effective chemical materials generation from cellulosic biomass without solid carbonized products by controlling the secondary reactions occurred between the cellulose crystallites. Figure 8-1 shows the summary of this dissertation.

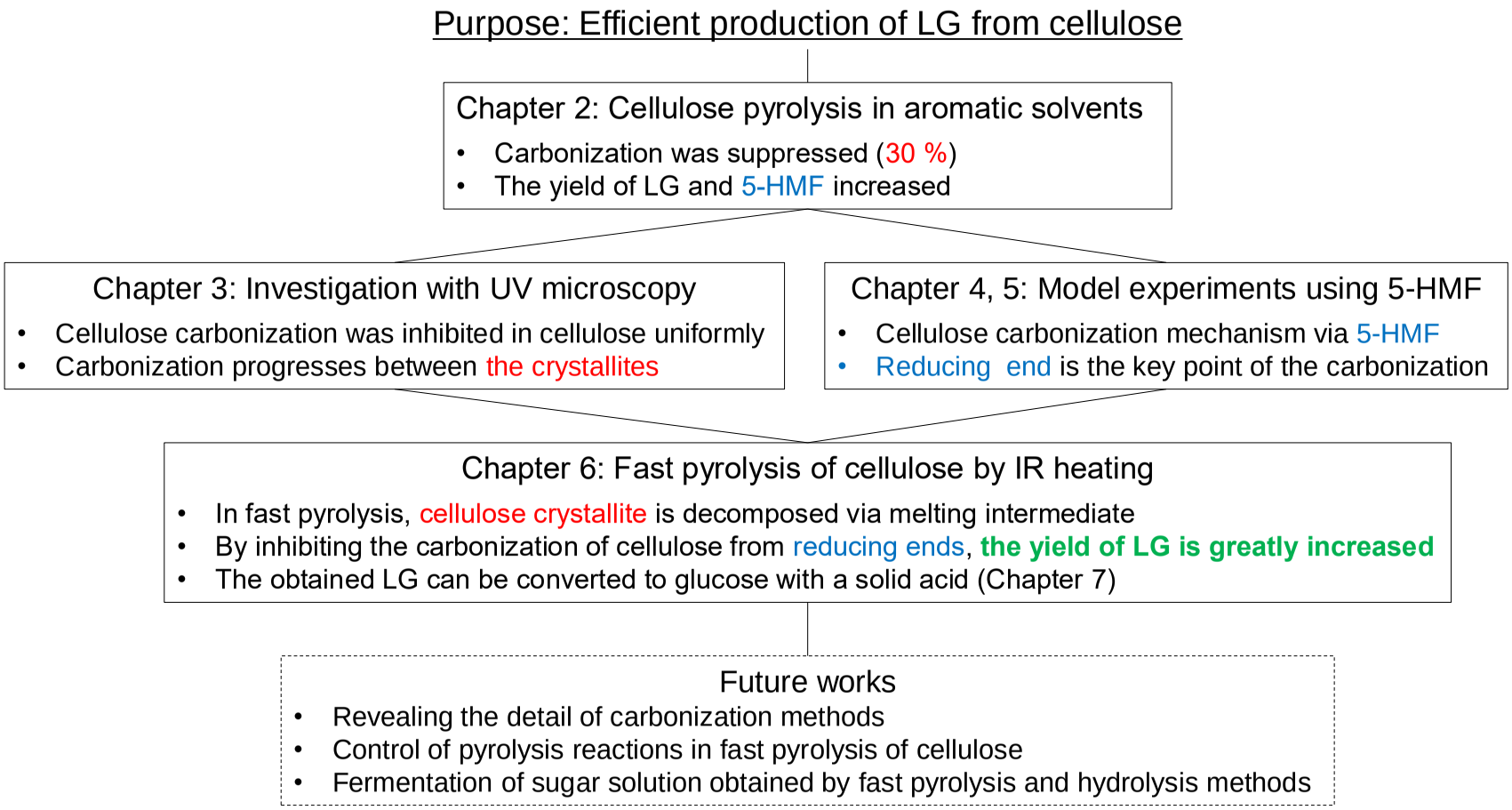

Figure 8-1. Summary of this dissertation

References

A. Pictet. (1918). On the transformation of levoglucoscine to dextrine. *Helv. Chim. Acta*, *1*, 226–230.

Agarwal, V., Dauenhauer, P. J., Huber, G. W., and Auerbach, S. M. (2012). Ab initio dynamics of cellulose pyrolysis: Nascent decomposition pathways at 327 and 600 °C. *J. Am. Chem. Soc.*, *134*(36), 14958–14972.

Agarwal, V., Huber, G. W., Conner, W. C., and Auerbach, S. M. (2011). Simulating infrared spectra and hydrogen bonding in cellulose Iβ at elevated temperatures. *J. Chem. Phys.*, *135*(13), 134506.

Amarasekara, A. S., Nguyen, L. H., Du, H., and Kommalapati, R. R. (2019). Kinetics and mechanism of the solid-acid catalyzed one-pot conversion of d-fructose to 5, 5′-[oxybis(methylene)]bis[2-furaldehyde] in dimethyl sulfoxide. *SN Appl. Sci.*, *1*(9), 964.

Ando, J., Huruta, N., Seto, M., and Akiyama, T. (1996). Kankyo no kagaku. Chapter 7, 87–96.

Antal, M. J., and Grønli, M. (2003). The art, science, and technology of charcoal production. *Ind. Eng. Chem. Res.*, 42(8), 1619–1640.

Asensio, J. L., Ardá, A., Cañada, F. J., and Jiménez-Barbero, J. (2013). Carbohydrate-aromatic interactions. *Acc. Chem. Res.*, *46*(4), 946–954.

Baccile, N., Laurent, G., Babonneau, F., Fayon, F., Titirici, M.-M., and Antonietti, M. (2009). Structural characterization of hydrothermal carbon spheres by advanced solid-state MAS ^{13}C NMR investigations. *J. Phys. Chem. C*, *113*(22), 9644–9654.

Banyasz, J. L., Li, S., Lyons-Hart, J. L., and Shafer, K. H. (2001). Cellulose pyrolysis: The kinetics of hydroxyacetaldehyde evolution. *J. Anal. Appl. Pyrolysis*, *57*(2), 223–248.

Béguin, P., and Aubert, J.P. (1994). The biological degradation of cellulose. *FEMS Microbiol. Rev.*, *13*(1), 25–58.

Blanco, P. H., Lad, J. B., Bridgwater, A. V, and Holm, M. S. (2018). Production of glucose from the acid hydrolysis of anhydrosugars. *ACS Sustain. Chem. Eng.*, *6*(10), 12872–12883.

Boutin, O., Ferrer, M., and Lédé, J. (1998). Radiant flash pyrolysis of cellulose - Evidence for the formation of short life time intermediate liquid species. *J. Anal. Appl. Pyrolysis*, *47*(1), 13–31.

Boutin, O., Ferrer, M., and Lédé, J. (2002). Flash pyrolysis of cellulose pellets submitted to a concentrated radiation: Experiments and modelling. *Chem. Eng. Sci.*, *57*(1), 15–25.

BP statistical Review of World Energy 2020.

Bradbury, A. G. W. W., Sakai, Y., and Shafizadeh, F. (1979). A kinetic model for pyrolysis of cellulose. *J. Appl. Polym. Sci.*, *23*(11), 3271–3280.

Bridgeman, T. G., Jones, J. M., Shield, I., and Williams, P. T. (2008). Torrefaction of reed canary grass, wheat straw and willow to enhance solid fuel qualities and combustion properties. *Fuel*, *87*(6), 844–856.

Bridgwater, A. V. (2012). Review of fast pyrolysis of biomass and product upgrading. *Biomass and Bioenergy*, *38*, 68–94.

Broido, A., Javier-Son, A. C., Ouano, A. C., and Barrall, E. M. (1973). Molecular weight decrease in the early pyrolysis of crystalline and amorphous cellulose. *J. Appl. Polym. Sci.*, *17*(12), 3627–3635.

Broido, A., and Nelson, M. A. (1975). Char yield on pyrolysis of cellulose. *Combust. Flame*, *24*, 263–268.

Capart, R., Khezami, L., and Burnham, A. K. (2004). Assessment of various kinetic models for the pyrolysis of a microgranular cellulose. *Thermochim. Acta*, *417*(1), 79–89.

Casanova, O., Iborra, S., and Corma, A. (2010). Chemicals from biomass: Etherification of 5-hydroxymethyl-2-furfural (HMF) into 5,5′(oxy-bis(methylene))bis-2-furfural (OBMF) with solid catalysts. *J. Catal.*, *275*(2), 236–242.

Chambel, P., Oliveira, M. B., Andrade, P. B., Fernandes, J. O., Seabra, R. M., and Ferreira, M. A. (1998). Identification of 5,5'-oxy-dimethylene-bis(2-furaldehyde) by thermal decomposition of 5-hydroxymethyl-2-furfuraldehyde. *Food Chem.*, *63*(4), 473–477.

Cheng, C. H., Lehmann, J., Thies, J. E., Burton, S. D., and Engelhard, M. H. (2006). Oxidation of black carbon by biotic and abiotic processes. *Org. Geochem.*, *37*(11), 1477–1488.

Chheda, J. N., and Dumesic, J. A. (2007). An overview of dehydration, aldol-condensation and hydrogenation processes for production of liquid alkanes from biomass-derived carbohydrates. *Catal. Today*, *123*(1–4), 59–70.

Chidambaram, M., and Bell, A. T. (2010). A two-step approach for the catalytic conversion of glucose to 2,5-dimethylfuran in ionic liquids. *Green Chem.*, *12*(7), 1253–1262.

Cho, J., Davis, J. M., and Huber, G. W. (2010). The intrinsic kinetics and heats of reactions for cellulose pyrolysis and char formation. *ChemSusChem.*, 3(10), 1162-1165.

Chun, Y., Sheng, G., Chiou, G. T., and Xing, B. (2004). Compositions and sorptive properties of crop residue-derived chars. *Environ. Sci. Technol.*, *38*(17), 4649–4655.

Czernik, S., and Bridgwater, A. V. (2004). Overview of applications of biomass fast pyrolysis oil. *Energy and Fuels*, *18*(2), 590–598.

Dasappa, S. (2014). Thermochemical conversion of biomass. *Transformation of Biomass*, John Wiley & Sons, Ltd. Ch.6, 133–157.

Dauenhauer, P. J., Colby, J. L., Balonek, C. M., Suszynski, W. J., and Schmidt, L. D. (2009). Reactive boiling of cellulose for integrated catalysis through an intermediate liquid. *Green Chem.*, *11*(10), 1555–1561.

Degenstein, J. C., Murria, P., Easton, M., Sheng, H., Hurt, M., Dow, A. R., Gao, J., Nash, J. J., Agrawal, R., Delgass, W. N., Ribeiro, F. H., and Kenttämaa, H. I. (2015). Fast pyrolysis of ^{13}C-labeled cellobioses: Gaining insights into the mechanisms of fast pyrolysis of carbohydrates. *J. Org. Chem.*, *80*(3), 1909–1914.

Degroot, W. F., Pan, W.P., Rahman, M. D., and Richards, G. N. (1988). First chemical events in pyrolysis of wood. *J. Anal. Appl. Pyrolysis*, *13*(3), 221–231.

Demirbaş, A. (2001). Biomass resource facilities and biomass conversion processing for fuels and chemicals. *Energy Convers. Manage.*, *42*(11), 1357–1378.

Dence, C.W. (1992) The determination of lignin. In Methods in Lignin Chemistry; Lin, S.Y.; Dence, C.W., Eds.; Springer-Verlag: Berlin, 33–61.

Di Blasi, C. (1994). Numerical simulation of cellulose pyrolysis. *Biomass and Bioenergy*, *7*(1–6), 87–98.

Ding, S. Y., Liu, Y. S., Zeng, Y., Himmel, M. E., Baker, J. O., and Bayer, E. A. (2012). How does plant cell wall nanoscale architecture correlate with enzymatic digestibility? *Science*, 338(6110), 1055–1060.

Dollimore, D., and Holt, B. (1973). Thermal degradation of cellulose in nitrogen. *J. Polym. Sci. Polym. Phys. Ed.*, *11*(9), 1703–1711.

Duff, S. J. B., and Murray, W. D. (1996). Bioconversion of forest products industry waste cellulosics to fuel ethanol: A review. *Bioresour. Technol.*, *55*(1), 1–33.

Ehara, K., and Saka, S. (2005). Decomposition behavior of cellulose in supercritical water, subcritical water, and their combined treatments. *J. Wood Sci.*, *51*(2), 148–153.

Elazzouzi-Hafraoui, S., Nishiyama, Y., Putaux, J. L., Heux, L., Dubreuil, F., and Rochas, C. (2008). The shape and size distribution of crystalline nanoparticles prepared by acid hydrolysis of native cellulose. *Biomacromolecules*, *9*(1), 57–65.

Emons, A. M. C., and Mulder, B. M. (2000). How the deposition of cellulose microfibrils builds cell wall architecture. *Trends in Plant Sci.*, 5(1), 35–40.

Esteghlalian, A., Hashimoto, A. G., Fenske, J. J., and Penner, M. H. (1997). Modeling and optimization of the dilute- sulfuric acid pretreatment of corn stover polar and switchgrass. *Bioresour. Technol.*, *59*(2–3), 129–136.

Fahlén, J., and Salmén, L. (2002). On the Lamellar structure of the tracheid cell wall. *Plant Biol.*, *4*(3), 339–345.

Falco, C., Perez Caballero, F., Babonneau, F., Gervais, C., Laurent, G., Titirici, M.M., and Baccile, N. (2011). Hydrothermal carbon from biomass: structural differences between hydrothermal and pyrolyzed carbons via ^{13}C solid state NMR. *Langmuir*, *27*(23), 14460–14471.

Fergus, B. J., Procter, A. R., Scott, J. A. N., and Goring, D. A. I. (1969). The distribution of lignin in sprucewood as determined by ultraviolet microscopy. *Wood Sci. Technol.*, *3*(2), 117–138.

Fidel, R. B., Laird, D. A., and Thompson, M. L. (2013). Evaluation of modified boehm titration methods for use with biochars. *J. Environ. Qual.*, *42*(6), 1771–1778.

Fisher, T., Hajaligol, M., Waymack, B., and Kellogg, D. (2002). Pyrolysis behavior and kinetics of biomass derived materials. *J. Anal. Appl. Pyrolysis*, *62*(2), 331–349.

Fratzl, P. (2003). Cellulose and collagen: From fibres to tissues. *Curr. Opin. Colloid Interface Sci.*, 8(1), 32–39

Fukazawa, K., and Imagawa, H. (1981). Quantitative analysis of lignin using an UV microscopic image analyser. variation within one growth increment. *Wood Sci. Technol.*, *15*(1), 45–55.

Fukutome, A., Kawamoto, H., and Saka, S. (2014). Gas- and coke/soot-forming reactivities of cellulose-derived tar components under nitrogen and oxygen/nitrogen. *J. Anal. Appl. Pyrolysis*, *108*, 98–108.

Fukutome, A., Kawamoto, H., and Saka, S. (2015). Processes forming gas, tar, and coke in cellulose gasification from gas-phase reactions of levoglucosan as intermediate. *ChemSusChem*, *8*(13), 2240–2249.

Fukutome, A., Kawamoto, H., and Saka, S. (2016). Gas-phase reactions of glyceraldehyde and 1,3-dihydroxyacetone as models for levoglucosan conversion during biomass gasification. *ChemSusChem*, *9*(7), 703–712.

Gani, A., and Naruse, I. (2007). Effect of cellulose and lignin content on pyrolysis and combustion characteristics for several types of biomass. *Renew. Energy*, *32*(4), 649–661.

Gardiner, D. (1966). The pyrolysis of some hexoses and derived di-, tri-, and poly-saccharides. *J. Chem. Soc. C Org.*, 1473–1476.

Gedye, R., Smith, F., Westaway, K., Ali, H., Baldisera, L., Laberge, L., and Rousell, J. (1986). The use of microwave ovens for rapid organic synthesis. *Tetrahedron Lett.*, *27*(3), 279–282.

Haas, T. J., Nimlos, M. R., and Donohoe, B. S. (2009). Real-time and post-reaction microscopic structural analysis of biomass undergoing pyrolysis. *Energy & Fuels*, *23*(7), 3810–3817.

Halpern, Y., and Patai, S. (1969). Pyrolytic reactions of carbohydrates. Part V. isothermal decomposition of cellulose in vacuo. *Isr. J. Chem.*, *7*(5), 673–683.

Helle, S., Bennett, N. M., Lau, K., Matsui, J. H., and Duff, S. J. B. (2007). A kinetic model for production of glucose by hydrolysis of levoglucosan and cellobiosan from pyrolysis oil. *Carbohydr. Res.*, *342*(16), 2365–2370.

Herrero, M. A., Kremsner, J. M., and Kappe, C. O. (2008). Nonthermal microwave effects revisited: On the importance of internal temperature monitoring and agitation in microwave chemistry. *J. Org. Chem.*, *73*(1), 36–47.

Hopkins, M. W., DeJenga, C., and Antal, M. J. (1984). The flash pyrolysis of cellulosic materials using concentrated visible light. *Sol. Energy*, *32*(4), 547–551.

Hosoya, T., Kawamoto, H., and Saka, S. (2007). Pyrolysis behaviors of wood and its constituent polymers at gasification temperature. *J. Anal. Appl. Pyrolysis*, *78*(2), 328–336.

Hosoya, Takashi, Kawamoto, H., and Saka, S. (2006). Thermal stabilization of levoglucosan in aromatic substances. *Carbohydr. Res.*, *341*(13), 2293–2297.

Hosoya, Takashi, Kawamoto, H., and Saka, S. (2008). Different pyrolytic pathways of levoglucosan in vapor- and liquid/solid-phases. *J. Anal. Appl. Pyrolysis*, *83*(1), 64–70.

Hosoya, Takashi, Nakao, Y., Sato, H., Kawamoto, H., and Sakaki, S. (2009). Thermal degradation of methyl β-D-glucoside. A theoretical study of plausible reaction mechanisms. *J. Org. Chem.*, *74*(17), 6891–6894.

Hudson, K. L., Bartlett, G. J., Diehl, R. C., Agirre, J., Gallagher, T., Kiessling, L. L., and Woolfson, D. N. (2015). Carbohydrate-aromatic interactions in proteins. *J. Am. Chem. Soc.*, *137*(48), 15152–15160.

IPCC. (2013). Climate Change 2013: The physical science basis. Contribution of working Group I to the fifth assesment areport of the intergovermental Panel on Climate change. Cambridge Universitiy Press, Cambridge, United Kingdom and New York, NY, USA, 1535.

Itabaiana Junior, I., Avelar Do Nascimento, M., De Souza, R. O. M. A., Dufour, A., and Wojcieszak, R. (2020). Levoglucosan: A promising platform molecule? *Green Chemistry*. 22(18), 5859–5880.

Jahirul, M. I., Rasul, M. G., Chowdhury, A. A., and Ashwath, N. (2012). Biofuels production through biomass pyrolysis- A technological review. *Energies*, 5(12), 4952–5001.

Julien, S., Chornet, E., Tiwari, P. K., and Overend, R. P. (1991). Vacuum pyrolysis of cellulose: Fourier transform infrared characterization of solid residues, product distribution and correlations. *J. Anal. Appl. Pyrolysis*, *19*, 81–104.

Kang, S., Li, X., Fan, J., and Chang, J. (2012). Characterization of hydrochars produced by hydrothermal carbonization of lignin, cellulose, d-xylose, and wood meal. *Ind. Eng. Chem. Res.*, *51*(26), 9023–9031.

Kashiwagi, T., and Nambu, H. (1992). Global kinetic constants for thermal oxidative degradation of a cellulosic paper. *Combust. Flame*, *88*(3–4), 345–368.

Katō, K. (1967). Pyrolysis of cellulose. *Agric. Biol. Chem.*, *31*(6), 657–663.

Katō, K., and Komorita, H. (1968). Pyrolysis of cellulose. *Agric. Biol. Chem.*, *32*(1), 21–26.

Kawamoto, H., and Saka, S. (2006). Heterogeneity in cellulose pyrolysis indicated from the pyrolysis in sulfolane. *J. Anal. Appl. Pyrolysis*, *76*(1–2), 280–284.

Kawamoto, Haruo. (2016). Review of reactions and molecular mechanisms in cellulose pyrolysis. *Curr. Org. Chem.*, *20*(23), 2444-2457.

Kawamoto, Haruo, Hosoya, T., Ueno, Y., Shoji, T., and Saka, S. (2014). Thermal stabilization and decomposition of simple glycosides in the presence of aromatic substances in closed ampoules: The role of OH···π hydrogen bonding. *J. Anal. Appl. Pyrolysis*, *109*, 41–46.

Kawamoto, Haruo, Murayama, M., and Saka, S. (2003). Pyrolysis behavior of levoglucosan as an intermediate in cellulose pyrolysis: polymerization into polysaccharide as a key reaction to carbonized product formation. *J. Wood Sci.*, *49*(5), 469–473.

Kawamoto, Haruo, Ueno, Y., and Saka, S. (2013). Thermal reactivities of non-reducing sugars in polyether—Role of intermolecular hydrogen bonding in pyrolysis. *J. Anal. Appl. Pyrolysis*, *103*, 287–292.

Kersten, S., and Garcia-Perez, M. (2013). Recent developments in fast pyrolysis of ligno-cellulosic materials. *Curr. Opin. Biotechnol.*, 24(3), 414–420.

Keskiväli, J., Wrigstedt, P., Lagerblom, K., and Repo, T. (2017). One-step Pd/C and $Eu(OTf)_3$ catalyzed hydrodeoxygenation of branched C_{11} and C_{12} biomass-based furans to the corresponding alkanes. *Appl. Catal. A Gen.*, *534*, 40–45.

Kim, D. Y., Nishiyama, Y., Wada, M., Kuga, S., and Okano, T. (2001). Thermal decomposition of cellulose crystallities in wood. *Holzforschung*, *55*(5), 521–524.

Klemm, D., Heublein, B., Fink, H. P., and Bohn, A. (2005). Cellulose: Fascinating biopolymer and sustainable raw material. *Angewandte Chemie* , 44(22), 3358–3393.

Kokot, S., Czarnik-Matusewicz, B., and Ozaki, Y. (2002). Two-dimensional correlation spectroscopy and principal component analysis studies of temperature-dependent IR spectra of cotton-cellulose. *Biopolymers*, *67*(6), 456–469.

Kumar, A., Jones, D., and Hanna, M. (2009). Thermochemical biomass gasification: A review of the current status of the technology. *Energies*, *2*(3), 556–581.

Kwon, G.J., Kim, D.Y., Kimura, S., and Kuga, S. (2007). Rapid-cooling, continuous-feed pyrolyzer for biomass processing: Preparation of levoglucosan from cellulose and starch. *J. Anal. Appl. Pyrolysis*, *80*(1), 1–5.

Kwon, G. J., Kuga, S., Hori, K., Yatagai, M., Ando, K., and Hattori, N. (2006). Saccharification of cellulose by dry pyrolysis. *J. Wood Sci.*, *52*(5), 461–465.

Lédé, J., Blanchard, F., and Boutin, O. (2002). Radiant flash pyrolysis of cellulose pellets: Products and mechanisms involved in transient and steady state conditions. *Fuel*, *81*(10), 1269–1279.

Lédé, J., Li, H. Z., Villermaux, J., and Martin, H. (1987). Fusion-like behaviour of wood pyrolysis. *J. Anal. Appl. Pyrolysis*, *10*(4), 291–308.

Lichtenegger, H., Müller, M., Paris, O., Riekel, C., and Fratzl, P. (1999). Imaging of the helical arrangement of cellulose fibrils in wood by synchrotron X-ray microdiffraction. *J. Appl. Crystallogr.*, *32*(6), 1127–1133.

Liu, Y. S., Baker, J. O., Zeng, Y., Himmel, M. E., Haas, T., and Ding, S. Y. (2011). Cellobiohydrolase hydrolyzes crystalline cellulose on hydrophobic faces. *J. Biol. Chem.*, *286*(13), 11195–11201.

Luo, G., Chandler, D. S., Anjos, L. C. A., Eng, R. J., Jia, P., and Resende, F. L. P. (2017). Pyrolysis of whole wood chips and rods in a novel ablative reactor. *Fuel*, *194*, 229–238.

Maria, del C. Fernandez, A., Francisco, Javier, C., Jesus, J.B., and Gabriel, C. (2005). Molecular recognition of saccharides by proteins. Insights on the origin of the carbohydrate-aromatic interactions. *J. Am. Chem. Soc.*, *127*(20).

Majumdar, A., Mukhopadhyay, S., and Yadav, R. (2010). Thermal properties of knitted fabrics made from cotton and regenerated bamboo cellulosic fibres. *Int. J. Therm. Sci.*, *49*(10), 2042–2048.

Mamleev, V., Bourbigot, S., and Yvon, J. (2007). Kinetic analysis of the thermal decomposition of cellulose: The main step of mass loss. *J. Anal. Appl. Pyrolysis*, *80*(1), 151–165.

Manyà, J. J. (2012). Pyrolysis for biochar purposes: A review to establish current knowledge gaps and research needs. *Environ. Sci. Technol.*, 46(15), 7939–7954.

Matsuoka, S., Kawamoto, H., and Saka, S. (2011a). Thermal glycosylation and degradation reactions occurring at the reducing ends of cellulose during low-temperature pyrolysis. *Carbohydr. Res.*, *346*(2), 272–279.

Matsuoka, S., Kawamoto, H., and Saka, S. (2011b). Reducing end-group of cellulose as a reactive site for thermal discoloration. *Polym. Degrad. Stab.*, *96*(7), 1242–1247.

Matsuoka, S., Kawamoto, H., and Saka, S. (2012). Retro-aldol-type fragmentation of reducing sugars preferentially occurring in polyether at high temperature: Role of the ether oxygen as a base catalyst. *J. Anal. Appl. Pyrolysis*, *93*, 24–32.

Matsuoka, S., Kawamoto, H., and Saka, S. (2014). What is active cellulose in pyrolysis? An approach based on reactivity of cellulose reducing end. *J. Anal. Appl. Pyrolysis*, *106*, 138–146.

Matsuoka, S., Kawamoto, H., and Saka, S. (2016). Reactivity of cellulose reducing end in pyrolysis as studied by methyl glucoside-impregnation. *Carbohydr. Res.*, *420*, 46–50.

Mayes, H. B., and Broadbelt, L. J. (2012). Unraveling the reactions that unravel cellulose. *J. Phys. Chem. A*, *116*(26), 7098–7106.

McHenry, M. P. (2009). Agricultural bio-char production, renewable energy generation and farm carbon sequestration in Western Australia: Certainty, uncertainty and risk. *Agric. Ecosyst. Environ.*, 129(1–39), 1–7.

Mettler, M. S., Paulsen, A. D., Vlachos, D. G., and Dauenhauer, P. J. (2012). The chain length effect in pyrolysis: Bridging the gap between glucose and cellulose. *Green Chem.*, *14*(5), 1284–1288.

Milne, T. A., and Evans, R. J. (1998). Biomass Gasifier "Tars": Their Nature, Formation, and Conversion, National Renewable Energy Laboratory, Golden, CO.

Milosavljevic, I., Oja, V., and M. Suuberg, E. (1996). Thermal Effects in Cellulose Pyrolysis: Relationship to Char Formation Processes. *Ind. Eng. Chem. Res.*, *35*(3), 653–662.

Mok, W. S. L., and Antal, M. J. (1983). Effects of pressure on biomass pyrolysis. II. Heats of reaction of cellulose pyrolysis. *Thermochim. Acta*, *68*(2–3), 165–186.

Musha, Y., and Goring, D. A. I. (1975). Distribution of syringyl and guaiacyl moieties in hardwoods as indicated by ultraviolet microscopy. *Wood Sci. Technol.*, *9*(1), 45–58.

Nelson, M. L., and Tripp, V. W. (1953). Determination of the leveling-off degree of polymerization of cotton and rayon. *J. Polym. Sci.*, *10*(6), 577–586.

Nimlos, M. R., Blanksby, S. J., Qian, X., Himmel, M. E., and Johnson, D. K. (2006). Mechanisms of glycerol dehydration. *J. Phys. Chem. A*, *110*(18), 6145–6156.

Nishiyama, Y. (2009). Structure and properties of the cellulose microfibril. *J. Wood Sci.*, 55(4), 241–249.

Nishiyama, Y., Kim, U. J., Kim, D. Y., Katsumata, K. S., May, R. P., and Langan, P. (2003). Periodic disorder along ramie cellulose microfibrils. *Biomacromolecules*, *4*(4), 1013–1017.

Nomura, T., Kawamoto, H., and Saka, S. (2017). Pyrolysis of cellulose in aromatic solvents: Reactivity, product yield, and char morphology. *J. Anal. Appl. Pyrolysis*, *126*, 209–217.

Nomura, T., Minami, E., and Kawamoto, H. (2020). Carbonization of cellulose cell wall evaluated with ultraviolet microscopy. *RSC Adv.*, *10*(13), 7460–7467.

Nordin, S. B., Nyren, J. O., and Back, E. L. (1974). An indication of molten cellulose produced in a laser beam. *Text. Res. J.*, *44*(2), 152–154.

O'Sullivan, A. C. (1997). Cellulose: The structure slowly unravels. *Cellulose*, *4*(3), 173–207.

Paethanom, A., Nakahara, S., Kobayashi, M., Prawisudha, P., and Yoshikawa, K. (2012). Performance of tar removal by absorption and adsorption for biomass gasification. *Fuel Process. Technol.*, *104*, 144–154.

Pastorova, I., Botto, R. E., Arisz, P. W., and Boon, J. J. (1994). Cellulose char structure: a combined analytical Py-GC-MS, FTIR, and NMR study. *Carbohydr. Res.*, *262*(1), 27–47.

Patwardhan, P. R., Satrio, J. A., Brown, R. C., and Shanks, B. H. (2009). Product distribution from fast pyrolysis of glucose-based carbohydrates. *J. Anal. Appl. Pyrolysis*, *86*(2), 323–330.

Pereira, B. L. C., Oliveira, A. C., Carvalho, A. M. M. L., Carneiro, A. de C. O., Santos, L. C., and Vital, B. R. (2012). Quality of wood and charcoal from eucalyptus clones for ironmaster use . *Int. J. For. Res.*, *2012*, 1–8.

Perez Locas, C., and Yaylayan, V. A. (2008). Isotope labeling studies on the formation of 5-(Hydroxymethyl)-2-furaldehyde (HMF) from sucrose by Pyrolysis-GC/MS. *J. Agric. Food Chem.*, *56*(15), 6717–6723.

Perkins, G., Bhaskar, T., and Konarova, M. (2018). Process development status of fast pyrolysis technologies for the manufacture of renewable transport fuels from biomass. *Renewable Sustainable Energy Rev.*, 90, 292–315.

Pictet, A. (1918). Sur la transformation de la lévoglucosane en dextrine. *Helv. Chim. Acta*, *1*(1), 226–230.

Piskorz, J., Radlein, D., Scott, D. S., and Czernik, S. (1989). Pretreatment of wood and cellulose for production of sugars by fast pyrolysis. *J. Anal. Appl. Pyrolysis*, *16*(2), 127–142.

Piskorz, J., Radlein, D., and Scott S. S. (1986). On the mechanism of the rapid pyrolysis of cellulose, *J. Anal. Appl. Pyrolysis*, 9(2), 127–142.

Prins, M. J., Ptasinski, K. J., and Janssen, F. J. J. G. (2006). Torrefaction of wood. Part 1. Weight loss kinetics. *J. Anal. Appl. Pyrolysis*, *77*(1), 28–34.

Rabemanolontsoa, H., and Saka, S. (2016). Various pretreatments of lignocellulosics. *Bioresour. Technol.*, *199*, 83–91.

Radlein, D. S. T. A. G., Grinshpun, A., Piskorz, J., and Scott, D. S. (1987). On the presence of anhydro-oligosaccharides in the sirups from the fast pyrolysis of cellulose. *J. Anal. Appl. Pyrolysis*, *12*(1), 39–49.

Rafsanjani, A., Stiefel, M., Jefimovs, K., Mokso, R., Derome, D., and Carmeliet, J. (2014). Hygroscopic swelling and shrinkage of latewood cell wall micropillars reveal ultrastructural anisotropy. *J. R. Soc. Interface*, *11*(95), 20140126.

Reynolds, J. G., and Burnham, A. K. (1997). Pyrolysis decomposition kinetics of cellulose-based materials by constant heating rate micropyrolysis. *Energy & Fuels*, *11*(1), 88–97.

Richards, G. N. (1987). Glycolaldehyde from pyrolysis of cellulose. *J. Anal. Appl. Pyrolysis*, *10*(3), 251–255.

Rieger, R., and Müllen, K. (2010). Forever young: Polycyclic aromatic hydrocarbons as model cases for structural and optical studies. *J. Phys. Org. Chem.*, 23, 315-325.

Rowland, S. P., and Roberts, E. J. (1972). The nature of accessible surfaces in the microstructure of cotton cellulose. *J. Polym. Sci. Part A-1 Polym. Chem.*, *10*(8), 2447–2461.

Ruel, K., Barnoud, F., and Goring, D. A. I. (1978). Lamellation in the S2 layer of softwood tracheids as demonstrated by scanning transmission electron microscopy. *Wood Sci. Technol.*, *12*(4), 287–291.

Saha, N., Saba, A., and Reza, M. T. (2019). Effect of hydrothermal carbonization temperature on pH, dissociation constants, and acidic functional groups on hydrochar from cellulose and wood. *J. Anal. Appl. Pyrolysis*, *137*, 138–145.

Saka, S, Whiting, P., Fukazawa, K., and Goring, D. A. I. (1982). Comparative studies on lignin distribution by UV microscopy and bromination combined with EDXA. *Wood Sci. Technol.*, *16*(4), 269–277.

Saka, S. (2001). Biomass Energy and Environment.

Sanders, E. B., Goldsmith, A. I., and Seeman, J. I. (2003). A model that distinguishes the pyrolysis of D-glucose, D-fructose, and sucrose from that of cellulose. Application to the understanding of cigarette smoke formation. *J. Anal. Appl. Pyrolysis*, *66*(1), 29–50.

Sasaki, M., Kabyemela, B., Malaluan, R., Hirose, S., Takeda, N., Adschiri, T., and Arai, K. (1998). Cellulose hydrolysis in subcritical and supercritical water. *J. Supercrit. Fluids*, *13*(1–3), 261–268.

Scheirs, J., Camino, G., and Tumiatti, W. (2001). Overview of water evolution during the thermal degradation of cellulose. *Eur. Polym. J.*, *37*(5), 933–942.

Schroeter, J., and Felix, F. (2005). Melting cellulose. *Cellulose* ,12(2), 159–165).

Scifinder. (2014). *Scifinder*, Chemical Abstracts Service: Columbus, OH; https://scifinder.cas.org (Accessed October 13, 2020); calculated using Advanced Chemistry Development (ACD/Labs) Software V11.02. 1994-2020.

Sekiguchi, Y., Frye, J. S., and Shafizadeh, F. (1983). Structure and formation of cellulosic chars. *J. Appl. Polym. Sci.*, *28*(11), 3513–3525.

Sekiguchi, Y., and Shafizadeh, F. (1984). The effect of inorganic additives on the formation, composition, and combustion of cellulosic char. *J. Appl Polym Sci.* 29(4) 1267-1286.

Seshadri, V., and Westmoreland, P. R. (2012). Concerted reactions and mechanism of glucose pyrolysis and implications for cellulose kinetics. *J. Phys. Chem. A*, *116*(49), 11997–12013.

Shafizadeh, F. (1982). Introduction to pyrolysis of biomass. *J. Anal. Appl. Pyrolysis*, *3*(4), 283–305.

Shafizadeh, F, and Bradbury, A. G. W. (1979). Thermal degradation of cellulose in air and nitrogen at low temperatures. *J. Appl. Polym. Sci.*, *23*(5), 1431–1442.

Shafizadeh, Fred, Furneaux, R. H., Cochran, T. G., Scholl, J. P., and Sakai, Y. (1979). Production of levoglucosan and glucose from pyrolysis of cellulosic materials. *J. Appl. Polym. Sci.*, *23*(12), 3525–3539.

Shafizadeh, Fred, and Sekiguchi, Y. (1983). Development of aromaticity in cellulosic chars. *Carbon N. Y.*, *21*(5), 511–516.

Sharifzadeh, M., Sadeqzadeh, M., Guo, M., Borhani, T. N., Murthy Konda, N. V. S. N., Garcia, M. C., Wang, L., Hallett, J., and Shah, N. (2019). The multi-scale challenges of biomass fast pyrolysis and bio-oil upgrading: Review of the state of art and future research directions. *Prog. Energy Combust. Sci.*, 71, 1–80.

Shoji, T., Kawamoto, H., and Saka, S. (2014). Boiling point of levoglucosan and devolatilization temperatures in cellulose pyrolysis measured at different heating area temperatures. *J. Anal. Appl. Pyrolysis*, *109*, 185–195.

Shoji, T., Kawamoto, H., and Saka, S. (2017). Complete inhibition of char formation from cellulose in fast pyrolysis with aromatic substance. *J. Anal. Appl. Pyrolysis*, *124*, 638–642.

Smith, R. C., and Howard, H. C. (1937). Aromatization of cellulose by heat. *J. Am. Chem. Soc.*, *59*(2), 234–236.

Soares, S., Ricardo, N. M. P., Jones, S., and Heatley, F. (2001). High temperature thermal degradation of cellulose in air studied using FTIR and ^{1}H and ^{13}C solid-state NMR. *Eur. Polym. J.*, *37*(4), 737–745.

Sørensen, H., Rosenberg, P., Petersen, H., and Sørensen, L. (2000). Char porosity characterisation by scanning electron microscopy and image analysis. *Fuel*, *79*(11), 1379–1388.

Silverstein R. M., Bassler G. C., and Morrill T. C. (1986) "Spectrometric Identification of Organic Compounds," Japanese Edition, ed. by S. Araki, Y. Mashiko and O. Yarnamoto, Tokyo-Kagakudojin, Tokyo.

Sun, Y., and Cheng, J. (2002). Hydrolysis of lignocellulosic materials for ethanol production: a review. *Bioresour. Technol.*, *83*(1), 1–11.

Suzuki, J., Azuma, J., Koshijima, T., Okamura, K., and Okamoto, H. (1983). Characterization of mono- and oligosaccharides produced by CO_2 laser irradiation on cellulose. *Chem. Lett.*, *12*(4), 481–484.

Tang, M., and Bacon, R. (1964a). Carbonization of cellulose fibers—I. Low temperature pyrolysis. *Carbon N. Y.*, *2*(3), 211–220.

Tang, M. M., and Bacon, R. (1964b). Cnization of cellulose fibers—I. Low tearbomperature pyrolysis. *Carbon N. Y.*, *2*(3), 211–220.

Teixeira, A. R., Mooney, K. G., Kruger, J. S., Williams, C. L., Suszynski, W. J., Schmidt, L. D., Schmidt, D. P., and Dauenhauer, P. J. (2011). Aerosol generation by reactive boiling ejection of molten cellulose. *Energy Environ. Sci.*, *4*(10), 4306–4321.

Thibodeaux, D. P., and Evans, J. P. (1986). Cotton Fiber Maturity by Image Analysis. *Text. Res. J.*, *56*(2), 130–139.

Tillman, D. A. (1978). Chapter 2 - The present use of wood as a fuel, Wood as an Energy Resource (33-64): Academic Press.

Titirici, M. M. M., Antonietti, M., and Baccile, N. (2008). Hydrothermal carbon from biomass: a comparison of the local structure from poly- to monosaccharides and pentoses/hexoses. *Green Chem.*, *10*(11), 1204–1212.

Tschiersky, H., and Baltes, W. (1989). Curie-point pyrolysis and gas chromatography/mass spectrometry of 5,5′-oxydimethylenebis(2-furfural). *J. Anal. Appl. Pyrolysis*, 17(1), 91–93.

Uddin, M. N., Techato, K., Taweekun, J., Rahman, M. M., Rasul, M. G., Mahlia, T. M. I., and Ashrafur, S. M. (2018). An overview of recent developments in biomass pyrolysis technologies. *Energies* , 11(11), 3115.

Zandvoort, I., Wang, Y., Rasrendra, C. B., van Eck, E. R. H., Bruijnincx, P. C. A., Heeres, H. J., and Weckhuysen, B. M. (2013). Formation, moecular sructure, and mrphology of hmins in bomass cnversion: Influence of fedstock and pocessing cnditions. *ChemSusChem*, *6*(9), 1745–1758.

Venderbosch, R., and Prins, W. (2010). Fast pyrolysis technology development. *Biofuels, Bioprod. Biorefining*, *4*(2), 178–208.

Sivers, M., and Zacchi, G. (1995). A techno-economical comparison of three processes for the production of ethanol from pine. *Bioresour. Technol.*, *51*(1), 43–52.

Wang, S., Dai, G., Yang, H., and Luo, Z. (2017). Lignocellulosic biomass pyrolysis mechanism: A state-of-the-art review. *Prog. Energy Combust. Sci.*, 62, 33–86).

Watanabe, A., Morita, S., and Ozaki, Y. (2006). Study on temperature-dependent changes in hydrogen bonds in cellulose Iβ by infrared spectroscopy with perturbation-correlation moving-window two-dimensional correlation spectroscopy. *Biomacromolecules*, *7*(11), 3164–3170.

Weldekidan, H., Strezov, V., and Town, G. (2018). Review of solar energy for biofuel extraction. In *Renewable Sustainable Energy Rev.*, 88, 184–192.

West, R. M., Liu, Z. Y., Peter, M., Gärtner, C. A., and Dumesic, J. A. (2008). Carbon–carbon bond formation for biomass-derived furfurals and ketones by aldol condensation in a biphasic system. *J. Mol. Catal. A Chem.*, *296*(1–2), 18–27.

Westerhof, R. J. M., Oudenhoven, S. R. G., Marathe, P. S., Engelen, M., Garcia-Perez, M., Wang, Z., and Kersten, S. R. A. (2016). The interplay between chemistry and heat/mass transfer during the fast pyrolysis of cellulose. *React. Chem. Eng.*, *1*(5), 555–566.

Whittaker, R. H. (1979). *Seibutsugunshu to Seitaikei, 2nd edn.* 1979.

Wrigstedt, P., Keskiväli, J., Perea-Buceta, J. E., and Repo, T. (2017). One-pot transformation of carbohydrates into valuable furan derivatives via 5-Hydroxymethylfurfural. *ChemCatChem*, *9*(22), 4244–4255.

Xu, B., and Huang, Y. (2004). Image analysis for cotton fibers Part II: Cross-sectional measurements. *Text. Res. J.*, *74*(5), 409–416.

Xu, B., Pourdeyhimi, B., and Sobus, J. (1993). Fiber cross-sectional shape analysis using image processing techniques. *Text. Res. J.*, *63*(12), 717–730.

Yuan, J. H., Xu, R. K., and Zhang, H. (2011). The forms of alkalis in the biochar produced from crop residues at different temperatures. *Bioresour. Technol.*, *102*(3), 3488–3497.

Zeng, K., Gauthier, D., Soria, J., Mazza, G., and Flamant, G. (2017). Solar pyrolysis of carbonaceous feedstocks: A review. *Sol. Energy*, *156*, 73–92.

Zhang, X., Golding, J., and Burgar, I. (2002). Thermal decomposition chemistry of starch studied by ^{13}C high-resolution solid-state NMR spectroscopy. *Polymer*, *43*(22), 5791–5796.

Zhou, L., Nguyen, T.H., and Adesina, A. A. (2012). The acetylation of glycerol over amberlyst-15: Kinetic and product distribution. *Fuel Process. Technol.*, *104*, 310–318.

Zickler, G. A., Wagermaier, W., Funari, S. S., Burghammer, M., and Paris, O. (2007). In situ X-ray diffraction investigation of thermal decomposition of wood cellulose. *J. Anal. Appl. Pyrolysis*, *80*(1), 134–140.

Acknowledgments

The author would like to express his sincerest gratitude to Professor Haruo Kawamoto, Department of Socio-Environment Energy Science, Graduate School of Energy Science, Kyoto University, for his kindest guidance and encouragement during the entire course of this work.

The author is wishes to express to Professor Toshiyuki Takano, Division of forest and Biomaterials Science, Graduate School of Energy Science, Kyoto University, for his valuable suggestion and critical reading of this manuscript.

The author is deeply grateful to Associate Professor Hideyuki Okumura, Socio-Environmental Energy Science Department, Graduate School of Energy Science, Kyoto University, for his valuable suggestion and critical reading of this manuscript.

The author is very grateful to Assistant Professor Eiji Minami, Department of Socio-Environment Energy Science, Graduate School of Energy Science, Kyoto University, for his helpful comments and discussion.

The author deeply appreciates Assistant Professor Takada Masatsugu, International Advanced Energy Science Research and Education Center, Kyoto University, for his kind assistance with regard to UV microscopy.

This research was made possible by the cooperation and assistance of the members in the Laboratory for Energy Ecosystems, Kyoto University.

The ^{1}H NMR analysis in this research was carried out with great supports of Professor Kazuhiro Irie, Division of Food Science and Biotechnology, Graduate School of Agriculture, Kyoto University.

Finally, the author would like to express his sincere thanks to his family.

List of Publications

Original Papers

Nomura, T., Kawamoto, H., and Saka, S. (2017). Pyrolysis of cellulose in aromatic solvents: Reactivity, product yield, and char morphology. *Journal of Analytical and Applied Pyrolysis,* **126**, 209-217. (*Chapter 2*)

Nomura, T., Minami, E., and Kawamoto, H. (2020). Carbonization of cellulose cell wall evaluated with ultraviolet microscopy. *RSC Advances,* **10**, 7460-7467. (*Chapter 3*)

Nomura, T., Minami, E., and Kawamoto, H. (2020). Hydroxymethylfurfural as an intermediate of cellulose carbonization. *ChemistryOpen,* accepted. (*Chapter 4*)

Nomura, T., Minami, E., and Kawamoto, H. Benzene-ring structure formation via 5-HMF in cellulose carbonization *in preparation.* (*Chapter 5*)

Nomura, T., Mizuno, H., Minami, E., and Kawamoto, H. (2020). Fast pyrolysis of cellulose by infrared heating. *Energies*, **14**, 1842-1854. (*Chapter 6*)

Nomura, T., Maruichi, Y, H., Minami, E., and Kawamoto, H. Hydrolysis of levoglucosan with solid acid by microwave heating. *in preparation.* (*Chapter 7*)

International conferences

Nomura, T., Kawamoto, H., and Saka, S., Controlled pyrolysis of cellulose in aromatic solvent: reactivity, product selectivity, and char morphology, International Cellulose Conference, Fukuoka, Japan, October, 17-20, 2017. (*Chapter 2*)

Nomura, T., Kawamoto, H., and Saka, S., PYROLYSIS OF CELLULOSE IN AROMATIC SOLVENT : REACTIVITY, PRODUCT SELECTIVITY AND CHAR MORPHOLOGY, pyro 2018, Kyoto, Japan, June, 3-8, 2018 (*Chapter 2*)

Nomura, T., Minami, E., and Kawamoto, H., Solid carbonized product formation via 5-HMF during cellulose pyrolysis, 20th International Symposium on Wood, Fiber and Pulping Chemistry, September 9-11, 2019, Tokyo, Japan. *(Chapters 3* and *4*)

【国内学会】

野村 高志、河本 晴雄、坂 志朗：セルロース熱分解に及ぼす非プロトン性添加物の影響、Oral、第 66 回日本木材学会大会、名古屋、2016 年 3 月 27-29 日(29)、P29-03-0915、p.129.

野村 高志、河本 晴雄、坂 志朗：芳香族溶媒中でのセルロースの熱分解反応制御、Oral、第 67 回日本木材学会大会、福岡、2017 年 3 月 17-19 日(17)、P17-10-1700.

野村 高志、河本 晴雄、坂 志朗：芳香族溶媒中での熱分解により生成するセルロースチャーの形態（Morphology of char produced from cellulose pyrolysis in aromatic solvent）、Oral、セルロース学会第 24 回年次大会 2017 Cellulose R&D、岐阜、2017 年 7 月 13-14 日(14)、K19、pp.39-40.

野村 高志、河本 晴雄、坂 志朗：芳香族溶媒を用いたセルロースの熱分解反応制御（Controlled pyrolysis of cellulose in aromatic solvent）、Oral、第 26 回日本エネルギー学会大会、名古屋、2017 年 8 月 1-2 日(2)、3-5-2、pp.94-95.

野村 高志、髙田 昌嗣、河本 晴雄、坂 志朗：セルロース炭化過程の紫外線顕微鏡観察、Oral、第 68 回日本木材学会大会、京都、2018 年 3 月 14-16 日(14)、P14-08-1300.

野村 高志、河本 晴雄：5-ヒドロキシメチルフルフラール －セルロース炭化におけるキー中間体－（5-hydroxymethylfurfural -key intermediate in cellulose carbonization-）、Poster、セルロース学会第 25 回年次大会 2018 Cellulose R&D、宇治、2018 年 7 月 5-6 日(6)、P038、p.85.

野村 高志、河本 晴雄：5-ヒドロキシメチルフルフラールを経由したセルロースの炭化機構（Cellulose carbonization mechanism via 5-hydroxymethylfurfural）、Oral、第 27 回日本エネルギー学会大会、東京、2018 年 8 月 8-9 日(9)、3-5-1、pp.106-107. doi:10.20550/jietaikaiyoushi.27.0_106

野村 高志、河本 晴雄：セルロース炭化中間体としての 5-HMF の熱分解反応特性、Oral、第 69 回日本木材学会大会、函館、2019 年 3 月 14-16 日(14)、P14-06-1400.

野村 高志、南 英治、河本 晴雄：セルロース炭化における 5-HMF からのベンゼン環形成挙動（Benzene ring formation via 5-HMF in cellulose carbonization）、Oral、セルロース学会第 26 回年次大会 2019 Cellulose R&D、福岡、2019 年 7 月 11-12 日(12)、K20、pp.43-44.

野村 高志、南 英治、河本 晴雄：セルロース炭化における 5-HMF からのベンゼン環形成挙動（Benzene ring formation via 5-HMF in cellulose carbonization）、Oral、第 28 回日本エネルギー学会大会、吹田、2019 年 8 月 7-8 日(8)、3-5-2、pp.98-99. doi:10.20550/jietaikaiyoushi.28.0_98

野村 高志、南 英治、河本 晴雄：固体酸触媒とマイクロ波加熱による木材急速熱分解物の糖化、Oral、第 70 回日本木材学会大会、鳥取、2020 年 3 月 16-18 日(16)、P16-02-1330.

水野 ひなの、野村 高志、南 英治、河本 晴雄：赤外線イメージ炉を用いたセルロースの急速熱分解、Oral、第 70 回日本木材学会大会、鳥取、2020 年 3 月 16-18 日(16)、P16-02-1345.

松尾 佳奈、野村 高志、南 英治、河本 晴雄：赤外線イメージ炉を用いたブナ木材の急速熱分解、Oral、第 70 回日本木材学会大会、鳥取、2020 年 3 月 16-18 日(16)、P16-02-1400.

【受賞・表彰】

第 68 回日本木材学会大会 学生優秀口頭発表賞（野村 高志受賞）「野村 高志、髙田 昌嗣、河本 晴雄、坂 志朗：セルロース炭化過程の紫外線顕微鏡観察」、日本木材学会、表彰日：H30.3.15.